



UNIVERSITA' DEGLI STUDI DI VERONA

*DIPARTIMENTO DI
Neuroscienze, Biomedicina e Movimento*

*SCUOLA DI DOTTORATO DI
SCIENZE DELLA VITA E DELLA SALUTE*

*DOTTORATO DI RICERCA IN
MEDICINA BIOMOLECOLARE
Curriculum Biochimica
XXXI ciclo/2015-2018*

**ERYTHROCYTES AS CARRIERS OF OXALATE DECARBOXYLASE
FROM *BACILLUS SUBTILIS*:
AN INNOVATIVE APPROACH FOR THE TREATMENT
OF HYPEROXALURIA**

S.S.D. BIO/10

Coordinatore: Prof.ssa Lucia De Franceschi




Tutor: Prof. Daniele Dell'Orco

Prof.ssa Barbara Cellini

Dottoranda: Dott.ssa Carolina Conter

Quest'opera è stata rilasciata con licenza Creative Commons Attribuzione – non commerciale
Non opere derivate 3.0 Italia . Per leggere una copia della licenza visita il sito web:

<http://creativecommons.org/licenses/by-nc-nd/3.0/it/>

-  **Attribuzione** Devi riconoscere una menzione di paternità adeguata, fornire un link alla licenza e indicare se sono state effettuate delle modifiche. Puoi fare ciò in qualsiasi maniera ragionevole possibile, ma non con modalità tali da suggerire che il licenziante avalli te o il tuo utilizzo del materiale.
-  **NonCommerciale** Non puoi usare il materiale per scopi commerciali.
-  **Non opere derivate** —Se remixi, trasformi il materiale o ti basi su di esso, non puoi distribuire il materiale così modificato.

Erythrocytes as carriers of oxalate-degrading enzymes: an innovative approach for the treatment of hyperoxaluria
Carolina Conter
Tesi di Dottorato
Verona, 10 dicembre 2018

INDEX

Abstract	3
Sommario	5
1. Introduction	7
1.1 The etiology of Hyperoxaluria	8
1.2 Primary Hyperoxaluria	9
1.3 Secondary Hyperoxaluria	12
1.4 Biochemical properties of AGT	14
1.4.1 The major and minor allelic form of AGT	17
1.4.2 The role of misfolding and aggregation in PH1	19
1.5 Current and future strategies for the treatment of Hyperoxaluria	21
1.6 Oxalate degrading-enzymes	29
1.6.1 Oxalate decarboxylase from <i>B. subtilis</i>	30
1.6.2 Use of OxDC in the treatment of Hyperoxaluria	34
1.7 Drug delivery by red blood cells	36
2. Aim of the research	39
3. Materials and Methods	42
3.1 Materials	43
3.2 Expression vectors and site-directed mutagenesis	43
3.3 OxDC, OxDC-DSSN and G2 clone expression and purification	45
3.4 AGT expression and purification	46
3.5 OxDC and OxDC-DSSN decarboxylase activity assay	46

3.6 OxDC and OxDC-DSSN oxidase activity assay	47
3.7 Measurement of oxalate decarboxylase and oxidase activity in function of pH	48
3.8 Determination of the AGT transaminase activity	49
3.9 Spectroscopic techniques	49
3.10 Aggregation studies	50
3.11 Aggregation kinetics: the minimalistic/"Ockham's razor" Finke-Watzy two-step model	51
3.12 Size exclusion chromatography	52
3.13 Cross-linking	53
3.14 Cell culture	53
3.15 Xfect protein transfection	53
3.16 Western Blot	54
3.17 Viability assay	55
3.18 RBC loading	55
3.19 Combinatorial Incorporation of Synthetic Oligonucleotides During Gene Shuffling (ISOR)	56
3.20 Screening of libraries	57
3.21 Molecular modeling and hydrophobic patches analysis	58
3.22 Calculation of electrostatic potential maps and predicted p _{Ka}	59
3.23 Determination of the consensus sequence	59
4. Biochemical characterization of OxDC and OxDC-DSSN at neutral pH	61
<i>Background Information</i>	62
<i>Results and Discussion</i>	64

4.1 Kinetic and structural properties of OxDC and OxDC-DSSN	64
4.2 Stability and aggregation propensity of OxDC and OxDC-DSSN at pH 4.2 and 7.2	70
4.3 Oxalate detoxification ability of OxDC and OxDC-DSSN in a PH1 cellular model	74
<i>Conclusions</i>	78
5. Loading of <i>B. subtilis</i> OxDC in human and murine red blood cells	79
<i>Background Information</i>	80
<i>Results and Discussion</i>	82
5.1 Stabilities studies of OxDC in human RBCs loading buffer	82
5.2 OxDC loading in human RBCs	85
5.3 OxDC loading in murine RBCs	86
<i>Conclusions</i>	87
6. Protein engineering strategy to select an improved form of OxDC at neutral pH	88
<i>Background Information</i>	89
<i>Results and Discussion</i>	93
6.1 Rational approach	93
6.2 Irrational approach	100
6.2.1 Identification of target mutations by the consensus based-approach	101
6.2.2 Library construction with the ISOR method and screening of the OxDC variants upon expression in <i>E. coli</i>	104
6.2.3 Analysis of the G2 clone	107

<i>Conclusions</i>	110
7. Opposite effect of polymorphic mutations on the electrostatic aggregation of human alanine:glyoxylate aminotransferase: implications for the pathogenesis of PH1	112
<i>Background Information</i>	113
<i>Results and Discussion</i>	114
7.1 <i>In silico</i> analysis of the AGT surface	114
7.2 Effect of pH and ionic strength on the aggregation propensity of AGT-Ma	115
7.3 Effects of the P11L and I340M polymorphic mutations on the aggregation process	119
7.4 Modulation of AGT-Mi aggregation by common PH1-causing mutations	126
<i>Conclusions</i>	130
8. Conclusions	132
Annex	135
Bibliography	138

ABSTRACT

Hyperoxaluria is a pathologic condition due to genetic and non-genetic causes that leads to the deposition of calcium oxalate (CaOx) crystals at first in the urinary system and, in the most severe forms, in the whole body. The disease can be due to either an increased endogenous oxalate production (primary hyperoxaluria or PH) or an increased intestinal oxalate absorption (secondary hyperoxaluria or SH). Three forms of PH are known. They are inherited disorders caused by the deficit of enzymes involved in liver glyoxylate metabolism. The most common and most severe form is PH1. Two curative therapies are currently available for the treatment of PH1: pyridoxine administration (PN) and liver transplantation. However, The first is only effective in 10-30% of the patients, while the second is a very invasive and risky procedure. Thus, the development of new therapeutic strategies represents an urgent need.

In this regard, we hypothesized that a possible approach could be the use of an oxalate-degrading enzyme, which would reduce plasma oxalate concentration thus counteracting the formation of CaOx. Oxalate Decarboxylase (OxDC) from *B. subtilis* is an hexameric Mn-dependent enzyme belonging to the bicupin family that catalyses the cleavage of the oxalate C-C bond to give carbon dioxide and formate. A mutated form of the enzyme, called OxDC-DSSN, shows a reduced decarboxylase specific activity, but is endowed with the ability to catalyse an oxalate oxidation reaction. It should be underlined that OxDC displays an optimum pH around 4 and a deep characterization of the enzyme at neutral pH is still lacking. Based on these considerations, the aim of my PhD was the study of the biochemical features of OxDC at neutral pH and their possible improvement by protein engineering techniques. Moreover, since the direct administration of a non-human protein would elicit a remarkable immune reaction, we thought to encapsulate OxDC in red blood cells (RBCs) and use loaded RBCs as oxalate-degrading bioreactors.

The data obtained indicate that:

- 1) OxDC and OxDC-DSSN (i) display optimal activity at pH 4.2 but retain a detectable residual activity at pH 7.2, the intracellular pH of RBCs, (ii) do

not undergo major structural changes at neutral pH, (iii) are able to detoxify oxalate endogenously produced in a cellular model of PH1.

- 2) OxDC can be efficiently encapsulated in human and murine RBCs and does not lose catalytic activity during the encapsulation process.
- 3) by using directed evolution approaches, a mutated form of OxDC could be engineered that is more resistant to thermal stress and aggregation under physiological conditions as compared with wild-type OxDC.

Overall these data provide the proof-of-principle for the feasibility of a therapy for PH based on the administration of RBCs-loaded with an oxalate-degrading enzyme. Future studies will be focused on the testing of the ability of wild-type and engineered OxDC to detoxify oxalate in a mouse model of PH1.

SOMMARIO

L'iperossaluria è una condizione patologica caratterizzata da un aumento dell'escrezione urinaria di ossalato. A seconda delle cause questa malattia può avere due espressioni cliniche differenti: l'iperossaluria primaria (PH) è dovuta a deficit enzimatici che causano l'aumento della produzione endogena di ossalato, mentre l'iperossaluria secondaria (SH) è causata da un aumento di ossalato esogeno (ad esempio in seguito ad un aumentato apporto con la dieta).

L'ossalato è un acido dicarbossilico che deriva dall'ossidazione epatica del gliossilato, un intermedio di alcune reazioni metaboliche. Poiché nell'uomo non può essere metabolizzato, va incontro ad escrezione mediante le urine. Nei casi di PH, l'aumento nei livelli di ossalato sintetizzati ed escreti provoca la deposizione di cristalli insolubili di ossalato di calcio (CaOx) dapprima nei reni e nel tratto urinario. Il conseguente danno renale determina l'aumento della concentrazione di ossalato anche a livello plasmatico, e la deposizione di CaOx in tutto il corpo. Quest'ultima condizione, detta ossalosi sistemica, porta in molti casi alla morte del paziente. Oltre alle terapie volte a migliorare la funzione renale, le quali non curano la malattia perché sono indirizzate più ai sintomi che non alle cause della patologia, le uniche cure disponibili sono la terapia con piridossina e il trapianto di fegato. Tuttavia, la terapia con piridossina è efficace solo per il 10-30% dei pazienti affetti dalla forma più comune di PH e il trapianto di fegato è un intervento molto invasivo e problematico. Pertanto, sarebbe auspicabile la ricerca di strategie idonee per lo sviluppo di terapie innovative.

E' noto che alcuni microrganismi sono in grado di produrre enzimi che degradano l'ossalato, fra i quali il più studiato è l'ossalato decarbossilasi da *Bacillus subtilis* (OxDC). OxDC converte l'ossalato in formiato e CO₂. È nota una forma mutata dell'enzima, chiamata OxDC-DSSN, la quale presenta una ridotta attività decarbossilasica, ma possiede attività ossalato ossidasica. Tuttavia, non è possibile somministrare direttamente OxDC ai pazienti affetti da PH, in quanto si svilupperebbe una significativa risposta immunitaria. Inoltre, è importante sottolineare che l'OxDC ha un optimum di pH attorno a 4 e molti studi si sono limitati a valutarne le proprietà a pH acido, tralasciando la caratterizzazione

dell'enzima a pH neutro. Tale aspetto non rappresenta solo un'importante premessa per il suo utilizzo all'interno degli eritrociti, ma può anche fornire informazioni importanti per gli impieghi dell'enzima a livello industriale.

Lo scopo principale del mio progetto di dottorato è stato quello di studiare le proprietà di OxDC a pH neutro e di porre le basi per lo sviluppo di un approccio terapeutico basato sull'incapsulamento dell'enzima all'interno degli eritrociti, i quali funzionerebbero da bioreattori proteggendolo dalla degradazione e impedendo la risposta immunitaria del paziente.

I dati ottenuti indicano che:

- (1) OxDC e OxDC-DSSN (i) mostrano un'attività ottimale a pH 4.2 ma conservano un'attività misurabile anche al pH 7.2 presente all'interno degli eritrociti, (ii) a pH neutro non vanno incontro a cambiamenti strutturali rispetto a pH 4.2 e (iii) sono in grado di detossificare l'ossalato endogeno prodotto in un modello cellulare di PH1.
- (2) OxDC può essere efficientemente incapsulata sia negli eritrociti umani che murini e durante il processo di loading non perde attività catalitica.
- (3) mediante approcci di evoluzione diretta è possibile ottenere una forma mutante di OxDC che presenta una aumentata termostabilità e una minore tendenza all'aggregazione rispetto all'enzima wild-type.

In conclusione, questi dati confermano l'applicabilità di una terapia basata sulla somministrazione di enzimi che degradano l'ossalato incapsulati in eritrociti come possibile cura per l'iperossaluria. A tal proposito, in futuro verrà testata la capacità di degradare l'ossalato in un modello murino di malattia da parte dell'enzima wild-type e della forma ingegnerizzata di OxDC.

1

INTRODUCTION

1.1 The etiology of Hyperoxaluria

Hyperoxaluria is a pathologic condition characterized by an increased urinary excretion of oxalate (Bhasin *et al.* 2015). Oxalate, in the form of its calcium salt (CaOx), is a highly insoluble end product of metabolism in humans (Cochat *et al.* 2013) and it is excreted by urine. The excretion of more than 40-45 mg/24 hours of urinary CaOx is considered pathological (Bhasin *et al.* 2015). Primary hyperoxaluria (PH) and secondary hyperoxaluria (SH) are two different clinical expressions of the disease. PH comprises a group of rare inborn errors of glyoxylate metabolism that result in high endogenous oxalate production mainly by the liver (Marengo *et al.*, 2008; Danpure *et al.*, 2004; Harambas *et al.*, 2011). In contrast, SH is caused by an increased intestinal oxalate absorption, as a consequence of various factors such as (i) high oxalate diet, (ii) fat malabsorption, (iii) alterations of the intestinal oxalate-degrading microorganisms, or (iv) genetic variations of the intestinal oxalate transporters (Robijn *et al.* 2011). The clinical phenotype of the two disease forms is qualitatively similar, and mainly related to the high urinary oxalate concentration leading to the production of CaOx stones, and to the consequent formation of diffuse renal calcifications (nephrocalcinosis) and stones (nephrolithiasis) (Robijn *et al.* 2011). However, PHs are usually characterized by an early-onset and are associated with more serious consequences for human health. In fact, the continuous CaOx deposition that occurs in the kidneys of PH patients frequently leads to remarkable kidney damage and to the consequent End Stage Renal Disease (ESRD). In ESRD, the progressive deterioration of the urinary tract finally causes renal failure and accumulation of CaOx crystals in other compartments like blood vessel, bones, retina, heart and the central nervous system (Osswald *et al.*, 1979; Beck *et al.*, 2013). These events generate a potentially fatal condition named systemic oxalosis (Beck *et al.*, 2013, Hoppe 2012), whose main manifestations are reported in Table 1.

Table 1. Symptoms of systemic oxalosis in PH1.

TISSUE	CLINICAL SYMPTOMS
Kidney and urinary tract	Urolithiasis, nephrocalcinosis, renal failure
Bone	Bone pain, multiple fractures and osteosclerosis
Eye	Retinopathy and optic atrophy
Heart	Heart block, myocarditis and cardioembolic stroke
Nerves	Peripheral neuropathy
Deep vasculature	Vasospasm

1.2 Primary Hyperoxaluria

Three genetic defects are currently known to cause PH. The corresponding disease forms are named primary hyperoxaluria Type I (PH1), Type II (PH2) and Type III (PH3). All of them are inherited recessive disorders caused by the deficit of a hepatic enzyme involved in the metabolism of glyoxylate, which results in glyoxylate accumulation and oxidation to oxalate (Salido *et al.*, 2012). (Fig 1).

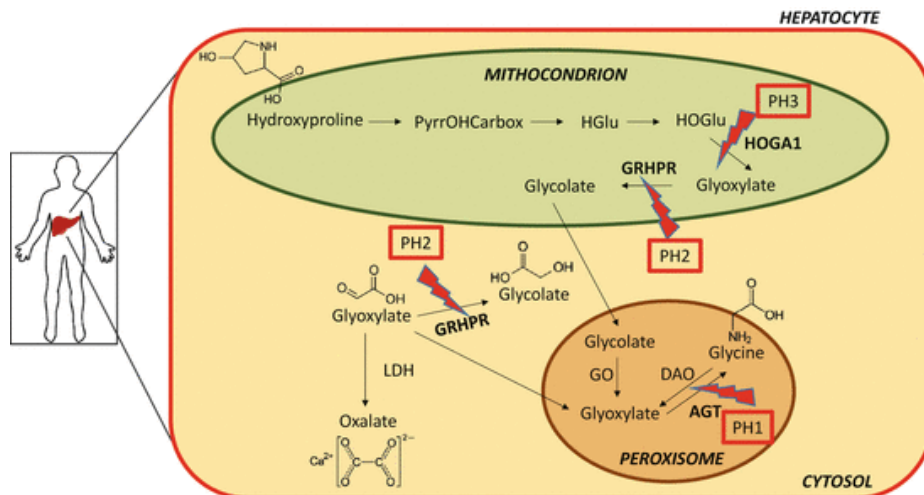


Figure 1. Molecular mechanisms of PH1, PH2 and PH3. HOGA: 4-hydroxy-2-oxoglutarate aldolase; GRHPR: glyoxylate reductase/hydroxypyruvate reductase; AGT: alanine:glyoxylate aminotransferase; GO: glycolate oxidase; LDH: lactate dehydrogenase (Oppici *et al.*, 2017).

- (i) PH1 is the most common and most severe form of PH (70-80% of the patients). It has an estimated prevalence ranging from 1 to 3 per million population and an estimated incidence rate of 1:120,000 live births per year in Europe and North America (Cochat *et al.*, 2013, Kopp *et al.*, 1995). However, the incidence is usually higher in geographically isolated countries such as Canary Islands and in populations where consanguineous marriages are common. The disease accounts for less than 1% of paediatric patients showing ESRD in Europe, but this percentage increases to more than 10% in Kuwait and Tunisia (Coulter-Mackie *et al.*, 2003).

PH1 is caused by mutations on the *AGXT* gene that encodes alanine:glyoxylate aminotransferase (AGT), a liver enzyme responsible for glyoxylate detoxification inside peroxisomes (Danpure *et al.*, 2005). AGT is a pyridoxal 5'- phosphate (PLP)-dependent enzyme that catalyses a transamination reaction in which the amino group of L-alanine is transferred to glyoxylate, leading to the formation of pyruvate and glycine. In the absence of functional AGT, a build-up of glyoxylate in peroxisomes occurs, followed by its translocation to the cytosol where it is oxidized to oxalate by lactate dehydrogenase (LDH) (Figure 1). The production of huge amounts of oxalate leads to a fast and conspicuous generation of CaOx stones at first in renal tissues and then, when supersaturation of CaOx in plasma occurs, to CaOx deposition in many other organs and tissues with consequent systemic clinical effects.

The clinical manifestations of PH1 can be various. First symptoms can appear from early infancy to the sixth decade (median age: 4-6 years) and mainly consist in nephrolithiasis, although some patients can present with ESRD in the first five years of life, thus underlying the severity of the disease. In adulthood PH1 presents with a mild-to-moderate reduction of kidney function and with recurrent renal stones. Moreover, 20-50% of individuals receiving a diagnosis of

PH1 present the late stages of chronic kidney disease or ESRD (Milliner *et al.*, 2002).

Overall, more than 150 mutations on the *AGXT* gene have been identified and associated with PH1 (Williams *et al.*, 2009, Mandrile 2014). Besides deletion and insertions, which represent about 25% of all known mutations, the vast majority are point mutations that lead to single amino acid substitutions of residues spread over the entire protein structure. As already found for many other inherited diseases, missense mutations often map highly conserved residues that are supposed to be crucial for the preservation of the enzyme structure and function (Montioli *et al.*, 2014).

- (ii) PH2, which accounts for approximately 10% of PH cases (Hoppe *et al.*, 2015), is caused by the deficit of glyoxylate reductase-hydroxypyruvate reductase (GRHPR). GRHPR is the enzyme that converts glyoxylate into glycolate and hydroxypyruvate to D-glycerate (Figure 1). GRHPR is ubiquitous, but the majority is intrahepatic (Creegen *et al.*, 2003), where it localizes in the cytosol of hepatocytes and partly inside mitochondria. The protein is also expressed in other tissues, including renal tubules where it likely contributes significantly to the kidney damage occurring in PH2 (Giafi *et al.*, 1998). The absence of hepatic GRHPR in PH2 patients leads to increased glyoxylate and hydroxypyruvate accumulation, two products that are converted by LDH to oxalate and L-glycerate, respectively. In fact, glyceric aciduria is one of the distinctive features of PH2 (Salido *et al.*, 2012). PH2 patients normally suffer from less severe symptoms with respect to those affected by PH1 and rarely progress to ESRD (Marangella *et al.*, 1994).
- (iii) PH3 accounts for 10% of PH cases and it is caused by the deficit of 4-hydroxy-2-oxoglutarate aldolase (HOGA1), encoded by the

HOGA1 gene (Figure 1). HOGA1 is located in the mitochondrial matrix and is responsible of the last step of the hydroxyproline degradation pathway, the cleavage of 4-hydroxy-2-oxoglutarate into pyruvate and glyoxylate (Phang *et al.*, 2001). Since this reaction produces glyoxylate, it is difficult to understand how HOGA1 dysfunction could lead to glyoxylate accumulation. It has been reported that the absence of HOGA1 results in increased concentration of 4-hydroxy-2-oxoglutarate, which could be transformed into glyoxylate by an unidentified cytosolic aldolase (Monico *et al.*, 2005). Although the enzyme is abundant in hepatocytes, the finding that it is also expressed at renal level has raised the possibility that it could contribute to the mechanism of renal damage in PH3. Nevertheless, a clear explanation of PH3 pathogenesis has not been provided until now (Salido *et al.*, 2012). PH3 patients show a mild phenotype with recurrent urolithiasis and nephrocalcinosis during the first decade of life, occasionally leading to reduce kidney function starting from childhood or adolescence. Moreover, systemic oxalosis has never been reported in PH3 patients (Cochat and Rumsby, 2013).

1.3 Secondary Hyperoxaluria

SH results from an increased intestinal absorption of exogenous oxalate (Bhasin *et al.*, 2015). It is usually associated with a milder phenotype with respect to PH. Despite the fact that ESRD has been reported as a possible clinical manifestation, systemic oxalosis is less common and may only occur in severe cases of inflammatory bowel disease or short bowel syndrome (Bhasin *et al.*, 2015). The molecular bases of SH can be various and span from environmental to genetic factors, including in particular:

- (i) Excessive intake of oxalate precursors. Dietary intake contributes to about 50% of the excreted urinary oxalate, thus proving that diet could be an important determinant in total oxalate excretion (Holmes *et al.*, 2001). Spinach and rhubarb are the main source of dietary oxalate whose daily intake must not exceed 1000 mg. However, it must be mentioned that the amount of oxalate effectively absorbed by the intestine could vary depending on the amounts of oxalate-binding cations present in the intestinal tract. In fact, ingested calcium or magnesium ions can complex oxalate producing insoluble salts and thus reducing the amount absorbed by the intestine.
- (ii) Fat malabsorption (enteric hyperoxaluria). An altered capacity to absorb fat-containing food increases the intestinal absorption of oxalate as a result of two different mechanisms: (i) dihydroxy bile acids and fatty acids increase the permeability of the intestinal mucosa to oxalate, and (ii) fatty acids complex with luminal calcium, thus increasing the amount of soluble oxalate available for intestinal absorption (Worcester *et al.*, 2012). This form of hyperoxaluria is often a consequence of partial gastrectomy, bariatric surgery or the use of gastrointestinal lipase inhibitors (Bhasin *et al.*, 2015, Karaolani *et al.*, 2014).
- (iii) Alteration in intestinal microflora. One of the microorganisms that colonize the intestinal tract is *Oxalobacter formigenes*, an aerobic gram negative bacterium that uses oxalate as its energy source, thus decreasing intestinal absorption (Mittal *et al.*, 2004, Hatch *et al.*, 2006). Oxalate enters the bacterium through an oxalate-formate antiporter on the cell membrane, and it is then metabolized to formate and CO₂ (Mittal *et al.*, 2004, Robijin *et al.*, 2011). Environmental influences, such as frequent antibiotic treatment, gastrointestinal disorders, or bariatric operations, often lead to a loss of intestinal colonization, and to a consequent increased absorption of free oxalate in the intestinal lumen (Hoppe *et al.*, 2005). In this regard, the

restoration of *O. formigenes* colonization has been proposed as an effective approach for the treatment of hyperoxaluria (see below).

1.4 Biochemical properties of AGT

PH1, the most recurrent and severe form of PH, is due to inherited mutations in the gene encoding AGT. AGT is a liver-specific enzyme present inside peroxisomes. It is a homodimer and each subunit is composed by 392 amino acids. According to its crystal structure (Zhang *et al.*, 2003), AGT belongs to the Fold Type I class of PLP-dependent enzymes (Figure 2). Each subunit comprises: a N-terminal extension composed by residues 1-21 wrapping over the surface of the neighbouring subunit, a large domain (residues 22-282) containing the dimerization interface and most of the active site and a C-terminal domain (residues 283-392) containing the peroxisomal targeting information.

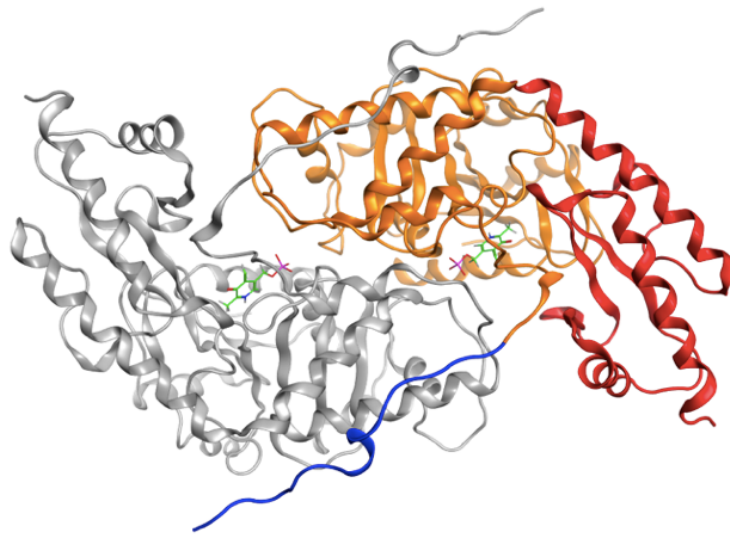


Figure 2. Representation of the AGT dimeric structure (PDB 3R9A). One subunit is colored grey; on the other subunit the N-terminal extension, the large domain and the C-terminal domain are shown in blue, orange and red, respectively. PLP is shown as green sticks. Oxygen, nitrogen and phosphorous atoms are shown in red, blue and purple, respectively.

As in all PLP-enzymes, the coenzyme is covalently bound to the amino group of a lysine residue (Lys209 in AGT) by means of a Schiff base linkage, forming a complex called internal aldimine (Amadasi *et al.*, 2007). Other weak interactions at the active site stabilize the AGT-PLP complex including: (i) a salt bridge between the pyridine nitrogen of PLP and Asp183, (ii) a base stacking interaction between Trp108 and the pyridine ring of PLP and (iii) hydrogen bonds between the hydroxyl group of PLP and Ser158 as well as between the phosphate group of PLP and Gly82, His83, Tyr260 and Thr263 (Figure 3) (Zhang *et al.*, 2003).

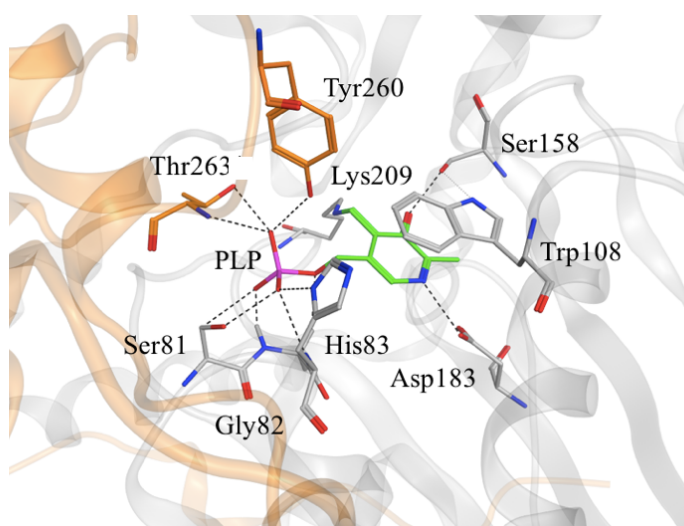


Figure 3. AGT active site. Particular of the AGT active site (PDB: 3R9A). PLP is shown as green sticks. Residues interacting with the coenzyme are shown as grey sticks (if belong to the same subunit of the coenzyme) or orange sticks (if belong to the neighboring subunit). Oxygen, nitrogen and phosphorous atoms are colored red, blue and fuchsia, respectively.

The active site is located in a cleft at the monomer-monomer interface and it is formed by residues belonging to both subunits, thus suggesting that the catalytic activity is strictly related to the folded dimeric structure. In this regard, it has been recently reported that the mutation of the interface residues Arg118, Phe238 and Phe240 produces a form of the enzyme stable in solution as monomer. Monomeric

AGT is devoid of catalytic activity but is able to bind PLP, which strongly promotes dimer formation (Dindo *et al.*, 2016).

A peculiar structural feature of AGT can be observed by looking to the surface of the protein, where it can be noticed an asymmetric distribution of charged residues, i.e. the presence of negative and positive patches. The latter condition can promote self-association processes mediated by electrostatic forces (Dindo *et al.*, 2017).

AGT catalyses the reversible transamination of L-alanine and glyoxylate to pyruvate and glycine, respectively, by a classical ping-pong mechanism (Figure 4). In the first half-reaction, after the binding of the substrate to the catalytic site of the enzyme in the internal aldimine form (AGT-PLP) and the formation of the Michaelis complex, the ϵ -amino group of Lys209 is replaced by the α -amino group of L-alanine, generating the external aldimine. The extraction of the C_{α} -proton from the external aldimine yields a quinonoid intermediate, which is then reprotonated at the $C4'$ of the coenzyme to give the ketimine intermediate. The latter form is then hydrolyzed to pyridoxamine 5'-phosphate (PMP) and pyruvate. In the second half transamination, following the same steps of the first half-reaction but in reverse order, glyoxylate reacts with the AGT-PMP complex and is converted to glycine, thus regenerating AGT-PLP (Cellini *et al.*, 2017).

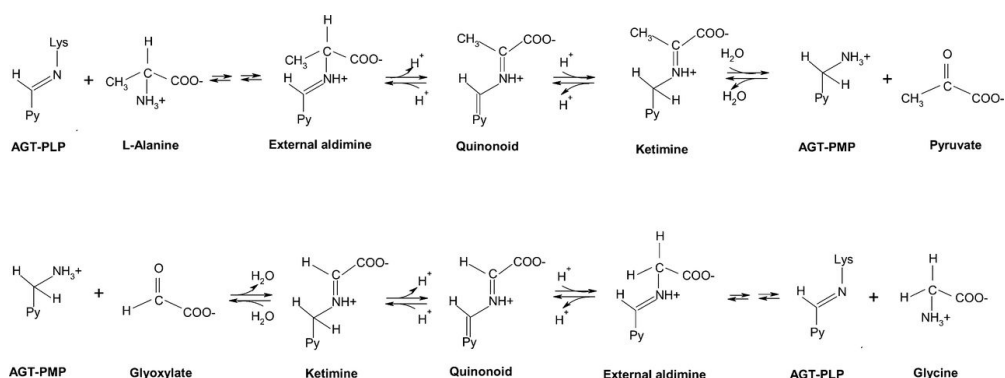


Figure 4. Mechanism of the transaminase reaction catalyzed by AGT.

AGT kinetic studies confirm that the enzyme is highly specific for the glyoxylate to glycine conversion, in agreement with the proposed physiological role of the enzyme in glyoxylate detoxification (Cellini *et al.*, 2017). In fact, the equilibrium constant of the overall transamination is about 9400 and the k_{cat} for the transamination reaction of the alanine/glyoxylate pair is about 150-fold higher with respect to that of the glycine/pyruvate pair (Cellini *et al.*, 2017). Moreover, it has been demonstrated that the enzyme possesses a higher affinity for PMP than for PLP, and the coenzymatic form PMP remains tightly bound to the apoprotein during the catalytic cycle, producing an enzyme more reactive toward oxoacids (Cellini *et al.*, 2017). The spectral changes occurring in AGT during the two half-transamination reactions have indicated that some conformational changes at the active site occurs. Through computational studies, it has been suggested that slight rearrangements of aromatic residues at the active site and a tilting of the coenzyme could take place and these structural re-orientations could be responsible for the tight PMP binding during catalysis (Cellini *et al.*, 2017).

1.4.1 The major and minor allelic form of AGT

AGT is encoded by the *AGXT* gene which is located on chromosome 2q37.3. This gene is present in human population as two polymorphic variants, named the “major allele” and the less common “minor allele”. The frequency of the minor allele varies from 2% in Japanese population, to 20% of Europeans and North Americans, to 28% in the Saami population (Purdue *et al.*, 1990, Purdue *et al.*, 1991). The minor allele differs from the major one for a 74-bp duplication in intron 1 and two point mutations (32C → T and 1020A → G) which cause the Pro11Leu and Ile340Met amino acid substitutions (Purdue *et al.*, 1991). The presence of the minor allele polymorphism is not pathogenic *per se*, but it could promote an increased susceptibility of AGT to the effect of several missense mutations, which are predicted to be non-pathogenic when associated with the major allele. For this reason, many investigations have been carried out to understand the differences between the two allelic forms of AGT at cellular and molecular level. Studies

performed in human hepatocytes suggest that the protein encoded by the minor allele (AGT-Mi) has a specific activity of about 70% as compared with that encoded by the major allele (AGT-Ma) (Purdue *et al.*, 1991, Lumb *et al.*, 2000). Moreover, while AGT-Ma is entirely located in peroxisomes, AGT-Mi shows a localization of about 95% peroxisomal and 5% mitochondrial (Purdue *et al.*, 1991). In cellular models it has been demonstrated that the partial mitochondrial localization of AGT-Mi is due to the presence of the P11L mutation, which creates a weak putative mitochondrial targeting sequence (MTS) at the N- terminus of the protein. Despite the presence of a putative MTS, a large part of AGT-Mi is not imported into mitochondria, probably because the protein quickly folds and dimerizes, thus avoiding the interaction with the mitochondrial import machinery that only acts on unfolded or partly-unfolded monomeric species (Lumb *et al.*, 1999).

Biochemical studies on the purified form of AGT-Ma and AGT-Mi (Cellini *et al.*, 2010, Salido *et al.*, 2012) have indicated that the P11L/I340M mutations do not affect either the UV-visible absorbance, dichroic and fluorescence features of AGT or the equilibrium dissociation constant for PLP ($K_{D(PLP)}$) value. This suggests the absence of gross conformational changes between the two allelic forms that share a similar active site architecture (Cellini B *et al.*, 2010). Nevertheless, AGT-Mi shows an approximately 30% decreased k_{cat} value for the overall transamination of the L-alanine/glyoxylate pair, in agreement with the reduced specific activity observed in human hepatocytes. Furthermore, yeast complementation assays (Hopper *et al.*, 2008) along with pulse-chase and cross-linking experiments performed on cell-free transcription/translation products (Coulter-Mackie *et al.*, 2006) have shown that AGT-Mi is less stable *in vivo* and is more susceptible to proteolytic degradation and aggregation in comparison to AGT-Ma (Cellini *et al.*, 2012).

Thermal and chemical unfolding experiments have provided evidence for a less stable dimeric structure and a decreased overall stability of both holo- and apoAGT-Mi as compared with the corresponding forms of AGT-Ma. The structural destabilization of AGT-Mi has been exclusively attributed to the P11L mutation (Cellini *et al.*, 2012). *In silico* analyses predict that its replacement by a leucine

residue could increase the flexibility of the N- terminal arm of AGT, possibly promoting its dissociation from the neighboring subunit (Dindo *et al.*, 2017).

Moreover, the perturbation of the N- terminal arm could also be transmitted to the AGT active site through a loop (residues 24-32), which contributes to the PLP binding site. Overall, the analyses on the differences between AGT-Ma and AGT-Mi, have allowed not only to better understand the structural features of AGT, but have also represented an important starting point to investigate the effect of pathogenic mutations associated with the major or the minor allele.

1.4.2 The role of misfolding and aggregation in PH1

In the last ten years, protein misfolding induced by missense mutations was demonstrated to be the molecular mechanism in a constantly growing number of inborn errors of metabolism. To attain functionality, proteins must fold into their three-dimensional native state structure during or following translation at the ribosomes (Sala *et al.*, 2017). To maintain proteostasis a cell must assume a correct balance between protein synthesis, folding and degradation. However, this balance is constantly altered by either mutations or environmental stress factors.

The vast majority of PH1-causing mutations are missense and they involve residues spread over the entire AGT sequence. Although this would suggest that a great variety of mechanisms could lead to AGT deficit, studies at molecular level strongly agree upon the finding that the main consequence of pathogenic mutations is protein misfolding. AGT misfolding can lead to various downstream effects, as outlined in Figure 6 (Oppici *et al.*, 2015, Pey *et al.*, 2013).

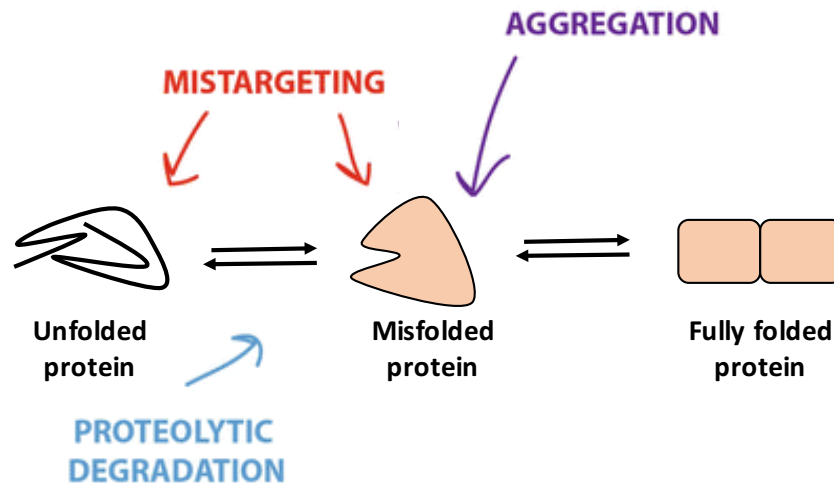


Figure 6. Tentative scheme describing the AGT folding pathway and the effects of mutations leading to folding defects. Most pathogenic mutations associated with PH1 cause folding defects that then lead to a variety of downstream effects including increased degradation or aggregation, destabilization or mistargeting.

It should be also underlined that most missense mutations are pathogenic only when present on the minor polymorphic form of the enzyme, while in other cases the same mutation can lead to different effects if present on the background of the major or the minor allele.

Pathogenic mutations altering AGT folding in PH1 can have the following consequences:

- (i) Destabilization of the dimeric structure. The mutations involved are residues located at monomer-monomer interface, as demonstrated for the G41R, G41V and G47R variants in the purified form (Cellini *et al.*, 2009, Cellini *et al.*, 2010a, Cellini *et al.*, 2010b) and in cellular systems (Fargue *et al.*, 2013, Montioli *et al.*, 2015). In some cases, substitutions of amino acid distant from the interface could give rise to indirect destabilizing effect on the quaternary structure, as proved for the F152I and G170R mutations which co-segregate with the minor allele polymorphism (Cellini *et al.*, 2009, Cellini *et al.*, 2010a).
- (ii) Reduction of intracellular stability. This point is related to proteolytic phenomena because in the presence of exposed flexible regions the proteolysis increase meaning the presence of a folding defect (Fontana *et al.*, 2014). Some pathogenic variants of AGT associated with the minor allele, such as G41R, A112D and I244T, and with the major allele, such as

G41R and A112D, show a high susceptibility to proteolytic degradation resulting in a reduced intracellular half-life (Cellini *et al.*, 2010b, Fargue *et al.*, 2013, Montioli *et al.*, 2015).

- (iii) Increased aggregation propensity. Two different mechanisms related to the aggregation process of AGT have been reported. Some variants, like F152I-Mi, undergo hydrophobic aggregation deriving from a destabilization of the dimeric structure which causes the population of monomeric intermediates exposing apolar surfaces (Cellini *et al.*, 2009, Fargue *et al.*, 2013, Montioli *et al.*, 2015). In other cases, variants undergo electrostatic aggregation in which interaction between patches of opposite charge create a native-like aggregation prone protein (Cellini *et al.*, 2010b, Oppici *et al.*, 2013b). AGT aggregates can deposit both in peroxisomes or in the cytosol, probably depending on the competition between the kinetics of aggregation and that of peroxisomal import (Fargue *et al.*, 2013, Oppici *et al.*, 2013b, Santana *et al.*, 2003). In fact, if the aggregation rate is higher with respect to the import rate, cytosolic aggregates are unable to reach the peroxisomal compartment as demonstrated for the Gly161 variant (Oppici *et al.*, 2013b).

1.5 Current and future strategies for the treatment of Hyperoxaluria

Hyperoxalurias are difficult-to-treat diseases. An early diagnosis and a focused therapy are crucial to avoid renal damage in patients. Classical treatments are addressed at preventing kidney failure or at restoring kidney function (Cochat *et al.*, 2012, Cochat *et al.*, 2013, Ben-Shalom *et al.*, 2015, Cellini 2017, Cochat *et al.*, 2013). In this regard, all patients affected by hyperoxaluria must assume a large daily intake of fluids (>31 per 1.73 m^2) to avoid CaOx concentration and prevent stones formation (Robijn *et al.*, 2011). Since in infants the assumption of fluids can be difficult, combination of haemodialysis and peritoneal dialysis may be used to further enhance oxalate elimination. The timing of haemodialysis and peritoneal dialysis should be coordinated as the latter may be more efficient in removing

oxalate in the later phases of the interdialytic period when rebound is much higher than in the earlier interdialytic phase (Bhasin *et al.*, 2015).

Other classical therapies are aimed at:

- (i) Decreasing the intake of oxalate by dietary restriction. This approach was not regarded as being very helpful, because dietary oxalate is supposed to contribute only marginally to the pathogenesis of the most severe forms of hyperoxaluria, where the highest amount of accumulating oxalate is of endogenous origin (Archer *et al.*, 1957; Zarembski *et al.*, 1969; Marshall *et al.*, 1972; Chadwick *et al.*, 1973). However, more recent studies have shown that diet contribution could be more significant than previously known (Holmes *et al.*, 2001).
- (ii) Preventing CaOx crystallization, by the administration of crystallization inhibitors (i.e. magnesium and potassium citrate) to decrease the amount of calcium oxalate available for precipitation (Bhasin *et al.*, 2015) or by hyper-hydration of the patient as mentioned above (Harambat *et al.*, 2011, Hoppe 2012).
- (iii) Removing CaOx stones by lithotripsy (Carasco *et al.*, 2015).
- (iv) Under more severe conditions, treating renal failure and associated uremia by dialysis or kidney transplantation (Carasco *et al.*, 2015). However, all the problems related to transplantation are well-known (Danpure *et al.*, 2005).

All these approaches address the symptoms of the disease rather than the causes and thus they do not represent a real cure and only slow down disease progression. Unfortunately, no true curative strategies are available for most disease forms, except for PH1.

In the case of PH1, two therapeutic approaches addressing the causes of the disease are currently in use: the administration of pharmacological doses of pyridoxine (PN), a B6 vitamer, and liver transplantation (Cellini *et al.*, 2014). In responsive patients, the administration of 10 mg/kg body weight of PN can enhance AGT expression and enzymatic activity (Cellini *et al.*, 2014). It is well-known that PN can be converted to PLP, the essential cofactor of AGT. PLP plays not only a prosthetic role for the protein, but also a chaperone role, because the binding of the

cofactor to the apo-form induces a strong stabilization that can be observed both at protein and at cellular level (Cellini *et al.*, 2014). In particular, recent papers have demonstrated that the coenzyme is able to induce dimer formation as well as to stabilize the dimer once folded (Oppici *et al.*, 2015a, Dindo *et al.*, 2017, Dindo *et al.*, 2018). This explains why PN-responsive patients usually bear mutations that compromise the correct folding of AGT by allowing the population of monomeric intermediates and/or by promoting intracellular aggregation (Oppici *et al.*, 2013, Fargue *et al.*, 2013a, Mesa-Torres *et al.*, 2013, Montioli *et al.*, 2015). Unfortunately, although very safe, PN administration is effective for only a minority (25-35%) of PH1 patients (Cochat *et al.*, 2012). The only alternative for unresponsive ones is liver transplantation. Liver transplantation is considered a form of enzyme replacement because it allows to substitute the entire pool of AGT thus restoring glyoxylate detoxification ability of the patients. However, it represents a very invasive intervention that comes with several side-effects (Cochat *et al.*, 2010). While this approach has been usually limited to PH1, recently it has been also employed with success in a PH2 patient (Dhondup *et al.*, 2018).

In the last years, an increased knowledge of the molecular bases of PH and SH has allowed to make big progresses in the development of new treatment strategies. The rationale of the approaches currently under development is outlined below, but most of them aim at either improving liver glyoxylate detoxification, or at preventing endogenous oxalate synthesis, based on the estimate that about 40% of oxalate production derives from the glycine/glyoxylate metabolism. Another category of therapies under development include those aimed at reducing the amount of exogenous oxalate absorbed at intestinal level.

The approaches currently under investigation include:

- (i) Gene therapy. It consists in the recovery of a defective enzymatic function by replacing a mutated gene with a normal copy. Being single-gene diseases, all three forms of PH could be cured by a gene therapy approach. The first attempts started on PH1 using liver-directed viral vectors to recover AGT expression in mice disease models. One employed two adeno-associated virus serotypes (AAV5 and AAV8) (Salido *et al.*, 2011), while the other employed helper-dependent

adenoviral vectors (Castello *et al.*, 2016). In both cases a reduction of urinary oxalate excretion was observed. However, the high dosage required reduces the safety of this approach and prompt for the searching of new viral vectors endowed with a better specificity and safety profile.

- (ii) Substrate reduction therapy (SRT). The principle of this strategy is the reduction of an accumulating substrate using small molecules that inhibit the enzymes working upstream of the mutated one in the same metabolic pathway (Guerard *et al.*, 2018, Shemesh *et al.*, 2015, Smid *et al.*, 2016). In the three forms of PH, various SRT strategies have been designed to reduce the amount of glyoxylate endogenously produced, with the direct consequence of preventing oxalate formation. They are based on the use of either small-molecule or RNA interference (RNAi) therapeutics directed against two different targets: (i) glycolate oxidase (GO), which is a flavin-dependent enzyme belonging to the hydroxyacid oxidases family that catalyses the conversion of (S)-2-hydroxy acids and molecular oxygen to 2-oxo acids and hydrogen peroxide. The protein is considered a suitable target for SRT in PH, because it is the enzyme mainly involved in glyoxylate production in human hepatocytes (Booth *et al.*, 2006, Mdluli *et al.*, 2005). (ii) LDH, which catalyses the conversion of lactate to pyruvate and back, with the concomitant conversion of NAD^+ to NADH. LDH is the enzyme directly involved in glyoxylate-to-oxalate conversion in the cytosol of liver hepatocytes. In 2016, Higuera *et al.* identified a compound named 4-carboxy-5[(4-chlorophenyl) sulfanyl]-1,2,3-thiadiazole (CCPST) which is able to inhibit GO in primary cultures of hepatocytes deriving from mice knock-out for the *AGXT* gene. Upon *in vivo* oral administration to *AGXT* knock-out mice, it reduces urinary oxalate excretion by 30-50%. Notwithstanding this very promising result, a more detailed investigation of toxicity is necessary to test the biosafety of this compound. Very recently, Moya-Garzon *et al.* have studied the effect of salicylic acid derivatives on the inhibition of GO. Most of the identified

compounds are able to reduce the production of oxalate in hyperoxaluric hepatocytes by acting as GO inhibitors. However, more detailed studies are ongoing in order to design molecules with an improved affinity and specificity for the enzyme (Moya-Garzon *et al.*, 2018).

In the last years, very promising SRT strategies for the treatment of PH have been designed taking advantage of the RNAi technologies. RNAi is based on the use of 19-21 bp RNA molecules which bind and degrade a specific mRNA, thus preventing the expression of the corresponding protein (Alagia *et al.*, 2016). The first attempt in this direction was made by Dutta *et al.* in 2016 using a Dicer-substrate RNAi produced by Dicerna Therapeutics, which is delivered by nanoparticles and targets the *HAOI* gene encoding GO. Preclinical studies have highlighted a remarkable suppression of GO expression and activity, associated with a decreased urinary oxalate excretion in mice and monkey models of hyperoxaluria. A subsequent study has been performed in 2016 by Liebow *et al.*, who tested a RNAi named ALN-GO1 produced by Alnylam Therapeutics and administered by subcutaneous injection. ALN-GO1 exerted a potent silencing of *HAOI* gene and reduced urinary oxalate in mice, rats and non-human primates (Liebow *et al.*, 2016). Based on these data the company developed Lumasiran, a drug based on ALN-GO1 conjugated to N-acetylgalactosamine, for an efficient delivery to hepatocytes. Lumasiran is currently tested in a phase 1/2 clinical trial in patients affected by PH1.

Very recently, the possibility to target LDH by RNAi has been evaluated by Lai *et al.* (Lai *et al.*, 2018). This approach could be mentioned as SRT because the reduction of hepatic LDH would block glyoxylate-to-oxalate conversion, thus achieving efficient oxalate reduction. In this work the authors hypothesized that the reduced expression of hepatic LDH, which converts glyoxylate into oxalate, could avoid the accumulation of oxalate in PH patients. They found that targeting *LDHA* gene by RNAi actually decreases oxalate production and prevents CaOx crystals precipitation in mouse and primate disease models. Nowadays,

this RNAi developed by Dicerna Pharmaceuticals is in phase 1 clinical trial. However, a deep investigation about biosafety is needed.

- (iii) Pharmacological chaperones. One of the approaches under development in the last decades for the treatment of protein misfolding diseases is the use of chemical or pharmacological chaperones (PCs) which are small molecules able to improve the folding and restore the activity of misfolded proteins (Powers *et al.*, 2009). The term chemical chaperones usually refers to low molecular weight molecules that non-specifically stabilize a misfolded protein without directly interacting with it. Some research groups have analysed the action of chemical chaperones in PH1. Phenylbutyric acid (PBA), betaine, glycerol and trimethylamine N-oxide (TMAO) have been tested. However, only glycerol and betaine were found to exert a stabilizing effect of the pathogenic variants F152I-Mi, G170R-Mi, and I244T-Mi (Coulter-Mackie *et al.*, 2006, Coulter-Mackie *et al.*, 2008). On the other hand, PCs usually exert a specific binding and stabilize misfolded proteins against denaturation and proteolytic degradation (Ringe *et al.*, 2009). When a disease is due to an enzymatic deficit, compounds acting as PCs are either (i) vitamin derivatives functioning as coenzymes, or (ii) competitive inhibitors of the enzyme involved. Both classes of molecules are usually endowed with a high binding affinity and specificity, two features that allow them to be effective at very low concentrations (Ringe *et al.*, 2009). The use of PCs as therapy has been successful for the treatment of various inborn disorders such as lysosomal storage diseases and phenylketonuria (Powers *et al.*, 2009). Based on the finding that in some AGT variants the folding defect only or mainly affects the apo-form, and that this is also true for mutations responsive to Vitamin B6 at clinical level (Cellini *et al.*, 2011, Monico *et al.*, 2005, Hoyer-Kuhn *et al.*, 2014), the possible chaperone role of the coenzyme has been evaluated. Studies carried out on purified proteins and in a cellular model of PH1 have revealed that PLP not only shifts the equilibrium from the less stable apo-form to the

more stable holo-form of AGT, but also binds apomonomeric and apodimeric folding intermediates promoting the acquirement and the maintenance of the dimeric structure that is crucial for functionality (Cellini *et al.*, 2009, Cellini *et al.*, 2010a, Cellini *et al.*, 2012, Mesa-Torres *et al.*, 2013, Mesa-Torres *et al.*, 2014, Pey *et al.*, 2011). As a confirmation of the chaperone role of PLP, it has been recently reported that mutations located at the AGT monomer-monomer interface that cause structural alterations on the apo-form but not on the holo-form, are responsive to PN administration *in vitro*. Interestingly, the responsiveness seems to inversely correlate with the degree of conformational alteration of each variant, thus implying that a kind of threshold could exist, above which the coenzyme is not able to rescue for the folding defect of a variant (Dindo *et al.*, 2018). Another parameter that could influence B6 responsiveness is the type of vitamer. In fact, even though PN is the only vitamer used in clinics, also pyridoxal (PL) and pyridoxamine (PM), can be internalized by cells (Ueland *et al.*, 2015). The comparison of the effectiveness of the three B6 vitamers in a cellular model of PH1 has revealed that PN and PM are more effective than PL in the rescue of folding-defective variants of AGT (Oppici *et al.*, 2015). The reason underlying this difference is that PM and PL administration, differently from PN, avoids the intracellular accumulation of pyridoxine phosphate (PNP) that competes with PLP for AGT binding and inhibits catalytic activity. Considering the safety of vitamins administration, and the fact that PM is already in the market for the treatment of diabetes Type II, these data hold promise for a possible future improvement of the therapy with Vitamin B6, which could completely or at least partly relief disease symptoms, provided that responsive mutations are identified and that the more effective vitamer is administered.

The possibility to use substrate analogs acting as competitive inhibitors has been also evaluated in PH1. In particular, aminoxyacetic acid (AOA) has been analysed because it is a well-known ligand of the

protein. AOA binds the AGT active site by mimicking the position of the substrate L-alanine (Andy *et al.*, 1995) and is supposed to form an oxime with the carbonylic group of PLP, similarly to what happens in other PLP-dependent enzymes. AOA behaves as a tight-binding inhibitor, but when administered to cells expressing AGT misfolded variants it plays a chaperone role for the most common mutations leading to PH1 such as F152I, G170R and I244T, due to its ability to specifically bind the enzyme and to dissociate from it in the presence of the physiological substrate. However, it lacks of specificity because it interacts with many PLP enzymes as well as with free PLP, thanks to its highly reactive aminic group (Andy *et al.*, 1995). To overcome the low specificity of AOA, which makes it unsuitable for clinical use, a preliminary structure activity relationship analysis has been performed. This study allowed to identify a number of AOA derivatives among which 2-aminooxy-3-phenylpropionic acid was found to work as PC (Oppici *et al.*, 2015).

- (iv) Intestinal oxalate degradation. A class of approaches under development aiming at reducing the burden of oxalate includes treatments directed to the consumption of intestinal oxalate. It has been mentioned that the intestine exerts a double function by (i) contributing to the absorption of dietary oxalate, and (ii) working as alternative pathway for the elimination of oxalate. It is well known how *Oxalobacter formigenes* plays a fundamental role in degrading intestinal oxalate, thus promoting a reduction in oxalate absorption which in turn reduces urinary oxalate excretion (Hatch *et al.*, 2008, Hatch *et al.*, 2013, Hoppe *et al.*, 2011). Clinical studies have underlined a correlation between the lack or decreased activity of *O. formigenes* and the development of recurrent oxalate stone disease. Since the elimination of intestinal oxalate could induce a concentration-dependent transport into the intestinal lumen, the possibility that intestine colonization with *O. formigenes* could represent a treatment option in PH1 has been tested. In animal models,

the oral administration of *O. formigenes* leads to a net reduction of the levels of oxalate in urine and plasma, due to the complete colonization of the intestinal tract that effectively induces a progressive excretion of endogenous oxalate. Studies based on this approach are presented since 2002, when Duncan *et al.*, demonstrated that *O. formigenes* administration was able to reduce urinary oxalate in four human subject. More recently Hoppe *et al.*, reported very encouraging results producing an oral formulations of *O. formigenes* with a good safety profile and leading to the reduction in urinary oxalate levels, as shown in a Phase 1 trial in PH patients (Hoppe *et al.*, 2006). In 2011, Hoppe *et al.* have also reported the effectiveness of the same treatment in two patients affected by infantile oxalosis (Hoppe *et al.*, 2011).

Moreover, a company named OxThera developed a lyophilized form of *O. formigenes* named Oxabact. Unfortunately, phase I/II clinical trials have not completely confirmed the results obtained in animal models. In fact, no significant differences were seen between control and treated group, probably due to a high heterogeneity in urinary oxalate excretion among patients.

Following the idea that any approach able to decrease oxalate levels could reduce CaOx supersaturation and remarkably counteract stone formation in all forms of hyperoxaluria, it has been proposed that oxalate degrading-enzymes could be suitable candidates to carry out oxalate degradation in hyperoxaluric patients (Grujic *et al.*, 2009). Among oxalate-degrading enzymes, oxalate decarboxylase (OxDC) is the most studied as new curative approach for PH1 patients. We will better explain this aspect in the chapter 4.

1.6 Oxalate degrading-enzymes

Oxalate is an end-product of metabolism in humans and other vertebrates (Smith *et al.*, 1978). On the other hand, some bacteria, fungi and plants produce enzymes able to catabolize oxalate. In bacteria, oxalate-degrading enzymes are mainly involved

in the adaptation to pH stress conditions (Tanner *et al.*, 2000), while in fungi and plants they take part of defence mechanisms in response to infection by pathogens (Wojtaszek *et al.*, 1997; Dumas *et al.*, 1995; Zhang *et al.*, 1995). The three major pathways of oxalate catabolism are (i) oxidation, (ii) decarboxylation in form of oxalyl-CoA, and (iii) direct decarboxylation. Oxalate oxidases, also known as germins, cleave oxalic acid to two molecules of carbon dioxide (CO₂) with the concomitant generation of hydrogen peroxide (H₂O₂). Oxalyl-CoA decarboxylase is a bacterial enzyme that converts oxalyl-CoA to formyl-CoA and CO₂ employing thiamine pyrophosphate as cofactor. Finally, OxDC catalyzes the direct decarboxylation of oxalate to formate and CO₂ (Just *et al.*, 2004).

1.6.1 Oxalate decarboxylase from *B. subtilis*

Among oxalate-degrading enzymes, OxDC from *B. subtilis* is the most extensively characterized from a biochemical point of view. It is a metalloenzyme that requires manganese (II) and O₂ to catalyse the conversion of oxalate to formate and CO₂ (Zhu *et al.*, 2016). The resolution of the enzyme crystal structure (Anand *et al.*, 2002; Just *et al.*, 2004) has revealed that OxDC is a 264 kDa homohexameric protein made up of two trimeric units (Figure 7A). The cupin domain I is made up of a continuous stretch of amino acid residues (56-233), while the cupin domain II is formed by residues 234-379 and 8-55 that contribute to one β -strand of the second cupin barrel and by two short helices (Figure 7B and C). A Mn(II) ion is located in the centre of each cupin domain and has an octahedral geometry in which four interactions are contributed by highly conserved amino acid side chains (His95, His97, His140, and Glu101 for the cupin domain I and His273, His275, His319, and Glu280 for the cupin domain II). The OxDC trimer is stabilized by interlocking claw-like α -helical protrusions of adjacent monomers. In the hexameric structure two trimeric layers are packed face to face and a large solvent channel extends entirely through the hexamer.

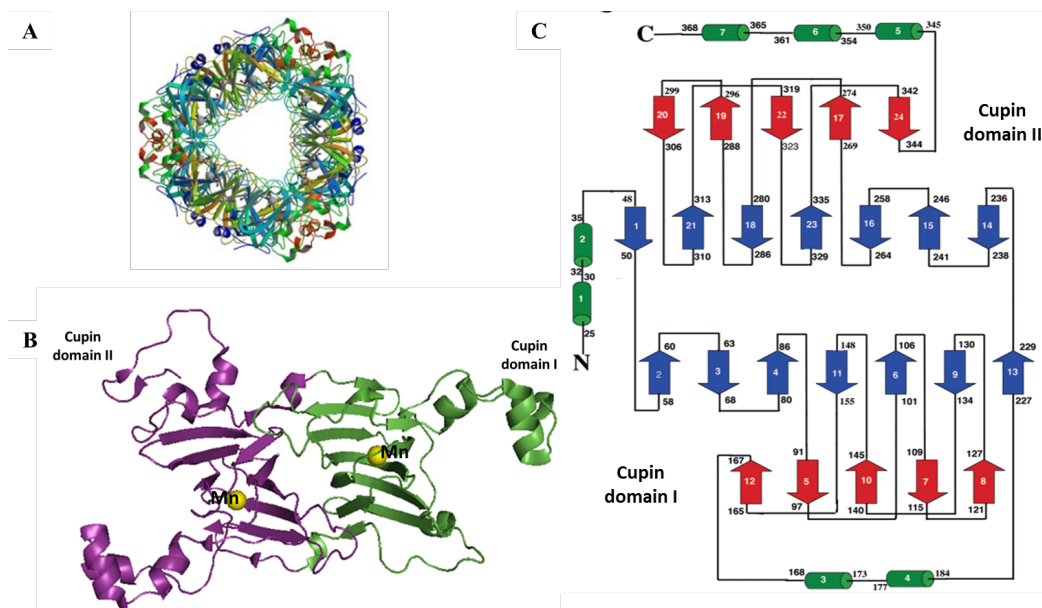


Figure 7. Structural representation of OxDC from *B. subtilis*. (A) Crystal structure of the OxDC hexamer. Each bicupin monomer is differently coloured. Grey spheres represent Mn (II) ions. (B) Crystal structure of the OxDC monomer. The cupin domain I and cupin domain II are coloured green and purple, respectively. The yellow spheres show the position of the two Mn(II) centers (PDB: 1J58). (C) Topology diagram of OxDC. The six-stranded β -sheets that form the front of the cupin barrel are blue, the five-stranded α -sheets that form the back are red, α -helices are green. The first and last residue numbers of each secondary structural element are shown (Anand *et al.*, 2002).

The proposed catalytic mechanism of OxDC has been extensively studied and is illustrated in Figure 8. The enzyme requires oxygen for catalysis, although the reaction does not involve any direct oxidation (Reinhardt *et al.*, 2003). In the first step of reaction, oxalate in the monoprotonated form binds both Mn (II) and the side chain guanidinic group of an Arg residue at the active site. Then, dioxygen oxidizes the catalytically important Mn (II) ion to Mn(III), which can then oxidize the bound substrate to the appropriate radical intermediate. Oxidation reaction is thought to take place with the concomitant formation of a Mn-bound superoxide. Then, an active site glutamate residue probably mediates a proton-coupled electron transfer in the initial complex to give a Mn(II)-bound oxalate radical anion, which undergoes heterolytic bond cleavage to release CO₂. After decarboxylation, a Mn(II)-bound radical anion of formate is produced, which can then be protonated by the active site glutamate, again with electron transfer from the metal, to yield

Mn(III)-bound formate (Svedružić *et al.*, 2007; Zhu *et al.*, 2016). It is well known that OxDC has an optimum pH of 4.2 and a K_m for oxalate of 5 mM (Burrel *et al.*, 2007).

The identity of the catalytically active Mn containing site is still highly debated (Just *et al.*, 2007). Recently, it has been postulated that the cupin domain I is the one responsible for the decarboxylase activity, while the cupin domain II exclusively plays a structural role. This hypothesis is supported by numerous structural and kinetic evidences as well as by site-directed mutagenesis studies. In particular, the presence in the crystal structure of a formate molecule bound to the active site and the identification of a suitable proton donor (Glu162) have been only detected in the cupin domain I (Anand *et al.*, 2002; Just *et al.*, 2004). Moreover, mutation of residues in the putative active site of the cupin domain I completely abolishes the OxDC catalytic activity (Just *et al.*, 2004).

Recently, it has been discovered that, besides the involvement of Glu162, also the oxidation state of the bound metal ion plays a crucial role during catalysis of the OxDC reaction. For many years it has been suggested that the enzyme used dioxygen to generate Mn ions in the oxidation state Mn(III) or Mn(IV). Zhu *et al.*, (Zhu *et al.*, 2016) have demonstrated using paramagnetic resonance spectroscopy that under acidic condition and in the presence of oxalate and dioxygen the oxidation state of manganese is Mn(III). So, the new vision of the catalytic mechanism of OxDC is based on a removal of electrons from the substrate by the cofactor Mn(III). This process then generates a radical intermediate in which the barrier to the C-C bond cleavage is significantly decreases, followed by the other reaction steps cited above (Figure 8).

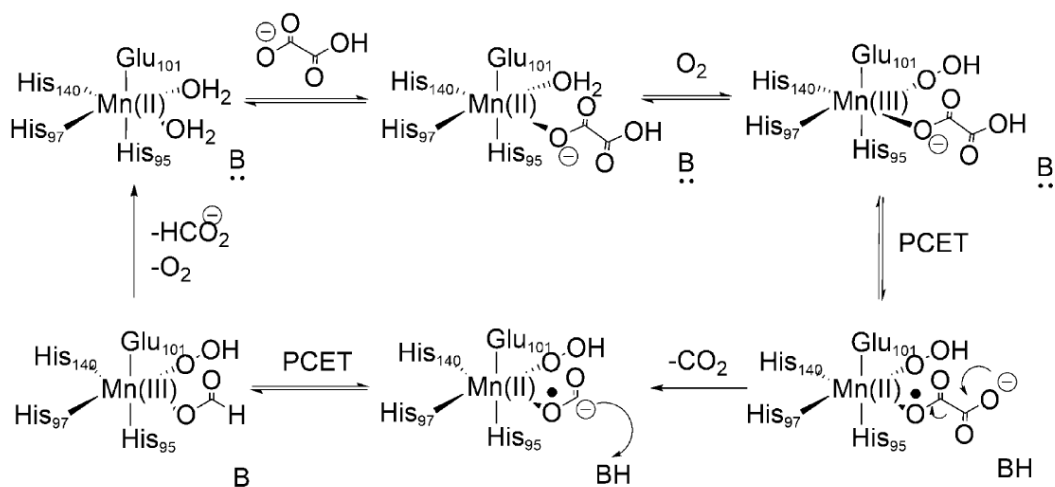


Figure 8. Proposed catalytic mechanism for the oxalate decarboxylase reaction.

Crystallography studies have identified in cupin domain I the presence of a channel for oxalate diffusion that can exist in an “open” or “closed” form as a result of the conformational rearrangement of a lid structure formed by residues 161–165. The open-closed conformational change seems to be important to (i) allow access of the substrate to the active site, (ii) move Glu162 in an optimal position to protonate the formyl radical intermediate, and (iii) release the products (Just *et al.*, 2007).

In addition to the decarboxylase reaction, wild type OxDC is also able to catalyse the oxygen-dependent oxidation of oxalate to carbon dioxide in a reaction that is coupled with the formation of hydrogen peroxide (H₂O₂). However, the turnover number for the oxidase activity is 0.2% that of the decarboxylase activity (Tanner *et al.*, 2001). It has been demonstrated that the substitution of the four amino acids in the OxDC lid from Ser161, Glu162, Asn163, Ser164 to Asp, Ser, Ser, Asn respectively (161-164 SENS→DSSN) (Burrell *et al.*, 2007), gives rise to an OxDC variant named OxDC-DSSN, characterized by an undetectable decarboxylase activity and a 116-fold increased oxidase activity (Table 2) as compared with wild-type OxDC. Burrell and co-workers solved the OxDC SENS161-4DSSN crystal structure and they did not find significant differences with respect to wild type OxDC (Burrell *et al.*, 2007). Moreover, the mutant still had full occupancy of manganese ions. The only significant structural difference was the conformation of

the lid itself, which is intermediate between those of the open and closed forms of the wild-type enzyme. While the loss of decarboxylase activity was expected, considering the absence of Glu162 that acts as proton donor, further studies will be necessary in order to completely understand the structural reasons explaining the improved oxidase activity.

Table 2. Kinetics parameters of wild type OxDC and OxDC-DSSN.

<i>Oxalate decarboxylase activity</i>		
Enzyme	V_{\max} (U mg ⁻¹)	K_m (mM)
Wild-type	27.6 ± 1.8	8.1 ± 0.8
OxDC-DSSN	0.04	n.d.
<i>Oxalate oxidase activity</i>		
Wild-type	0.038 ± 0.03	0.27 ± 0.11
OxDC-DSSN	4.4 ± 0.1	3.2 ± 0.2

a: expressed as formate production;

b: expressed as hydrogen peroxide production; *Data from* Burrell M. R. *et al.*, 2007;

n.d.: not determined.

1.6.2 Use of OxDC in the treatment of hyperoxaluria

As described above, the symptoms of the various forms of hyperoxalurias arise from oxalate accumulation and the consequent formation of CaOx stones. (Cochat and Groothoff, 2013; Canales *et al.*, 2014; Hoppe *et al.*, 2003). Thus, any approach able to decrease oxalate levels could in principle reduce CaOx supersaturation and remarkably counteract stone formation (Salido *et al.*, 2006; Salido *et al.*, 2012). On these bases, the possibility that OxDC could be a suitable candidate to carry out oxalate degradation in hyperoxaluric patients has come out (Hoppe *et al.*, 2005). The idea is that the degradation of intestinal oxalate should reduce the absorption from exogenous sources and possibly promote the clearance of the endogenous pool (Grujic *et al.*, 2009, Cowley *et al.*, 2017, Langman *et al.*, 2016). In agreement with

this hypothesis, studies performed in mice demonstrated that an efficient enteric secretion was able to reduce renal oxalate burden (Hatch *et al.*, 2011). On these bases, a crystalline cross-linked formulation of OxDC, called OxDC-CLEC, has been proposed as oral drug for the treatment of hyperoxaluria. It has been found to have a detectable residual activity at neutral pH, corresponding to about 2% that observed at its optimum pH of 4.2 (Grujic *et al.*, 2009). The oral administration of OxDC-CLEC is able to significantly reduce both urinary (44%) and fecal oxalate (72%) in AGT knockout mice (AGT1KO), a model of PH1, as well as in mice challenged with ethylene glycol (EG), which represent a general model of hyperoxaluria because EG is readily absorbed throughout the intestine and metabolized in the liver to oxalate (Grujic *et al.*, 2009; Salido *et al.*, 2006). Interestingly, in 2016 Langman *et al.*, have implemented the use of OxDC in humans by using ALLN-177A, a crystal form of the enzyme filled into capsules (1,500 units/capsule). In a double-blind, placebo controlled, phase-I study of ALLN-177 in healthy volunteers with diet-induced hyperoxaluria, they demonstrated that ALLN-177 significantly reduced urinary oxalate excretion by efficiently degrading dietary oxalate in the gastrointestinal tract thereby reducing its absorption. Thus, ALLN-177 has been proposed as a new approach for the treatment of secondary hyperoxalurias. Sasikumar and co-workers have designed another approach to reduce intestinal oxalate absorption by using a genetically engineered strain of *L. plantarum* that constitutively expresses and secretes OxDC from *B. subtilis* (Sasikumar *et al.*, 2014). The *in vivo* oxalate degradation ability of this strain has been demonstrated in rats which, upon treatment, showed significant reduction of urinary oxalate, calcium, uric acid, creatinine and serum uric acid as compared with untreated controls. Moreover, no CaOx crystals were detected in the kidneys of treated animals.

The approach based on the use of OxDC could be useful for the treatment of both primary and secondary hyperoxalurias. Very recently, the Allena Pharmaceuticals has completed the clinical trial concerning the ALLN-177A and it has developed the drug Reloxaliase (see <https://clinicaltrials.gov>; Government trial Identifiers: NCT03847090), an orally-administered recombinant oxalate-degrading enzyme formed by 142 mg of OxDC (equivalent to 3,750 units of enzyme activity).

Reloxaliase is being evaluated in the ongoing pivotal Phase 3 URIROX-1 for patients with enteric and/or secondary hyperoxaluria. Moreover, for the first time, this drug has been proposed and it has been granted separate orphan drug designations by FDA for the treatment of primary hyperoxaluria and for the treatment of pediatric hyperoxaluria. However, the administration of oxalate-degrading enzyme would be unsuitable in case of systemic oxalosis, where an increased plasmatic oxalate concentration is observed in PH1 patients, leading to a very serious and often fatal condition (Osswald *et al.*, 1979). In this regard, it should be pointed out that oxalate-degrading enzymes cannot be directly administered in humans, because they would elicit a remarkable immune response.

1.7 Drug delivery by red blood cells

Erythrocytes or red blood cells (RBCs) drug delivery is one of the most promising therapeutic approaches for the administration of selected drugs in order to improve their therapeutic action and reducing their toxicity. RBCs constitute the largest population of blood cells and are the main carriers of oxygen to the body's cells and tissues. RBCs constitute potential biocompatible vectors for different bioactive substances, including drugs and proteins (Barker *et al.*, 2001). Loading procedures exploit the capacity of RBCs placed in hypotonic solutions to form pores large enough to enable the entrance of particles with a molecular weight up to 50000 Da (Gutierrez *et al.*, 2004).

Initial attempts for the encapsulation of drugs in RBCs were undertaken in the 1970s, subsequently extended to the encapsulation of enzymes and peptides with therapeutic activity (Gutierrez *et al.*, 2004, Magnani *et al.*, 2002, Zocchi *et al.*, 1989, Noel-Hocquet *et al.*, 1992). The use of RBCs as carriers has several advantages. RBCs are highly biocompatible, easy to handle, provide an encapsulated drug with a systemic clearance similar to their normal life (120 ± 20 days) (Magnani *et al.*, 1988, Guyton *et al.*, 1996) and protect the encapsulated drug from premature degradation by the immune system.

From a therapeutic perspective, RBCs may be employed for three main purposes: (i) to act as a reservoir for the drug, providing the sustained release of the same into

the body, (ii) to selectively direct the drugs to the reticulo-endothelial system (RES) of the liver, spleen and bone marrow, and (iii) to act as bioreactors in which an enzyme is encapsulated and is able to metabolize its physiological substrate without leaving the cell. The applications of this carrier system are currently very numerous, even though more clinical studies are required to confirm its pharmacokinetic and pharmacodynamic advantages (Biagiotti *et al.*, 2011). Beside the numerous advantages, the use of RBCs as carrier also presents some disadvantages (Jain *et al.*, 1997; Moss *et al.*, 2000; Valbonesi *et al.*, 2001; Sugai *et al.*, 2001; Lvarez *et al.*, 2005). The major problem encountered in the use of biodegradable materials or natural cells as drug carriers is that they are removed *in vivo* by the RES. This seriously limits their half-life and in some cases may also pose toxicological problems. Moreover, due to their biological origin, RBCs may present greater variability and are more liable to contamination as compared with other carrier systems. Finally, encapsulated drugs may alter the physiology of the erythrocyte and/or induce a rapid leakage from the RBC.

Notwithstanding the possible shortcomings, RBC loading techniques were recently used in the treatment of phenylketonuria. Phenylketonuria (PKU) is an autosomal recessive genetic disease caused by the deficit of phenylalanine hydroxylase, the enzyme that converts L-phenylalanine to L-tyrosine (Scriver *et al.*, 2001). PKU patients accumulate high levels of phenylalanine in the bloodstream, with pathologic consequences mainly consisting in mental retardation. One of the available therapies for PKU is the administration of phenylalanine ammonia lyase (PAL), a cyanobacteria-derived enzyme able to degrade phenylalanine into metabolically harmless products (trans-cinnamic acid and trace amounts of ammonia) (Hoskins *et al.*, 1982). PAL is usually administered in complex with polyethylene glycol, to increase stability and limit immunogenicity (see www.ClinicalTrials.gov; Government trial Identifiers: phase I NCT00634660; phase II NCT00925054, NCT01560286, NCT00924703 and NCT01212744; phase III NCT01819727 and NCT01889862). Recently, Rossi L. and co-workers (Rossi *et al.*, 2014) developed erythrocytes loaded with recombinant PAL from *Anabaena variabilis*, as bioreactors able to overcome the accumulation of phenylalanine in the bloodstream in a murine model of PKU. They demonstrated that PAL-loaded RBCs

are able to decrease blood Phe levels and do not induce the generation of antibodies as the recombinant enzyme. These results have opened new perspectives for the use of RBCs as carrier in enzyme administration therapies for other disorders due to enzyme deficiencies.

2

AIM OF THE RESEARCH

Hyperoxaluria is a pathologic condition characterized by the deposition of calcium oxalate crystals at first in the urinary system and, in the most severe forms, in the whole body. Primary hyperoxalurias (PHs) are rare inborn errors of glyoxylate metabolism leading to an increased production of endogenous oxalate. Secondary hyperoxalurias (SHs) result from an increased intestinal absorption or an increased intake of exogenous oxalate.

Among PHs, Primary Hyperoxaluria Type I (PH1) is a rare disease caused by mutations in the gene encoding alanine:glyoxylate aminotransferase (AGT), an enzyme that utilizes pyridoxal 5'-phosphate (PLP) as coenzyme to catalyse the transamination of L-alanine and glyoxylate to pyruvate and glycine. AGT deficiency allows glyoxylate accumulation and its oxidation to the metabolic end-product oxalate.

Hyperoxaluria is a difficult-to-treat disease. The therapeutic strategies currently available are either poorly effective or very invasive. Thus, many efforts have been dedicated in the last years to the development of innovative and non-invasive treatment strategies. In this regard, we focused our attention on the possible use of oxalate-degrading enzymes, and in particular on oxalate decarboxylase (OxDC) from *B. subtilis*. OxDC is a 264 kDa homo-hexamer belonging to the cupin-like family, that converts oxalate to formate and CO₂. The mutation of the sequence of the loop (161-164) from Ser-Glu-Asn-Ser to Asp-Ser-Ser-Asn, abolishes the decarboxylase activity, but enhances a secondary oxalate oxidase activity of the enzyme, thus converting OxDC into OxDC-DSSN, which metabolizes oxalate to carbon dioxide and hydrogen peroxide. Both enzymes could be effective in preventing oxalate accumulation, but their biochemical properties under physiological conditions have not been investigated. Moreover, the therapeutic use of OxDC requires its activity at neutral pH, but the enzyme displays an optimal pH of activity around 4. Finally, the administration of non-human enzymes would elicit a remarkable immune response, we thought to the possibility of encapsulating the enzyme inside red blood cells (RBCs) to generate bioreactors able to metabolize plasmatic oxalate and reduce its urinary excretion.

Based on these considerations, my research activity during the PhD program has been focused on:

- (i) The biochemical characterization of OxDC and OxDC-DSSN at their optimum pH (4.2) and at the intracellular pH of RBCs (7.2);
- (ii) The analysis of the ability of both enzymes to metabolize oxalate in a cellular model of PH1;
- (iii) The setup of a protocol for OxDC loading in human and murine RBCs.
- (iv) The application of protein engineering techniques to select mutant forms of OxDC endowed with a higher activity or stability at physiological pH

In parallel with my main PhD project, I have also focused my attention on the study of the molecular mechanisms underlying the tendency of AGT to aggregation and the effect of polymorphic and pathogenic mutations associated with PH1.

3

MATERIALS AND METHODS

3.1 Materials

Potassium oxalate, formate, formate dehydrogenase (FDH) from *Candida boidinii*, bovine plasma thrombin, glycolate, Bradford reagent, nicotinamide adenine dinucleotide oxidate form (NAD⁺), lysozyme, leupeptine, pepstatin, imidazole, isopropyl β -D-1 thiogalactopyranoside (IPTG), pyridoxal 5-phosphate (PLP), L-alanine, sodium glyoxylate, rabbit muscle L-lactic dehydrogenase (LDH) and EDTA were purchased from SIGMA-Aldrich. 2,2'-azinobis-3-ethylbenzothiazoline-6-sulphonic acid (ABTS) and the EDTA free protease inhibitor cocktail were purchased from Roche. The rabbit anti-His (C-Term)-HRP antibody was purchased from Invitrogen, the Enhanced ChemiLuminescence® (ECL) reactive was purchased from Millipore. The Xfect™ Protein Transfection kit was purchased from Clontech Laboratories. Zeocin, geneticin (G418), PBS (phosphate-buffered saline), modified Ham's F12 Glutamax medium and trypsin were purchased from Life Technologies™. All other chemicals were of the highest purity available.

3.2 Expression vectors and site-directed mutagenesis

The cDNA of *B. subtilis* OxDC with a thrombin cleavage site and a 6-Histidine (6xHis) tag at the C-terminus cloned in a pET24a(+) vector (pET24a-OxDC) was purchased from GeneScript. This vector allows the expression of the recombinant protein in *E. coli* under the control of the lactose operon upon isopropyl β -D-1 thiogalactopyranoside (IPTG) addition to the culture medium.

The expression vector for OxDC-DSSN (pET24a-OxDC-DSSN) was obtained by introducing the S161D, E162S, N163S, and S164N mutations by site-directed mutagenesis on the pET24a-OxDC vector using the QuikChange II site-directed mutagenesis kit (Stratagene). The primers used were 5'-CTG CTG GTT TTT GAC GAT GGC AGC TTC AGC GAG AAC AGC ACC TTT CAA CTG ACC GAC TGG CTG GC-3' and its complement. Underlined codons indicate mutated amino acids.

The expression vectors for OxDC E162H, E162K and E162Q (pET24a-OxDC-E162H, pET24a-OxDC-E162K and pET24a-OxDC-E162Q) by site-directed mutagenesis on the pET24a-OxDC vector using the QuikChange II site-directed mutagenesis kit (Stratagene) in order to produce site-saturation mutagenesis of Glu162. The primers used were 5'-GAC GAT GGC AGC TTC AGC CAT AAC AGC ACC TTT CAA CTG-3' for E162H, 5'-GAC GAT GGC AGC TTC AGC AAA AAC AGC ACC TTT CAA CTG-3' for E162K and 5'-GAC GAT GGC AGC TTC AGC CAT AAC AGC ACC TTT CAA CTG-3' for E162Q. Underlined codons indicate mutated amino acids.

The primers used to produce the mixture of primers used in chapter 6.1 for the substitution of residues in the proximity of the active site were designed as shown below. The expression vectors for OxDC E60H, E60K, E60R, E99H, E99K, E99R, E198H, E198K and E198R (pET24a-OxDC-E60H, pET24a-OxDC-E60K and pET24a-OxDC-E60R, pET24a-OxDC-E99H, pET24a-OxDC-E99K, pET24a-OxDC-E99R, pET24a-OxDC-E198H, pET24a-OxDC-E198K) were obtained using the primers 5'-C CCA CAA CCG TCT CAT AAG GGT GGC TAC GC -3' for E60H, 5'- C CCA CAA CCG TCT AAA AAG GGT GGC TAC GC -3' for E60K, C CCA CAA CCG TCT AGA AAG GGT GGC TAC GC -3' for E60R, 5'-CGT GAG CTG CAC TGG CAC AAA CAT GCG GAA TGG GC-3' for E99H, 5'-CGT GAG CTG CAC TGG CAC AAA AAA GCG GAA TGG GC-3' for E99K, 5'-CGT GAG CTG CAC TGG CAC AAA AGA GCG GAA TGG GC-3' for E99R, 5'-C AGC AAC CTG CCG GGC AAA CAT AAG TAC ATT TTT GAG AAC C-3' for E198H, 5'-C AGC AAC CTG CCG GGC AAA AAA AAG TAC ATT TTT GAG AAC C-3' for E198K and 5'-C AGC AAC CTG CCG GGC AAA AGA AAG TAC ATT TTT GAG AAC C-3' for E198R. Underlined codons indicate mutated amino acids.

The pAGT-His construct and the expression vectors for AGT-Ma, AGT-Mi, and the P11L, I360M, F152I, G170R and I244T AGT-Mi mutants were already available (Cellini *et al.*, 2010)

All mutations were confirmed by DNA sequencing.

3.3 OxDC, OxDC DSSN and G2 clone expression and purification

E. coli BL21 (DE3) Codon plus cells transformed with the constructs pET24a-OxDC or pET24a-OxDC-DSSN were grown in Luria Broth (LB) in a total volume of 4.5 litres at 37 °C. Cells were grown with vigorous shaking to an OD of 0.3-0.4 at 600 nm and then heat-shocked at 42°C for 20 minutes. 5 mM MnCl₂ was added to the culture and protein expression was induced with 0.5 mM IPTG for 16 hours at 30°C. Cells were then harvested by centrifugation and resuspended in lysis buffer (50 mM Tris-HCl pH 8 containing 0.5 M NaCl, 20 mM imidazole and EDTA-free protease inhibitor cocktail). Lysozyme was added to a final concentration of 0.2 µg/mL and the culture was incubated for 20 minutes at room temperature. After a freeze-thaw cycle, leupetin (0.5 µg/mL) and pepstatin (0.7 µg/mL) were added and cell debris were removed by centrifugation (16000 x g for 30 minutes at 4°C). The lysate was loaded on a HiTrap™ TALON® crude column equilibrated with 50 mM Tris-HCl pH 8 containing 500 mM NaCl and 20 mM imidazole. A linear gradient (0-100% in 100 ml) was then applied with the same buffer containing 500 mM imidazole. OxDC-His and OxDC DSSN-His eluted approximately at 200 mM imidazole. Upon forced dialysis by Amicon ultra 10 devices (10000 kDa) and wash with storage buffer (50 mM Tris-HCl pH 8, 500 mM NaCl and 5 mM DTT), OxDC-His and OxDC-DSSN-His can be conserved at -80°C where they are stable for several months. The purification efficiency was evaluated by SDS-PAGE: 1 µg of OxDC or OxDC-DSSN were loaded per lane on 10% polyacrilimide gel along with the Precision plus protein Kaleidoscope™ (Bio-Rad) molecular mass markers. To remove the histidine tag, OxDC-His and OxDC-DSSN-His were incubated with 4U of thrombin per mg of protein in 50 mM Tris-HCl pH 8, 500 mM NaCl, 5 mM DTT buffer at 4°C for 16 hours with gentle mixing. The cleaved protein was then separated from thrombin excess by a Sephacryl S-300 column equilibrated and run in 50 mM Tris-HCl pH 8 containing 500 mM NaCl. Eluted proteins were concentrated to about 8 mg/ml using Amicon Ultra concentrators and stored at -80°C for at least 6 months.

Incorporation of Mg²⁺, Cd²⁺ and Co²⁺ in OxDC active site was carried out during the production of protein. The bivalent ions were added at 5 mM concentration in

the culture before the induction with IPTG. The proteins containing the new ions were purified exploit the His-tag tail as for wild-type enzyme. Through SDS-PAGE and WB analysis with anti-His antibodies we have monitored the incorporation of ions. The FDH assay (see chapter 3.7 in Materials and Methods) was carried out in order to evaluate the shift of optimum pH.

3.4 AGT expression and purification

AGT-Ma, AGT-Mi and mutant enzymes in their histidine-tagged form were expressed in *E. coli* and purified by the procedure already described (Cellini *et al.*, 2008). The apo form of each variant was prepared as previously described (Cellini *et al.*, 2007). AGT can be stored at 20 °C without loss of activity for more than 6 months. Protein concentration was determined by using the apparent molar absorption coefficient of 95400 M⁻¹ cm⁻¹ at 280 nm (Pace *et al.*, 1995). The PLP content was determined by releasing the coenzyme in 0.1 M NaOH and by using the apparent molar absorption coefficient of 6600 M⁻¹ cm⁻¹ at 388 nm.

3.5 OxDC and OxDC-DSSN decarboxylase activity assay

The oxalate decarboxylase activity was determined by a coupled spectrophotometric assay that determines formate production by using FDH, which catalyses the oxidation of formate to carbon dioxide, with the concomitant reduction of a molecule of NAD⁺ to NADH. Since NADH, differently from NAD⁺, absorbs the light at 340 nm, the conversion of formate to CO₂ causes the increase of the absorbance at 340 nm. The assay was carried out according to Magro *et al.* with minor modifications. The reaction was started by adding 1 µg of OxDC to a solution containing 63 mM potassium oxalate in 50 mM sodium acetate (NaAc). The reaction mixture was incubated at 25°C for 4 minutes and stopped by the addition of 10 µl of 1 N NaOH. For the coupled reaction the protocol of Magro *et al.*, (Magro *et al.*, 1988) was modified in order to optimize the assay for a 96-well plate reader. Briefly, 15 µl of the assay mixture were transferred in a 96-well plate and incubated over night with NAD⁺ (9 mM) and FDH (0.7 U) in 50 mM potassium

phosphate pH 7.8 to a final volume of 200 μl . The absorbance at 340 nm was measured after an incubation at 25 $^{\circ}\text{C}$, by using a micro plate reader (Tecan Infinity). A formate calibration curve (0-400 μM) and a blank were freshly performed for each experiment. The decarboxylase specific activity (U/mg) of was calculated by the equation:

$$AS = \frac{\left[\text{formate } (\mu\text{M}) * \left(\frac{200 \mu\text{l}}{15\mu\text{l}} \right) * (0.11\mu\text{l}) \right]}{\text{min} * \text{mg of enzyme}} \quad (2)$$

where one unit was defined as the amount of enzyme that produces 1 μmol of formate/min. The kinetic parameters of the decarboxylase reaction were determined by varying oxalate concentration from 0.1 mM to 250 mM. Data of initial velocity (v) as a function of substrate concentration were fitted to the Michaelis-Menten equation:

$$\frac{v}{Et} = \frac{k_{cat} [S]}{K_m + [S]} \quad (3)$$

where Et is the total enzyme concentration, S is substrate concentration, k_{cat} is the turnover number, and K_m is the Michaelis-Menten constant.

3.6 OxDC and OxDC-DSSN oxidase activity assay

Oxalate oxidase activity was determined spectrophotometrically using a continuous assay in which the production of hydrogen peroxide was coupled to the oxidation of ABTS by horseradish peroxidase (HRP) (Requena *et al.*, 1999). The oxidation of ABTS gives rise to a green and soluble end-product with an absorbance maximum at 420 nm ($\epsilon = 3.6 \times 10^4 \text{ M}^{-1} \text{ cm}^{-1}$). The reaction was started by adding 50 mM potassium oxalate to a mixture containing 5 μg of enzyme, 1 U of HRP, and 0.5 mM ABTS in 50 mM NaAc pH 4.2, to a final volume of 250 μl . The absorbance at 420 nm was continuously recorded by using a Jasco V-550 spectrophotometer with a temperature controlled cell-holder set at 25 $^{\circ}\text{C}$. Blank sample, containing all components except the enzyme, were taken immediately prior to the measurements of samples containing protein.

The oxidase specific activity (U/mg) was calculated by the equation:

$$AS = \frac{[\Delta Abs (min^{-1}) * 10^6 (M min^{-1}) * 0.00025 L]}{\epsilon_{ABTS} (M^{-1} cm^{-1}) * mg \text{ of enzyme}} \quad (4)$$

One unit of enzyme was defined as the amount consuming or producing 1 μ mol of substrate or product, respectively/min.

The kinetic parameters of the oxidase reaction were determined by measuring the oxidase activity at various oxalate concentrations from 10 mM to 200 mM. Data of initial velocity (v) as a function of substrate concentration were fitted to the Michaelis-Menten equation (3).

3.7 Measurement of oxalate decarboxylase and oxidase activity as a function of pH

For pH-dependence studies, decarboxylase and oxidase activity assays were carried out in the buffers reported in the Table 3 by using the previously reported procedures. In order to perform all the assays at physiological ionic strength (154 mM), we kept the NaCl concentration (140 mM) constant and we modulated buffer concentration according to its ionic strength contribution.

Table 3. Buffers used during pH-dependence experiments.

pH	Buffer composition
4.2	52 mM Sodium Acetate + 140 mM NaCl
5	21 mM Sodium Acetate + 140 mM NaCl
5.5	16.3 mM Sodium Acetate + 140 mM NaCl
5.5	15.5 mM Bis-Tris + 140 mM NaCl
6	18.5 mM Bis-Tris + 140 mM NaCl
6.5	26 mM Bis-Tris + 140 mM NaCl
7	58.3 mM Bis-Tris + 140 mM NaCl
7	15 mM Tris-HCl + 140 mM NaCl
7.2	16 mM Tris-HCl + 140 mM NaCl

3.8 Determination of the AGT transaminase activity

The catalytic activity for the overall transamination of the alanine/glyoxylate pair was determined by a coupled spectrophotometric assay, as previously described (Cellini *et al.*, 2007). The kinetic parameters of the P11L and I340M variants (0.1 μ M) were determined in the presence of saturating PLP concentrations by varying the substrate concentration at a fixed saturating co-substrate concentration. At different times, the reactions were stopped by adding TCA 10% (v/v). The residual activity of pathogenic and polymorphic variants as well as of AGT-Ma and AGT-Mi after aggregation was measured in presence of saturating PLP, substrate and co-substrate concentration at 0.1 μ M enzyme concentration, at 25°C in KP 0.1 M pH 7.4. After 10 minutes, the reactions were stopped by adding TCA 10% (v/v). The produced pyruvate was measured by a spectrophotometric assay using the coupled lactate dehydrogenase system (Cellini *et al.*, 2008).

3.9 Spectroscopic techniques

OxDC, OxDC-DSSN and AGT absorption measurements were made by a Jasco V-550 spectrophotometer at a scan speed of 50 nm/min and a bandwidth of 2 nm, by using 1 cm path length cuvettes.

Spectra of blanks, i.e. of samples containing all components except the enzyme, were taken immediately before the measurements of samples containing protein.

Intrinsic fluorescence emission spectra of OxDC and OxDC-DSSN were registered by a Jasco FP750 spectro-fluorometer equipped with a thermostatically controlled cell holder by using 1 cm path length quartz cuvettes. Protein spectra were registered from 300 to 550 nm (excitation at 280 nm) by using 5 nm bandwidths at a protein concentration of 0.5 mg/ml both at pH 7.2 and pH 4.2. Blank spectra were taken immediately prior to the measurements of samples containing protein.

Circular dichroism (CD) spectra were recorded on a Jasco J-710 spectropolarimeter equipped with a thermostatically controlled cell compartment at 25 °C at a OxDC and OxDC-DSSN concentration of 0.5 mg/ml or AGT concentration from was 1 to 15 µM. Routinely, three spectra were recorded at a scan speed of 50 nm/min⁻¹ with a bandwidth of 2 nm and averaged automatically, except where indicated. The cuvette path length was 1 cm.

All spectroscopic measurements were carried out both in 52 mM sodium acetate pH 4.2 containing 140 mM sodium chloride and in 16 mM Tris-HCl pH 7.2 containing 140 mM sodium chloride for OxDC and OxDC-DSSN whereas for AGT the buffer was 0.1 M KP pH 7.4.

Thermal stability studies on purified OxDC, OxDC-DSSN and AGT were performed by CD-monitored thermal unfolding. The CD signal at 222 nm of OxDC and OxDC-DSSN (0.5 mg/ml) at physiological ionic strength was registered at pH 4.2 and 7.2 at increasing temperature from 25 to 90 °C at a heating rate of 1.5 °C/min. For AGT the concentration was 10 µM in 0.1 M KP pH 7.4. The melting temperatures (T_m) was obtained by fitting the data to either a two- or a three-state unfolding model using the Origin Pro7 software according to the method of Pace (Pace *et al.*, 1989).

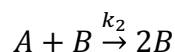
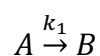
3.10 Aggregation studies

Dynamic Light Scattering (DLS) measurements were performed on a Zetasizer Nano S device (Malvern Instruments) equipped with a Peltier temperature controller by using disposable 12.5 × 45-mm cells with stopper. The aggregation kinetics of OxDC and OxDC-DSSN (0.5 mg/ml) were measured at 25 °C in buffers at physiological ionic strength at pH 4.2 or 7.2. Furthermore, the aggregation propensity of OxDC (0.1 mg/ml) in RBC loading buffer (10 mM NaHCO₃, 10 mM NaH₂PO₄, 20 mM glucose, pH 7.4, with additional 2 mM ATP, 1.5 mM GSH) was analyzed. The aggregation kinetics of AGT-Ma, AGT-Mi, P11L and I340M was determined at an enzyme concentration of 10 µM in KP at different pHs and ionic strengths, at 37°C. All the buffers were filtered immediately before measurement in order to eliminate any impurities.

The aggregation kinetics of OxDC and OxDC-DSSN (0.5 mg/ml) were also monitored by turbidimetry experiments measuring the change in the absorbance at 600 nm as a function of time at 25 °C. In the case of OxDOx, the process was monitored in the absence or presence of sodium glyoxylate (50 mM). All the aggregation studies were performed both in 16 mM Tris-HCl pH 7.2 and 140 mM sodium chloride and in 52 mM sodium acetate pH 4.2 and 140 mM NaCl buffers.

3.11 Aggregation kinetics: the minimalistic/“Ockham’s razor” Finke-Watzky two-step model

The minimalistic/ “Ockham’s razor” Finke–Watzky (F–W) two-step model was routinely used to analyze protein aggregation kinetic data. This model is characterized by nucleation and autocatalytic growth, yielding quantitative (average) rate constants for nucleation (k_1) and growth (k_2), respectively. It is described by the following scheme:



where A is the monomeric protein and B is the polymeric protein i.e. in oligomers that are past the nucleation stages. The F–W two-step model is an oversimplified, phenomenological kinetic model that consists of hundreds, if not thousands, of steps in most cases. The resultant k_1 and k_2 values are therefore averages of the true underlying steps. The classic F–W two-step mechanism assumes an initial zero concentration of aggregate, and so the rate equation becomes

$$-\frac{d[A]}{dt} = k_1[A] + k_2[A][B] \quad (5)$$

By mass balance,

$$[A]_0 = [A]_t + [B]_t \quad (6)$$

Combining these equations (5) and (6), integrating and solving for $[A]_t$ gives:

$$[A]_t = \frac{\frac{k_1}{k_2} + [A]_0}{1 + \frac{k_1}{k_2[A]_0} \exp(k_1 + k_2[A]_0)t} \quad (7)$$

where $[A]_0$ represents the initial monomeric concentrations and $[A]_t$ represents the loss of $[A]$ with time. Assuming that the initial $[B]_t$ is null, all data were fit using the integrated analytical equation (8) corresponding to the F-W two-step model:

$$[B]_t = [A]_0 - \frac{\frac{k_1}{k_2} + [A]_0}{1 + \frac{k_1}{k_2[A]_0} \exp(k_1 + k_2[A]_0)t} \quad (8)$$

where $[B]_t$ represents the concentration of aggregated protein at time t , $[A]_0$ represents the initial protein concentrations and k_1 and k_2 are the rate constants of nucleation and growth, respectively.

The pK_{spec} was calculated by the following equation:

$$Y = \frac{Y_H - Y_L}{1 + 10^{pK_{spec} - pH}} + Y_H \quad (9)$$

where Y_H and Y_L are the limit values of the rate constants k_1 and k_2 at high and low pH, respectively.

3.12 Size-exclusion chromatography

SEC analyses were performed on a Superdex 200 10/300 GL column at room temperature by an Akta FPLC system (GE Healthcare) using the Unicorn 5.01 (GE Healthcare) software. The injection volume was 100 μ L with detection at 280 nm, and the flow rate was 0.5 ml/min. The experiments were carried out at concentration of 0.5 mg/ml OxDC and OxDC-DSSN and ionic strength 154 mM in Tris-HCl pH 7.2.

3.13 Cross-linking

Cross-linking was performed with glutaraldehyde, a reagent used in a variety of applications. OxDC or OXDC-DSSN (monomer concentration 9 μM) were cross-linked in 52 mM sodium acetate pH 4.2 and 140 mM NaCl buffer with 1% glutaraldehyde and quenched by 1 M Tris-HCl pH 8 after 2 min. 7 μg of sample were analysed by SDS-PAGE (7.5%).

3.14 Cell culture

The PH1 cellular model used for the experiments reported in this thesis is made up of chinese hamster ovary (CHO) cells. In particular, we used two subtypes of this cell line: 1) CHO-GO cells, which stably expresses glycolate oxidase (GO) due to the transfection with the pCDNA3.1(-)Zeo-GO vector, and 2) CHO-GO-AGT cells, which stably express GO and wild type AGT thanks to the presence of the pCDNA3.1(+)-Neo-AGT vector. Both cell clones were provided by Prof. C.J. Danpure of the University College London.

The medium used for the growth of CHO-GO cells was the Ham's F12 Glutamax medium, supplemented with fetal bovine serum (10%, v/v), penicillin (100 units/ml) and streptomycin (100 $\mu\text{g}/\text{ml}$). 400 $\mu\text{g}/\text{ml}$ zeocin was used as selective agent for CHO-GO cells. 400 $\mu\text{g}/\text{ml}$ zeocin and 1 mg/ml geneticin were used as selective agents for CHO-GO-AGT cells. Cells were cultured at 37°C under O₂/CO₂ (19:1) atmosphere. Cell passaging was performed by treating with trypsin (0.01%) for 5 minutes at 37 °C. Cell counting was carried out by the Countesse™ apparatus.

3.15 Xfect protein transfection

The Xfect Protein Transfection Kit uses a cell-penetrating peptide, developed by Clontech, able to bind and transport active proteins directly into a wide variety of mammalian cell types.

For protein transfection experiments, CHO-GO cells were seeded in two 6 cm dishes at 0.3×10^6 cells/dish and grown until they reached 80% confluence.

Transfection was then performed by following manufacturer instructions. Briefly, 15 μl of the 1X Xfect Protein Transfection Reagent Stock were diluted in 85 μl of deionized H_2O ; in a second tube, 5 μg of OxDC-His or OxDC-DSSN-His were mixed with the Xfect Protein buffer in a total volume of 100 μl . Then the content of the second tube was added to the first one, gently vortexed and incubated at room temperature for 30 minutes. During the incubation step, the medium in the dish was aspirated and cells were washed once with PBS. Upon PBS removal, 1 ml of modified Ham's F12 Glutamax medium and 200 μl of the transfection reagent/protein mixture were added. Cells were then incubated at 37°C and 5% CO_2 for different times (1 hour, 6 hours and 24 hours). After incubation cell were harvested and assayed for the presence of the protein or used for subsequent experiments.

3.16 Western Blot

20 μg of cell lysate or 0.1 μg of purified proteins were loaded per lane on a 10% or 7.5% polyacrylamide gel along with the Precision plus protein Kaleidoscope™ (Bio-Rad) molecular mass markers. The gel was run for 60 minutes at 150 V and 25 mA. Proteins were then transferred from the gel to a nitrocellulose membrane using the iBlot device (Invitrogen) and blocked by incubation with 5% BSA (w/v) at 37° C for one hour. For OxDC-His and OxDC-DSSN-His detection, the membrane was incubated with an anti-His (C-Term)-HRP conjugate antibody (Invitrogen, dilution 1:5000) for 1hour at RT and the excess of antibody was then eliminated by washing the membrane for three times in TBST (50 mM Tris-HCl pH 7.5, 150 mM NaCl, 0.1% Tween 20) for 10 minutes. Band detection was performed by using the enhanced chemiluminescence (ECL) substrate reagent containing luminol and a peroxide solution. The horseradish peroxidase (HRP), conjugated with the primary antibody, in the presence of peroxide produces a radical of its substrate, the luminol. This makes a further reactions leading to the formation of a dianion in an excited electronically state that emits light when returns to the ground state. The light emission signal was acquired by the system Chemidoc (Biorad).

3.17 Viability assay

In order to assess the capacity of OxDC and OxDC-DSSN to detoxify oxalate in a cellular model of PH1, cells were seeded into a 96-well plate at 8.000 cells/well density. After 6 hours, OxDC or OxDC-DSSN transfection was performed as previously described and cells were incubated over night at 37°C and 5% CO₂. The subsequent day, glyoxylate production was induced by adding Hepes buffered glycolate pH 7.0 to a final concentration of 0.8 mM. Un-transfected CHO-GO and CHO-GO-AGT were used as negative and positive control, respectively. Cell viability was evaluated after further 24 hours incubation using a crystal violet assay. Briefly, cells were rinsed with PBS and incubated at room temperature for 5 min with a fixing and staining solution containing 4% formaldehyde and 0.5% Crystal Violet. Cells were then extensively washed with distilled water to remove the excess of dye and lysed with 1% SDS in PBS to allow crystal violet solubilization. The absorbance at 595 nm, which is proportional to the number of viable cells, was measured with a TECAN plate reader. Six replicates were performed for each assay condition.

3.18 RBC loading

Human blood was obtained from the Blood Transfusion Center of the Hospital “S. Maria della Misericordia”, Urbino (PU) Italy or “Policlinico G.B. Rossi”, Verona, Italy; blood was provided by healthy adult volunteers who signed an informed consent form before donation and samples were collected anonymously in heparinized tubes.

The use of human blood in the present study was approved by the research ethics committee of the University of Urbino (PU), Italy. OxDC was loaded into human RBCs by means of hypotonic dialysis, isotonic resealing and “reannealing”, essentially according to Magnani *et al.*, 1988 with these modifications: RBCs were pre-dialyzed in human RBCs buffer containing 10 mM NaHCO₃, 10 mM NaH₂PO₄, 20 mM glucose, pH 7.4, 2 mM ATP without GSH. After that RBCs were loaded with 36.4 IU of OxDC with RBCs at 70% hematocrit (Ht). 1 ml final volume was

dialyzed at + 4 °C in a cellulose tube (14 kDa cut-off) vs 50 ml of hypotonic solution (using the same buffer used for pre-dialysis) 60 mOsm measured by Osmometer Fiske Associates Model 210, Norwood, MA, USA. After dialysis the cells were approx. 90 mOsm. The GSH at 1.5 mM concentration was added during the resealing passage of loading. Unloaded (UL) RBCs (*i.e.* cells submitted to the same procedure without the addition of the enzyme) were used as controls. The amount of entrapped OxDC was quantified essentially by a kinetic assay as previously described (Magro *et al.*, 1988). Hematological parameters were measured by an automatic Coulter AcT 5 Diff Hematology Analyzer (Beckmann, Miami, FL). Percent RBC recovery was calculated from the number of RBCs submitted to the dialysis step and those recovered at the end of the loading procedure.

3.19 Combinatorial Incorporation of Synthetic Oligonucleotides During Gene Shuffling (ISOR)

The ISOR procedure was carried out based on the protocol developed by Rockah-Shmuel *et al.* 2014. The main steps are the following:

A) DNA preparation:

- (i) Amplification of OxDC gene using external primers in order to obtain about 25 μ g of starting DNA.
- (ii) Treatment of the DNA with 20 units of DpnI per 50 μ l of PCR for 1 h at 37°C in order to remove the residual template plasmid DNA.
- (iii) Purification and concentration of the DNA to a final concentration \geq 200 ng/ μ l.

B) Gene fragmentation

- (i) Preparation of a reaction solution mixing 20-25 μ g DNA with 100 mM Tris-HCl pH 7.5 and 10 mM MnCl₂ to generate a 200 μ l solution
- (ii) Preparation of the stop solution in a 200 μ l final volume containing 25 μ l of 500 mM EDTA pH 8.2 equilibrated to 85°C in a heating block.
- (iii) Addition of DNase I to a final concentration of 0.015 u/ μ g of DNA and incubation of all samples at 37°C

- (iv) Stop of the reaction by removal of 50 μ l aliquots every 0.5 min and mix with an aliquot of the EDTA stop solution kept at 85 °C. Incubation of each aliquot at 85°C for 15 min.
- (v) Loading of the samples on a 2% (w/v) agarose-TAE gel with a DNA ladder comprised of 50 or 100 bp bands. Each time point sample is run in a different well to see the DNA fragments which change in size range as a function of the DNase I digestion time. Excision of the part of gel which contains the fragments comprised from 50 to 250 bp and DNA extraction.
- (vi) Gel extraction and purification of the desired fragments using the GeneElute Plasmid miniprepr Kit (Sigma)

C) Incorporation of Oligonucleotides by assembly PCR

- (i) Reassembly of the gene by PCR. 100 ng of the purified fragments were mixed in the presence of 1-10 nM of library nucleotides, dNTP mix and high-fidelity polimerase in 50 μ l final volume. The program used for PCR analysis was: one denaturation step at 95°C for 2 min; 40 cycles composed by a denaturation step at 94°C (30 s); 13 hybridization steps separated by 2°C each, from 65°C to 41°C for 1.5 min each; an elongation step of 1 min/kb gene at 72°C and then a final 7 min elongation step at 72°C to allow full elongation of all assembled genes.
- (ii) Amplification of the assembly product by “nested” PCR using the external primer 5’ TCCCCATCGGTGATGTCGGCAT 3’ and its complement in 50 μ l final volume. Purification of the product of nested PCR.
- (iii) Treatment of the purified DNA using EcoRI and NdeI and ligation to pET21a to create the plasmid library. Transformation in DH5a E.coli cells.

3.20 Screening of libraries

To screen the library of the OxDC each single colony was picked up and added in a well of a sterile, clear, flat-bottomed lidded microtiter plate that contained 200 μ l

of LB medium supplemented with kanamidine. The 96-well plates were incubated at 37 °C overnight at 200 rpm agitation. 100 µl of each well were transferred in a new well with fresh 1 ml of LB and induced and lysed as described for the wild type enzyme (see chapter 3.3 of Materials and Methods). To normalize the data of specific activity, protein concentration was determined by Bradford assay. Specific activity was determined at either pH 5.5 and 6.5 by FDH assay reported in chapter 3.8 of this section and compared with the wild-type clone.

Each clone resulted positive was screened in triplicate in order to confirm the increase of activity respect to wild-type.

3.21 Molecular modelling and hydrophobic patches analysis

Molecular modelling analyses were performed by the software *Molecular Operating Environment (MOE 2015.1001 and MOE 2016.08)* developed by the Chemical Computing Group, starting from the available crystal structure of human AGT in complex with the tetratricopeptide repeat domain of human Pex5p (PDB: 3R9A) (Fodor *et al.*, 2001). We performed *in silico* mutagenesis on both AGT monomers by using the *Protein builder and rotamer explorer* tool of *MOE 2016.08*, which explores the conformational space of amino acid side chains within a protein in the presence of surrounding amino acids, ligands and solvent. The potential side chain conformations were visually inspected and calculated as the sum of the side chain strain energy, the van der Waals interaction energy with the environment, and the hydrogen bond interaction energy. The rotamer with the lowest values of energy were selected and analyzed. Upon modification of residues by the tool *Protein builder*, we performed an energetic minimization of the microenvironment around the mutation site. The side chain atoms of the mutated residue and of neighboring residues (within a distance of 6 Å) were minimized. All other atoms and all backbone atoms were kept fixed.

The analysis of the hydrophobic patches was performed by using the *Patch analyzer* tool of *MOE 2015.1001* by setting the size and energy cut-offs of the hydrophobic patches at 100 Å² and 0.25 kcal/mol, respectively. Salt-bridge interactions and hydrophobic interactions between residues were scored as positive if they fell

within 5 Å of each other in the structure. Hydrogen bonds were scored as present if the distance between the electronegative atoms (N & O) within O-H-N or O-H-O groups were ≈ 2.9 Å apart.

3.22 Calculation of electrostatic potential maps and predicted pK_a

The electrostatic potential maps of AGT-Ma and mutants were calculated by the Adaptive Poisson-Boltzmann Solver 1.3 tool (Baker *et al.*, 2001), using the non-linear Poisson-Boltzmann equation and modulating the ionic strength (setting ions charge, molar concentration and radius in Å of potassium phosphate buffer, to mimic the experimental conditions) and temperature. The graphic interface of the tool is integrated in UCSF Chimera version 1.1 (Pettersen *et al.*, 2004). The calculations were performed on the Opal web server (Ren *et al.*, 2010). Structure preparation and analysis of the protonation state of residues at different pH values were carried out by the PDB2PQR (Dolinsky *et al.*, 2004) (using CHARMM as forcefield) and PROPKA 3.0 (Olsson *et al.*, 2010) tools respectively, on the Opal web service. 2Dmaps were calculated by the tool Patch Analyzer of MOE 2016.08. For 2D views, structure preparation and protonation were performed directly by MOE 2016.08. Calculation of the predicted pK_a of AGT residues was obtained by the tool Residue pK_a of MOE 2016.08.

3.23 Determination of the consensus sequence

The *Bacillus subtilis* OxDC sequence was retrieved from GeneScript. We performed both a multiple sequence alignment (MSA) and a structure based sequence alignment (STRAP). The MSA was obtained by aligning the OxDC sequence with 200 homologous sequences with a % of identity between 35 and 95 (using the protein database Uniref90) using the MUSCLE and T-COFFEE programs and analyzed with the ConSurf Server (<http://consurf.tau.ac.il/2016/>). The STRAP alignment was obtained using EXPRESSO and PROMALS 3D softwares based on the MSA obtained previously to generate the conservation score

from structural information. The two outputs were combined using the Jalview program.

4

**BIOCHEMICAL
CHARACTERIZATION OF
OxDC AND OxDC-DSSN AT
NEUTRAL pH**

Background Information

The administration of oxalate-degrading enzymes is considered one of the new avenues in the therapeutic approaches directed to the treatment of hyperoxaluria. The rationale behind this strategy is to metabolize the excess of oxalate accumulating at intestinal and/or plasma level, so that to reduce the amount excreted by urine. Among oxalate-degrading enzymes, the best characterized is oxalate decarboxylase (OxDC) from *B. subtilis*. OxDC catalyses the conversion of oxalate into formate and carbon dioxide (Begley *et al.*, 2004; Svedružić *et al.*, 2005). As for other oxalate degrading-enzymes the optimum of catalytic activity is shown at acidic pH (Tanner *et al.*, 2000). The initial use of OxDC was focused on industrial and biotechnology applications, i.e. to prevent the formation of oxalate salt deposits in industrial processes such as papermaking (Sjöde *et al.*, 2008; Cassland *et al.*, 2010) and beer production (Hiatt *et al.*, 1987). Very recently, the potential of OxDC as medical application has been advanced. In fact, at diagnostic level, OxDC is used for the determination of oxalic acid concentration in food and complex biological samples such as blood and urine (Parkinson *et al.*, 1985; Allen *et al.*, 1989; Langman *et al.*, 1998). Finally, the enzyme has been proposed as a possible biological drug in the treatment of hyperoxaluria. The use of OxDC in hyperoxaluric patients is currently focused on its oral administration and the ability to degrade oxalate in the intestine, and thus is suitable for secondary hyperoxalurias (Grujic *et al.*, 2009). However, its use in primary hyperoxalurias has been also proposed, based on the possibility that consuming exogenous oxalate could promote the intestinal excretion of the endogenous pool (Hatch *et al.*, 2006).

Although the medical applications of OxDC exploit its ability to degrade oxalate under physiological conditions (Grujic *et al.*, 2009; Cowley *et al.*, 2010; Langman *et al.*, 2016), a deep characterization of OxDC at neutral pH is lacking. Moreover, it has been reported that a mutant form of OxDC, called OxDC-DSSN and characterized by the four mutations S161D-E162S-N163S-S164N, is endowed with an oxalate oxidase activity while the decarboxylase activity is completely abolished. If OxDC-DSSN displays any activity at neutral pH is unknown.

To fill these gaps, in the first part of my PhD, we performed a deep characterization of OxDC wild-type and OxDC DSSN at neutral pH in order to verify if the two proteins maintain their stability and functionality.

RESULTS AND DISCUSSION

4.1 Kinetic and structural properties of OxDC and OxDC-DSSN

Using a two-step purification process (see Materials and Methods) we obtained untagged OxDC and OxDC-DSSN with a yield of 20 mg of pure protein per litre of bacterial culture (Figure 9).

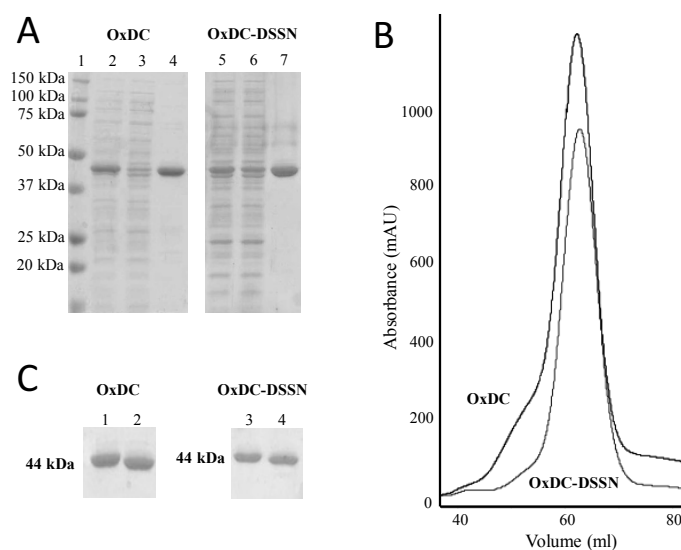


Figure 9. Purification of OxDC and OxDC-DSSN. (A) SDS-PAGE analysis of the various steps of OxDC-His and OxDC-DSSN-His purification. Lanes are coded as follows: 1 molecular weight markers; 2 and 5 soluble fraction of the cell lysate; 3 and 6 flow-through; 4 and 7 eluted OxDC-His and OxDC-DSSN-His, respectively. (B) Chromatographic profile of cleaved OxDC and OxDC-DSSN on a Sephacryl S-200 column. The buffer was 50 mM Tris- HCl pH 8 containing 500 mM NaCl. (C) SDS-PAGE analysis of OxDC-His (lane1), OxDC (lane 2), OxDC-DSSN-His (lane 3) and OxDC-DSSN (lane 4).

At pH 4.2 in the presence of *o*-phenylenediamine (*o*-PDA), purified OxDC displayed an oxalate decarboxylase specific activity of 83 U/mg in line with previous reports (Tanner *et al.*, 2001), thus suggesting that our purification strategy did not alter protein functionality and/or Mn²⁺ binding. Although *o*-PDA is a known OxDC activator (Emiliani *et al.*, 1964), it is highly toxic and not suitable for biomedical applications (*o*-PDA CAS No. 95-54-5). Thus, we also determined OxDC activity at pH 4.2 in the absence of *o*-PDA in the assay mixture and we found that it displayed a significantly lower decarboxylase specific activity (28 U/mg) and

a K_m for oxalate of 8 mM. As expected, the mutation of lid residues Ser161Asp, Glu162Ser, Asn163Ser, Ser164Asn in OxDC-DSSN completely abolished the decarboxylase activity, but gave rise to an enzyme displaying a detectable oxalate oxidase activity, in the same range of that already reported (Table 3) (Burrel *et al.*, 2007).

We measured the decarboxylase and oxidase activity of OxDC and OxDC-DSSN, respectively, in the pH range 4.2-7.2. The upper limit of the analysis was chosen taking into account the functional test of the two enzymes in a cellular model of PH1 (see below) because it represents the pH value of the cell cytosol (Martinez-Zaguilan *et al.*, 1991). Appropriate controls were performed to validate each assay in the whole pH range, as well as to evaluate possible buffer effects. The buffer used are reported in detail in the Material and Methods section. We found that the activity of both enzymes significantly decreases at increasing pH (Figure 10A and 10B), in line with previous reports (Reinhardt *et al.*, 2003; Twahir *et al.*, 2016). However, at pH 7.2 the two proteins retain 7% and 15% activity, respectively. It should be observed that the OxDC activity values do not significantly change in the range of pH 6-7.2. Considering that (i) assay calibration curves obtained at various pH values allow to exclude any influence of the coupled assay, and that (ii) in the pH range 6-7.2 the coefficient of variation inter-assay is below 15%, we cannot exclude that the observed differences could have a biological meaning possibly related to the biochemical mechanism of action of OxDC in the neutral range. Unfortunately, we could not increase the signal by increasing protein concentration or incubation time, because of the strong tendency of the protein to aggregation (see below).

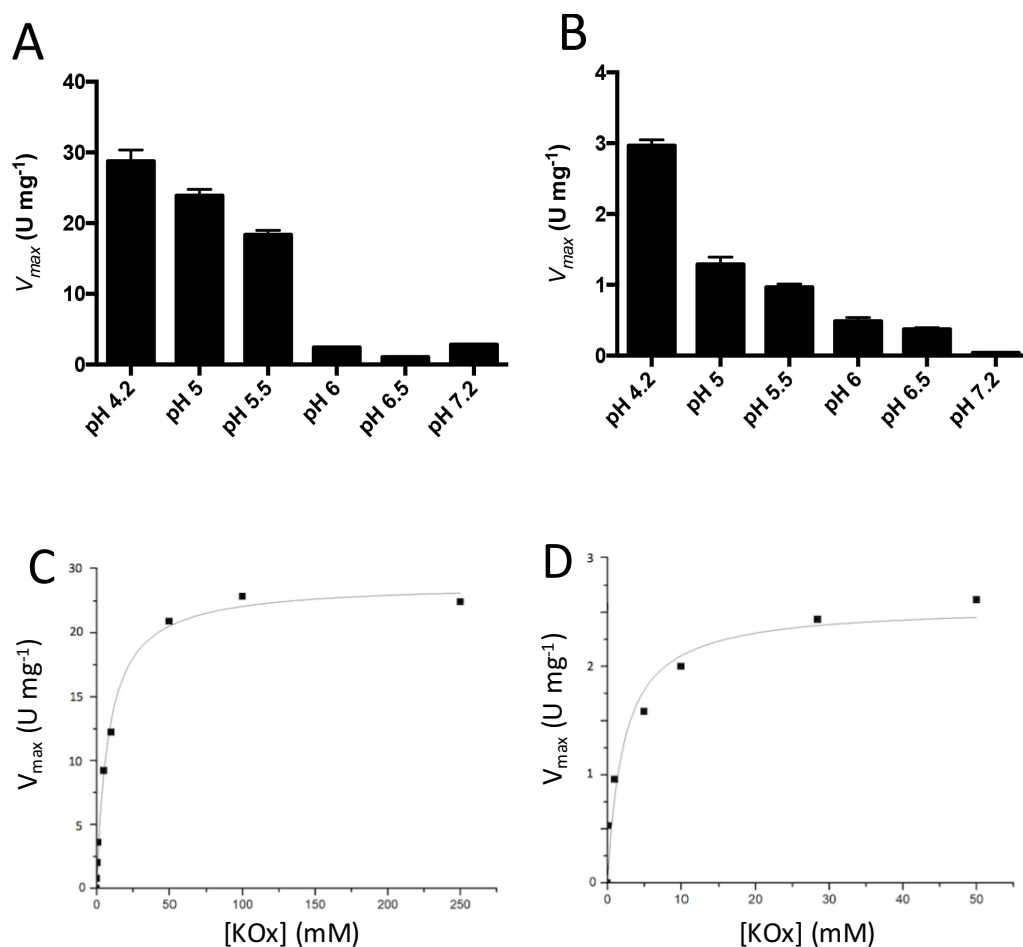


Figure 10. Effect of pH on OxDC and OxDC-DSSN activity. A and B: histograms representing specific activity values of OxDC decarboxylase activity (**A**) and OxDC-DSSN oxidase activity (**B**) at different pHs. Protein concentration was 10 μ g/ml. Data are representative of two independent experiments. Bar graphs represent the mean \pm SEM. The buffers used and the technical details are reported in Materials and Methods. **C and D:** Michaelis-Menten curves of the kinetic parameters of OxDC at pH 4.2 (**C**) and 7.2 (**D**). Enzyme activity was measured as described in Materials and Methods. The amount of enzyme used in each assay mixture was 1 μ g and 5 μ g for experiments carried out at pH 4.2 and 7.2, respectively. Each point represents the average of five replicates. One unit of OxDC is defined as 1 nmol of fomite formed per hour at 25°C.

Nevertheless, we determined the kinetic parameters for the decarboxylation or oxidation reaction at pH 7.2. As shown in Figure 10 C and 10D and Table 4, OxDC shows a 13-fold reduction in the V_{max} of the decarboxylation reaction, without significant alterations of the K_m value for oxalate as compared to pH 4.2. On the other hand, OxDC-DSSN shows a 7-fold reduced V_{max} for the oxidation reaction and a remarkably increased K_m for oxalate as compared to pH 4.2.

Table 4. Kinetic parameters for the oxalate decarboxylase and oxidase activity of OxDC and OxDC-DSSN, respectively, at pH 4.2 and 7.2.

	Decarboxylase activity				Oxidase activity		
	V_{max} (U mg ⁻¹)	K_m (mM)	k_{cat} (s ⁻¹)		V_{max} (U mg ⁻¹)	K_m (mM)	k_{cat} (s ⁻¹)
OxDC pH 4.2	28.0 ± 2.0	8.0 ± 0.8	20.0 ± 1.8	OxDC- DSSN pH 4.2	2.0 ± 0.1	0.30 ± 0.07	1.4 ± 0.2
OxDC pH 7.2	2.0 ± 0.4	2.0 ± 1.0	1.45 ± 0.15	OxDC- DSSN pH 7.2	0.35 ± 0.04	70.0 ± 20.0	0.85 ± 0.07

These findings are in contrast with previous results (Reinhardt *et al.*, 2003; Twahir *et al.*, 2016; Tanner *et al.*, 2000; Svedružić *et al.*, 2007) which reported that OxDC activity is undetectable at neutral pH due to the fact that only monoprotonated oxalate is a productive substrate. However, an in-depth analysis of the OxDC kinetic properties at neutral pH has never been performed. Moreover, a recent report suggests that the pH-dependence of catalytic activity could be also governed by small changes in the active site of the protein that could stabilize the +3 oxidation state of the Mn ion (Twahir *et al.*, 2016). In addition, Moomaw *et al.* reported that the change in oxalate oxidase activity as a function of pH is influenced by the protonation state of an active site Asp residue at position 241. All these considerations could possibly explain why the measured activity of OxDC and OxDC-DSSN at pH 7.2 does not correspond to that expected based on the amount of monoprotonated oxalate present in solution. In this regard, recent experimental evidences indicate that (i) OxDC activity is detectable in *E. coli* cells grown at pH 7 (Lee *et al.*, 2014) and (ii) an oral formulation of recombinant OxDC in its crystalline form shows 2% residual activity under physiological conditions and is able to metabolize intestinal oxalate in a mouse model of hyperoxaluria (Grujic *et al.*, 2009), and (iii) OxDC is able to degrade the oxalate contained in spinach leaves under conditions mimicking the intestinal environment (Mufarrij *et al.*, 2013). Finally, Albert *et al.*, demonstrated that HEK293 cells transfected with a construct encoding OxDC (HEK293-OxDC) exhibit a higher viability as compared to untransfected HEK293 cells when exposed to oxalate stress. Moreover, HEK293-

OxDC, but not HEK293 cells, are able to metabolize oxalate added to the medium, thus suggesting that OxDC is biologically active in the cytoplasm (Albert *et al.*, 2017). These results provide indirect evidence for the presence of residual enzymatic activity at neutral pH.

To investigate if any structural change could occur in OxDC and OxDC-DSSN at physiological pH, we compared their spectroscopic properties at acidic and neutral pH maintaining a physiological ionic strength. At pH 4.2, the two proteins exhibited almost identical far-UV (data not shown) and near-UV CD spectra (Figure 11A). No significant alterations were noticed at pH 7.2. Upon excitation at 280 nm (Figure 11B), both OxDC and OxDC-DSSN exhibited an intrinsic fluorescence emission spectrum with maximum at 329 nm, indicating a folded structure. However, the emission intensity of OxDC-DSSN was about 1.5-fold lower than that of OxDC, probably as a consequence of the fact that the mutation of lid residues could affect the orientation of some buried aromatic residues.

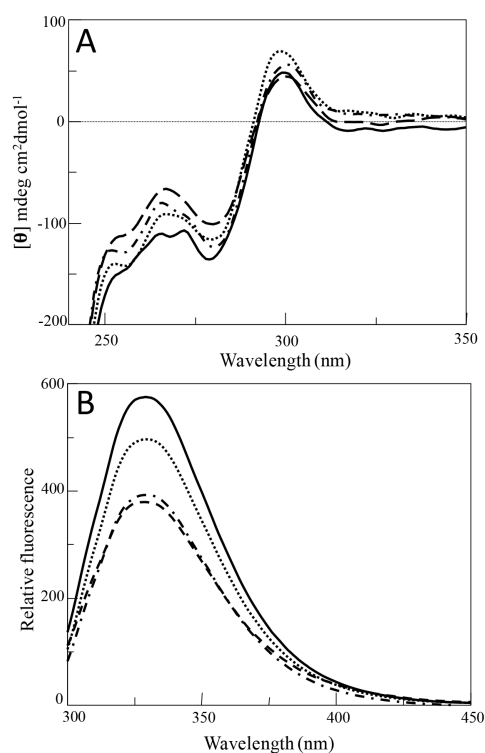


Figure 11. Spectroscopic features of OxDC and OxDC-DSSN (A) Near-UV CD spectra and **(B)** intrinsic fluorescence emission spectra (λ_{exc} 280 nm) of OxDC at pH 4.2 (—) or pH 7.2 (• •) and of OxDC-DSSN at pH 4.2 (---) or pH 7.2 (– • –). Spectra were registered at 0.5 mg/ml enzyme concentration in 52 mM sodium acetate pH 4.2, 140 mM NaCl or 16 mM Tris-HCl pH 7.2, 140 mM NaCl.

DLS analyses revealed that at both acidic and neutral pH OxDC and OxDC-DSSN display a peak with a diameter of 12 ± 1 nm, corresponding to an hexamer, and a second peak at approximately 200 nm, corresponding to aggregates (Figure 12A). Considering that the scattering intensity is proportional to the sixth power of a particle diameter (Plakoutsi *et al.*, 2004) the hexamer represents by far the most abundant species in solution, thus suggesting that neither the mutation of residues of the lid, nor the change of the pH, affects the quaternary structure of the enzyme. We confirmed these data by SEC experiments, which were only performed at pH 7.2 due to the technical limitations of the Superdex 200 10/300 GL column. In line with previous data, OxDC eluted from the column with a main peak at 10.8 ml, corresponding to the elution volume of a hexamer, along with a shoulder at 9.3 ml, corresponding to an aggregated form (Svedružić *et al.*, 2007). We found a similar elution profile for OxDC-DSSN, although the area of the hexamer is 1.5-fold lower with respect to that of OxDC (Figure 12B). Since no other peaks were present in the elution profile of OxDC-DSSN, and considering that the two proteins have a similar molar extinction coefficient at 280 nm, the reduced peak area is probably a consequence of the formation of high-molecular weight aggregates that do not enter the column bed (see below), as previously reported for other proteins (Cellini *et al.*, 2006; Bertoldi *et al.*, 2005). Since the technical features of the SEC column did not allow to carry out runs at pH 4.2, we could only perform cross-linking experiments that confirmed the presence of the hexamer for both proteins, along with tetrameric, dimeric and monomeric species deriving from the limited efficiency of the cross-linking reactions (data not shown).

Overall, spectroscopic data indicate that OxDC and OxDC-DSSN do not undergo gross changes of their secondary, tertiary and quaternary structure at neutral pH with respect to acidic pH. Although this is not surprising considering that the available crystal structures have been solved at neutral or alkaline pH (Anand *et al.*, 2002; Just *et al.*, 2004), the results confirm that the reduced catalytic activity observed at increasing pH does not depend on a significant conformational change of the protein. Rather, it is merely a catalytic problem related to the protonation

state of the substrate and/or of active site groups as discussed above (Svedružić *et al.*, 2005; Reinhardt *et al.*, 2003; Moomaw *et al.*, 2013).

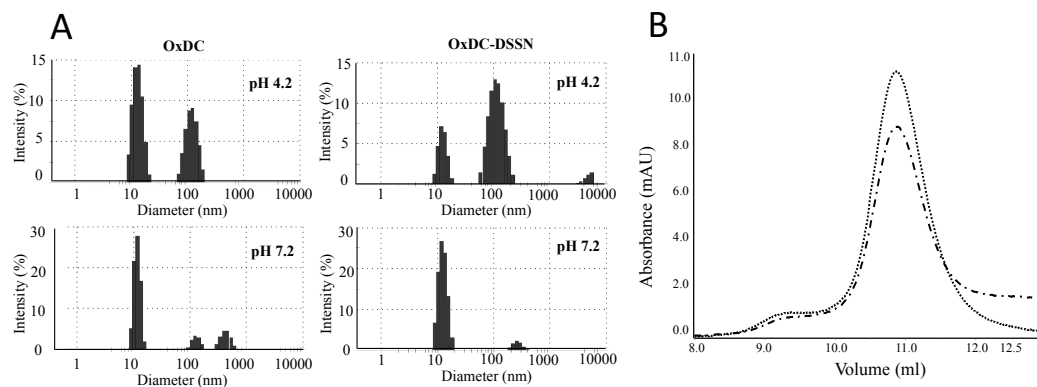


Figure 12. Analysis of the OxDC and OxDC-DSSN quaternary structure. (A) DLS analysis of the size distribution of 0.5 mg/ml OxDC and OxDC-DSSN at pH 4.2 (52 mM sodium acetate pH 4.2, 140 mM NaCl) and pH 7.2 (16 mM Tris-HCl pH 7.2, 140 mM NaCl). **(B)** Elution profile of OxDC (...) and OxDC-DSSN (-.-) at 0.5 mg/ml concentration loaded on a Superdex 200 10/300 GL column (GE Healthcare) equilibrated and run in 16 mM Tris-HCl pH 7.2 containing 140 mM NaCl. Detection was set at 280 nm.

4.2 Stability and aggregation propensity of OxDC and OxDC-DSSN at pH 4.2 and 7.2

Considering the possible use of OxDC and/or OxDC-DSSN as biological drugs, we compared their thermal stability at pH 4.2 and 7.2 and physiological ionic strength by monitoring the decrease of dichroic signal at 222 nm indicative of the secondary structure content. At pH 4.2 OxDC maintains its secondary structure up to 60°C and shows a transition with mid-point at 69°C to a conformation characterized by a higher signal, followed by a second transition with mid-point at 85 °C leading to the almost complete loss of secondary structure content (Figure 13A). This behaviour, which is frequently observed during acid protein unfolding (Uversky *et al.*, 2001) suggests a two-step process consisting in the first formation of a partly-folded intermediate characterized by a pre-molten globule like structure and its subsequent conversion to the fully-unfolded state. On the other hand, OxDC-DSSN undergoes a progressive loss of secondary structure from 36°C to 64°C, with a mid-point around 47°C, followed by an apparent recovery of secondary structure with

mid-point at 85°C and by the subsequent almost complete loss of the dichroic signal (Figure 13A). At pH 7.2, both OxDC and OxDC-DSSN show a classical two-state unfolding process with mid-point transitions at 38°C and 36°C, respectively.

Thus, although OxDC and OxDC-DSSN do not seem to undergo major structural changes at neutral pH, they are less resistant to thermal stress with respect to acidic pH. This finding is not easy to explain at structural level, but it can be speculated that the protonation state of key protein residues, whose identity is presently unknown, could be crucial for the maintenance of the native structure although it does not affect the overall conformation of the protein. In addition, it is worth nothing that OxDC-DSSN displays a lower resistance with respect to OxDC, thus suggesting that one or more of the mutations altering the reaction specificity could also induce some local conformational change that could promote unfolding.

Similar conclusions were also drawn by looking to the aggregation propensity of OxDC and OxDC-DSSN at pH 4.2 and 7.2, physiological ionic strength. Turbidimetry experiments (Figure 13B) did not reveal aggregation of both enzymes up to 60 min at pH 4.2, as well as for OxDC at pH 7.2. Accordingly, we did not notice the formation of significant amounts of aggregates in DLS analyses, as shown by the presence of the signal corresponding to the dimer throughout the analysis. On the other hand, for OxDC-DSSN at pH 7.2 we detected a time-dependent increase in the absorbance at 600 nm, indicative of an ongoing aggregation process. By fitting the signal changes at 600 nm vs time we estimated a $t_{1/2}$ of aggregation equal to 28.4 ± 0.3 min. Under the same experimental conditions, a rapid increase in DLS count rate occurred after a 6 min lag phase, followed by a decrease of the signal probably due to the precipitation of insoluble high molecular weight aggregates (Figure 13D). Accordingly, the signal of the OxDC-DSSN hexamer disappeared after 9 min and high molecular weight aggregates (200-1200 nm) appeared (Figure 13C). Finally, the increase of the count rate in DLS is paralleled by a progressive decrease of the CD signal at 222 nm, thus suggesting that aggregation is associated with an unfolding process (Figure 13E).

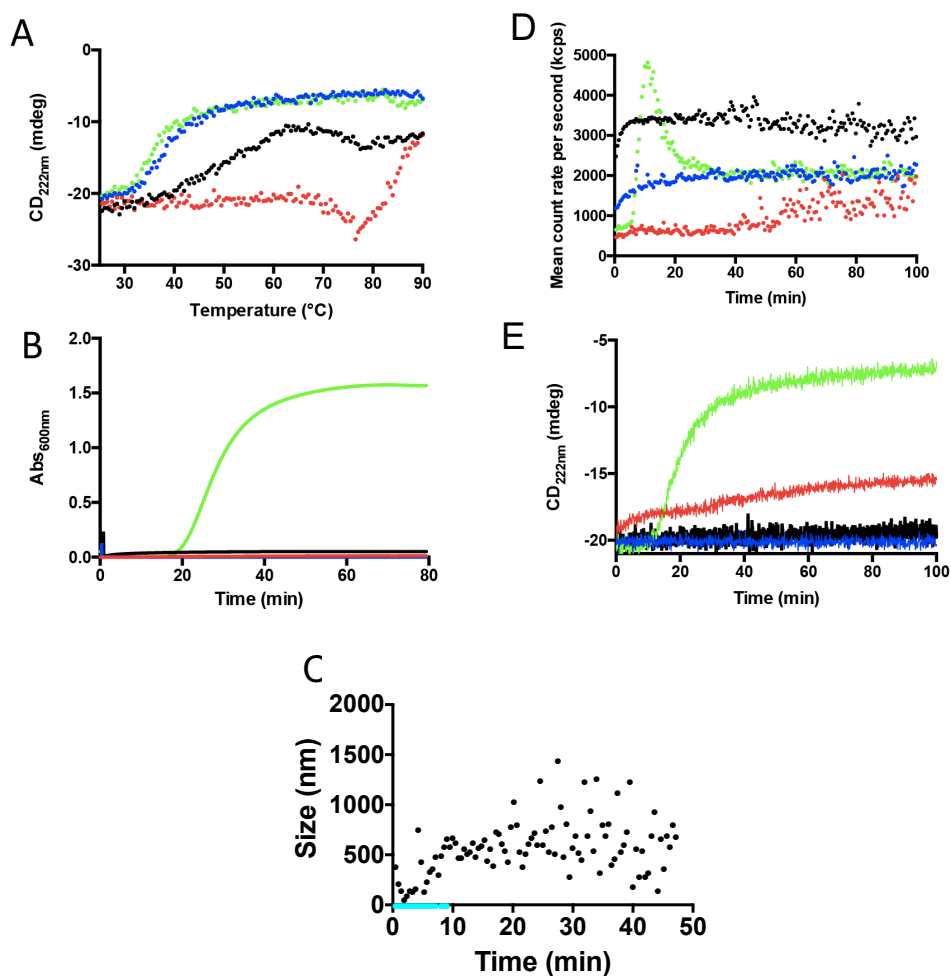


Figure 13. Thermal stability and aggregation propensity of OxDC and OxDC-DSSN at pH 4.2 and 7.2. (A) Change in the CD signal at 222 nm at increasing temperature from 25° to 90°C (heating rate 1.5°C/min). (B) Absorbance changes at 600 nm as a function of time, (C) time-dependent change of species (measured as nm) of OxDC-DSSN at pH 7.2, the hexamer and aggregates are represented by cyan and black dots, respectively (D) change in the total count rate (measured as kilo counts per second) and (E) CD signal at 222 nm as a function of time. All measurements were performed at 0.5 mg/ml enzyme concentration, in 16 mM Tris-HCl pH 7.2, 140 mM NaCl or 52 mM sodium acetate pH 4.2, 140 mM NaCl, at 25°C. The colour code is the following: red, OxDC pH 4.2; blue, OxDC pH 7.2; black, OxDC-DSSN pH 4.2; green, OxDC-DSSN pH 7.2.

Overall these results agree with thermal stability studies and confirm an enhanced propensity of OxDC-DSSN to unfold and aggregate at neutral pH with respect to OxDC. Crystallographic analyses did not reveal major structural differences between the two proteins (Burrell *et al.*, 2007). However, in OxDC-DSSN the lid remains in an intermediate form between the open and close position, as shown in

Figure 14, thus causing the exposure of residues located in the channel connecting the protein surface with the active site (Burrel *et al.*, 2007).

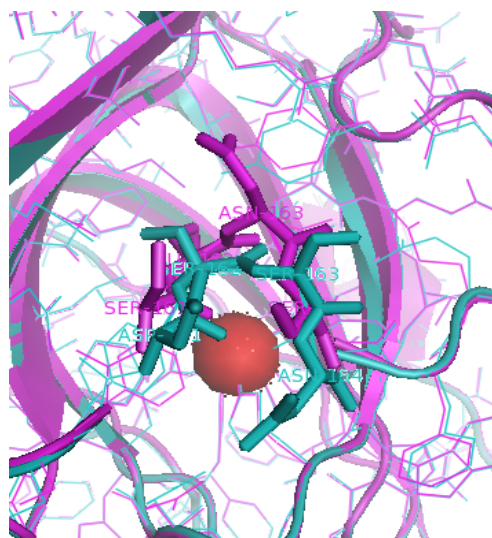


Figure 14. Superimposition of OxDC and OxDC-DSSN active sites. The OxDC structure (PDB code 1J58) is depicted in magenta whereas that of the OxDC-DSSN mutant (PDB code 1UW8) is coloured cyan. The main chain backbone of the lid regions (residues 161-164) are shown as sticks. Mn²⁺ ion is represented as red sphere. The figure was generated using PyMOL.

Based on these considerations, we hypothesized that the use of a substrate analogue, such as sodium glyoxylate (NaGlyox), could induce at least a partial closure of the active site channel and consequently prevent aggregation. Thus, in order to better understand the mechanism leading to OxDC-DSSN aggregation, we monitored the change in turbidity at pH 7.2 and physiological ionic strength upon addition of OxDC-DSSN to the buffer in the absence or presence of 50 mM NaGlyox (Figure 15). We found that NaGlyox prevents aggregation and, if added to the mixture during aggregation, it is able to stop the process, as shown by the progressive stabilization of the 600 nm absorbance signal to a value lower than that observed in the absence of ligand. The latter effect cannot be ascribed to dilution, since the addition of NaGlyox led to a less than 20% change in the overall volume of the mixture. Thus, we can conclude that the ligand at the active site is able to partly rescue for the conformational changes induced by amino acid substitutions in OxDC-DSSN. It should be mentioned that the addition of NaGlyox is not suitable

for the biotechnological application of the enzyme, since it would affect the enzymatic activity. Nevertheless, these findings confirm the hypothesis that OxDC-DSSN aggregation comes from the increased flexibility of the lid and could be instrumental for a possible future engineering of the protein.

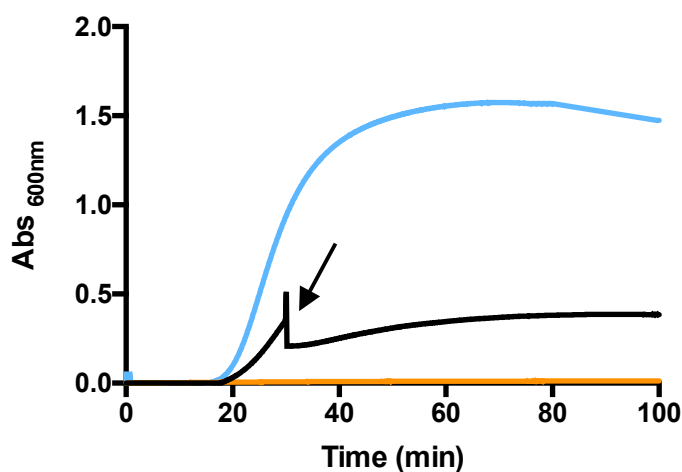


Figure 15. Time-dependent aggregation of OxDC-DSSN at pH 7.2 in absence or presence of sodium glyoxylate. Absorbance changes at 600 nm as a function of time of OxDC-DSSN at 0.5 mg/ml concentration in the absence (light blue) or presence (orange) of 50 mM sodium glyoxylate. The black line shows the absorbance changes occurring upon addition of sodium glyoxylate during aggregation (at the time indicated by the arrow). The buffer was 16 mM Tris-HCl pH 7.2, 140 mM NaCl, at 25°C.

4.3 Oxalate detoxification ability of OxDC and OxDC-DSSN in a PH1 cellular model

Considering the potential use of an oxalate-degrading enzyme for the treatment of hyperoxaluria, we wonder if at neutral pH the residual decarboxylase or oxidase activity of OxDC and OxDC-DSSN, respectively, endowed the two proteins with the ability of metabolizing oxalate in a cellular environment. To test this hypothesis, we employed a PH1 cellular model made up of CHO-GO cells (Benham *et al.*, 2006). CHO-GO cells overexpress glycolate oxidase (GO), an enzyme that converts glycolate into glyoxylate inside peroxisomes (Benham *et al.*, 2006). Thus, in the presence of glycolate in the culture medium, cells generate glyoxylate inside peroxisomes. Glyoxylate accumulates and is oxidized to oxalate in the cytosol, thus

promoting cell death (Figure 16). It follows that the highest is the ability to detoxify glyoxylate or oxalate, the highest is the cell survival in the presence of glycolate. In other words, cell viability in the presence of glycolate represents an indirect measure of the amount of oxalate or glyoxylate detoxification ability of the cells (Fargue *et al.*, 2018).

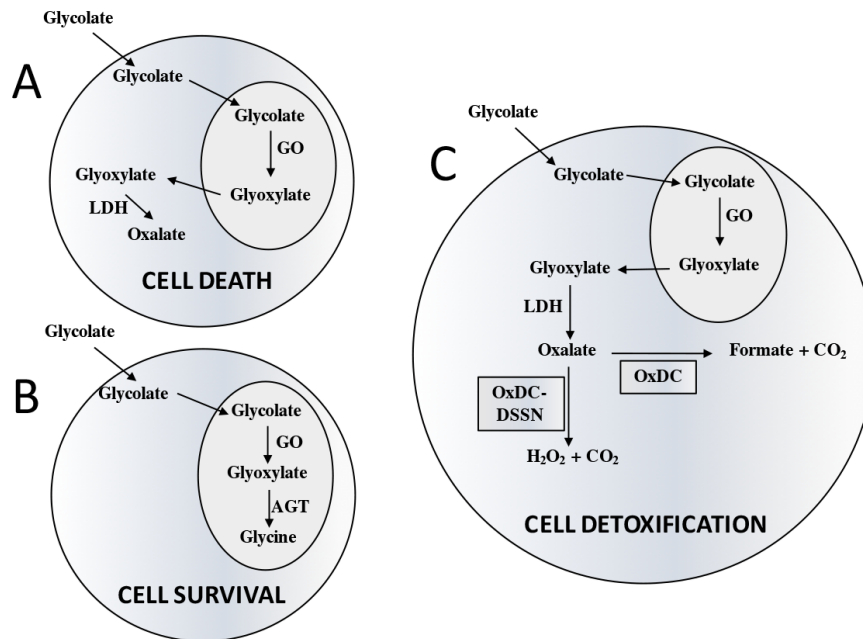


Figure 16. Schematic representation of oxalate detoxification in CHO-GO cells. (A) Negative control: CHO-GO cells **(B)** Positive control: CHO-GO-AGT cells; **(C)** CHO-GO cells after OxDC or OxDC-DSSN transfection. GO: glycolate oxidase; LDH: lactate dehydrogenase AGT: alanine:glyoxylate aminotransferase; CO₂: carbon dioxide; H₂O₂: hydrogen peroxide.

We transfected recombinant purified OxDC or OxDC-DSSN in CHO-GO cells by using the Xfect Protein Transfection Reagent. A preliminary experiment using OxDC-His (Figure 17A), revealed that the protein is detectable inside the cell starting from 1 hour incubation and reaches its maximum level after 24 hours. Thus, we evaluated the oxalate degradation ability of CHO-GO-OxDC cells and CHO-GO-OxDC-DSSN cells 24 h after protein transfection. As negative control we used non-transfected CHO-GO cells, which lack any detoxifying enzyme. As positive control, we used CHO-GO cells stably expressing AGT. AGT catalyzes the conversion of glyoxylate into glycine. Thus, it prevents oxalate formation and preserves cell viability (Figure 16).

As shown in Figure 17B, as compared with that of CHO-GO, the culture medium of CHO-GO-OxDC and CHO-GO-OxDC-DSSN cells treated with glycolate contains a lower amount of oxalate, in line with that present in the medium of CHO-GO-AGT cells. This would imply that transfected cells are able to detoxify the oxalate produced inside the cell. In particular, the residual activity at pH 7.2 of OxDC and OxDC-DSSN encapsulated inside CHO-GO cells (equal to 7 and 15%, respectively, as compared with the value at pH 4.2) was sufficient to reduce the concentration of oxalate released in the culture medium from 678 to 298 and 291 μM , respectively, over 24-h incubation at 37°C. To confirm these data, we determined the viability upon treatment with glycolate of each cell clone.

Although we verified that the protein transfection process did not affect cell viability *per se*, in order to exclude any possible bias for each cell clone we obtained the viability value from the ratio between each glycolate-treated sample and its untreated control. As expected, after treatment with glycolate CHO-GO cells and CHO-GO-AGT cells showed a viability of 18% and 80%, respectively (Figure 17C) (Oppici *et al.*, 2015). Interestingly, CHO-GO-OxDC cells and CHO-GO-OxDC-DSSN cells showed a significant increase in viability of about 1.8 and 1.6-fold respectively, as compared with CHO-GO cells. It should be noted that cells viability does not seem to correlate with the reduction in oxalate content. However, it should be taken into account that there is no direct proportionality between the glyoxylate/oxalate content and cell viability. Thus, a threshold value probably exists below which viability is preserved, thus explaining our data.

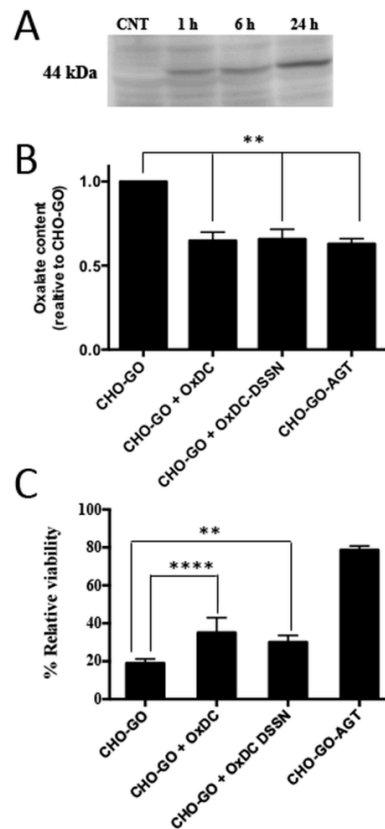


Figure 17. Indirect glycolate toxicity assay. (A) CHO-GO cells were transfected with OxDC-His. At different times cells were harvested and lysed. 20 μ g of lysate were subjected to SDS-PAGE and immunoblotted with anti-His (C-term) antibody (1:5000). GAPDH (indicated as CNT in the figure) was used as loading control. Lanes are coded as follows: CNT: non transfected CHO-GO cells; 1 h: cells harvested 1 hour after transfection; 6 h: cells harvested 6 hour after transfection; 24 h: cells harvested 24 hour after transfection. (B) Amount of oxalate present in the culture medium of the indicated cell clones upon 24 h treatment with 0.8 mM glycolate, expressed as percentage with respect to the negative control. Three replicates have been measured for each sample. Bars represent mean \pm SEM. * $P < 0.05$. (C) Histogram representative of cell viability after 24 hours of treatment with 0.8 mM glycolate expressed as percentage with respect to untreated control. Six replicates have been measured for each sample. Bars represent mean \pm SEM; ** $P < 0.01$, **** $P < 0.0001$.

Overall, these data indicate that both OxDC and OxDC-DSSN, although with a different efficiency, are able to degrade oxalate formed in the cell cytosol, thus suggesting that they could be able to metabolize oxalate under conditions similar to those present in biological fluids. These results are in line with those recently obtained in HEK293 cells (Albert *et al.*, 2017).

CONCLUSIONS

The use of OxDC for industrial and therapeutic applications has greatly attracted the interest of the scientific community in the last years. One of the main concerns on the use of this enzyme is related to its extremely low optimum pH of activity. In an attempt to explore the potential of OxDC as biological drug, we deeply investigated its biochemical properties at neutral pH. Our main findings indicate that OxDC wild-type and a mutated form showing oxalate oxidase activity (OxDC-DSSN) (i) retain detectable decarboxylase or oxidase activity, respectively, at neutral pH, (ii) do not undergo gross structural changes at neutral with respect to acidic pH, except for a reduced thermal stability associated in OxDC-DSSN to an enhanced propensity to unfolding and aggregation, and (iii) although with a different efficiency, are able to degrade oxalate in a cellular model of PH1.

These data provide the proof of principle for the possible use of oxalate degrading enzymes as biological drugs for the treatment of primary and enteric hyperoxalurias, pathologic conditions caused by the accumulation of oxalate from endogenous or exogenous sources, respectively.

In this regard, it should be mentioned that the direct administration of a bacterial enzyme is not feasible, because it would generate a remarkable immune response on the patients. Thus, as already done in other enzymatic deficits (Rossi *et al.*, 2014, Sarkissian *et al.*, 2008) appropriate delivery systems can be designed to profit from the metabolizing activity while being protected from the interaction with the immune system. In addition, the very low activity and stability of the enzyme at neutral pH implies that protein engineering techniques should be applied to select mutant forms endowed with improved fitness under physiological conditions. These two problems will be addressed in chapters 5 and 6 of this thesis.

5

**LOADING OF *B. subtilis* OxDC
IN HUMAN AND MURINE RED
BLOOD CELLS**

Background Information

The main hallmark of PH is the increased production of endogenous oxalate. In the most severe forms, the disease progresses to systemic oxalosis, a status where oxalate accumulates in plasma and deposits in various organs including heart, leading to serious and often fatal consequences (Beck *et al.*, 2013; Hoppe 2012). Under the latter condition, any treatment able to degrade plasmatic oxalate could represent an effective cure. One of the possibilities to reduce the plasmatic oxalate burden is the administration of an oxalate-metabolizing enzyme such as OxDC. However, the direct intravenous administration of OxDC is not feasible, because it would elicit a significant immune response. In this regard, an intriguing approach to prevent immunogenicity of exogenous proteins is their encapsulation inside red blood cells (RBCs). Indeed, RBCs can encapsulate large particles thanks to the unique ability of their membranes to be opened, thus allowing the entrance of enzymes that remain entrapped within the cells after resealing (Gutierrez-Millan *et al.*, 2004; Magnani *et al.*, 1988; Magnani *et al.*, 2002). Upon reinfusion, the enzyme is functional and able to perform his activity assuming that the substrate can enter RBCs. Since RBCs are able to internalize oxalate through the SLC4A1 ion channel (or band 3) transporter (Jennings and Adame, 1996), the possibility to apply this strategy to PH is attractive. In addition, the use of RBCs provides several advantages over alternative carriers, owing to their biocompatibility, the induction of little or no antigenic response, their long life-span in circulation, and their large internal capacity (Biagiotti *et al.*, 2011). A similar approach has been recently applied to phenylketonuria (PKU). PKU patients accumulate high levels of phenylalanine in the bloodstream, with pathologic consequences mainly consisting in mental retardation. One of the available therapies for PKU is the administration of phenylalanine ammonia lyase (PAL), a cyanobacteria-derived enzyme able to degrade phenylalanine to ammonia and trans-cinnamic acid (Hoskins *et al.*, 1982). It has been reported that RBCs loaded with recombinant PAL from *Anabaena variabilis* are able to avoid hyperphenylalaninemia in a murine model of PKU. Moreover, the therapy does not produce adverse immune reactions (Rossi *et al.*, 2014).

Based on these considerations, we thought that encapsulating OxDC inside RBCs and using them as bioreactors could allow to degrade plasmatic oxalate in the most severe forms of PH. The elimination of plasmatic oxalate would also reduce the amount of urinary oxalate and avoid the accumulation of insoluble calcium oxalate salt at kidney level, thus preventing stone formation. In order to use OxDC inserted in RBCs as a therapeutic bioreactor in PH, we setup loading conditions using the wild-type enzyme and human erythrocytes. This part of my PhD project was carried out in collaboration with the group of Prof. Magnani at the University of Urbino.

RESULTS AND DISCUSSION

5.1 Stabilities studies of OxDC in human RBCs loading buffer

The studies described in chapter 4 indicate that under conditions mimicking the RBCs cytoplasm OxDC maintains its functional and structural properties. However, since it is well-known in the literature that OxDC is sensible to changes in ionic strength (Tanner *et al.*, 2001), as preliminary step we tested the behaviour of the enzyme under the experimental conditions used for the human RBC loading procedure. In particular, we investigated the aggregation propensity of the protein in loading buffer at 0.1 mg/ml protein concentration and 4°C for 90 minutes, which is the time necessary for encapsulation. DLS analyses revealed that the total count rate in complete buffer was very high and the signal of the hexamer was detectable for only few minutes (data not shown). This result suggests that one or more components of the buffer could promote OxDC aggregation. Therefore, we performed the same analysis by excluding one component at a time, while preserving the basal buffer components. As shown in Figure 18 we found that GSH is responsible for OxDC aggregation. In fact, in the presence of complete human RBCs buffer, containing 3 mM GSH, the total count rate increases rapidly, thus indicating an aggregation process. In contrast, upon the elimination of GSH from the buffer no increase in count rate is observed up to 90 min. In agreement with these data, OxDC rapidly aggregates in the same buffer used for the studies at physiological ionic strength (see Figure 18) upon addition of 3 mM GSH.

An explanation of the effect of GSH at molecular level is not straightforward. Nevertheless, we noticed from the OxDC sequence that a Cys residue is present at the C-terminus (Cys383). Although Cys383 is not visible in the crystal structure we can speculate that, being the third to last residues, it should be exposed to the solvent. To understand if Cys383 was responsible for the aggregation of OxDC in the presence of GSH, we treated the protein with dinitrothiocyanobenzene (DNTB), which promotes the alkylation of cysteines with an exposed sulfhydryl group. We first confirmed that only one cysteine per monomer is titrated (data not shown), as expected. We then monitored the aggregation propensity of OxDC-DNTB, i.e. of

OxDC upon alkylation with DTNB. DLS analyses revealed that OxDC-DNTB is stable in complete human RBCs loading buffer up to 90 min (Fig 18B). This result agrees with the hypothesis that OxDC aggregation induced by GSH could involve Cys383. It can be speculated that GSH could directly bind Cys383 and cause a conformational change of the protein that makes it more susceptible to self-association.

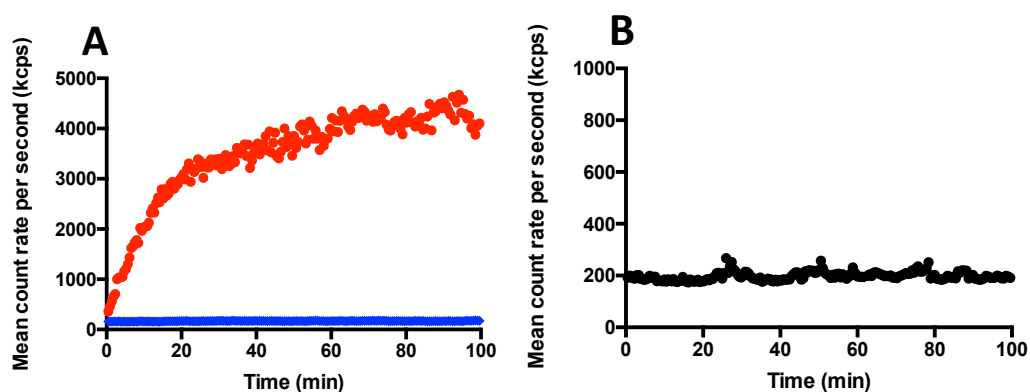


Figure 18. DLS analysis of OxDC aggregation. (A) Time dependence of total count rate (measured as kilocounts per second) of 0.1 mg/ml OxDC in complete human RBCs buffer (10 mM NaHCO₃, 10 mM NaH₂PO₄, 20 mM glucose, pH7.4, 2 mM ATP) in the presence (red), or absence (blue) of 3 mM GSH. (B) Time dependence of total count rate (measured as kilocounts per second) of OxDC alkylated with DNTB in human RBCs buffer (10 mM NaHCO₃, 10 mM NaH₂PO₄, 20 mM glucose, pH7.4, 2 mM ATP and 1.5 mM GSH) at 4°C. The experiment was carried out in presence of 0.1 mg/ml enzyme and 0.1 mM DNTB.

The finding that GSH promotes OxDC aggregation opened a big problem in view of RBCs loading, because GSH is very important to maintain erythrocytes integrity and its absence during the loading protocol could compromise the success and/or the efficiency of the procedure. For this reason, we decided to monitor OxDC aggregation in the presence of different concentrations of GSH, to look for a limit value to preserve OxDC stability. As shown in Figure 19, when GSH is reduced below 2 mM concentration, OxDC aggregation is prevented, as demonstrated by the low values of count rate and by the persistence of the signal of the hexamer up to 90 min. Based on these data, we decided to slightly modify the loading buffer using 1.5 mM GSH to prevent aggregation while possibly avoiding RBCs alterations.

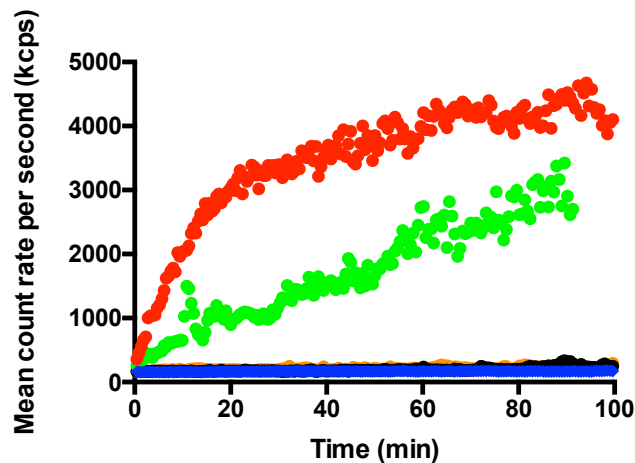


Figure 19. Aggregation of OxDC in human RBCs loading buffer in presence of different concentration of GSH. Time dependence of total count rate (measured as kilocounts per second) of 0.1 mg/ml OxDC in human RBCs loading buffer (10 mM NaHCO₃, 10 mM NaH₂PO₄, 20 mM glucose, pH7.4, 2 mM ATP) in the presence of GSH at 3 mM (red), 2 mM (black), 1.5 mM (orange), 1 mM (black), or 0.5 mM (blue), at 4°C.

As final control, we performed a standard decarboxylase assay at pH 4.2 after incubation of OxDC for different times (10, 30, 60 and 90 minutes) in the chosen formulation of the human RBCs loading buffer, i.e. 10 mM NaHCO₃, 10 mM NaH₂PO₄, 20 mM glucose, pH7.4, 2 mM ATP, 1.5 mM GSH. Results reported in Figure 20 reveal that after an initial decrease of about 15%, the catalytic activity remains stable up-to 90 minutes suggesting an almost unaltered functionality of OxDC.

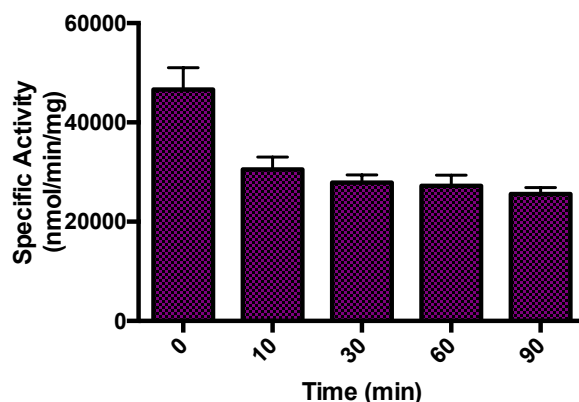


Figure 20. Specific activity of OxDC after incubation in RBCs loading buffer. Time-dependent loss of activity of OxDC measured by the FDH-coupled assay at pH 4.2 after incubation of OxDC in RBCs loading buffer (10 mM NaHCO₃, 10 mM NaH₂PO₄, 20 mM glucose, pH7.4, 2 mM ATP, 1.5 mM GSH) at 4°C.

5.2 OxDC loading in human RBCs

We used a loading procedure setup by the group of Prof. Magnani (Magnani *et al.*, 1988), that involves the following three steps:

- 1) hypotonic dialysis: upon exposure to a hypotonic solution a swelling of the erythrocyte membrane is observed, accompanied by an increased membrane permeability and by the formation of pores;
- 2) isotonic resealing: erythrocytes are incubated in a isotonic solution in the presence of the particle to be encapsulated, and the reduced osmotic pressure favours encapsulation;
- 3) “resealing”: erythrocytes are exposed to a hyperosmotic solution, which promotes the closure of the pores and the consequent encapsulation of the target particle.

We introduced minor modifications to the protocol due to the interference of GSH with OxDC aggregation. First, before the hypotonic dialysis step we decided to pre-dialyze RBCs to eliminate endogenous GSH. RBCs pre-dialysed were then dialysed in hypotonic solution in the presence of 36.4 IU of OxDC at 70% haematocrit. Then, since RBCs should not stay for long time in the absence of GSH, we added 1.5 mM GSH during the hyperosmotic resealing step.

The percentage of recovery was 79% calculated from the number of RBCs submitted to the dialysis step and those recovered at the end of the loading procedure. We then estimated the yield of OxDC internalization by performing an OxDC activity assay on the hemolysate of loaded RBCs. Based on the specific activity value of the enzyme, we could estimate that the yield of entrapment of OxDC was 26%. This value is in line with those previously observed by Rossi *et al.*, on the encapsulation of PAL (Rossi *et al.*, 2014).

In order to monitor the vitality and functionality of RBCs-loaded we determined the haematological parameters. The resulting corpuscular indices (MCV, MCH, MCHC) of loaded RBCs were in agreement with those of native cells (Rossi *et al.*, 2014) at 90% haematocrit.

5.3 OxDC loading in murine RBCs

To provide the necessary information for preclinical investigations, we also determined the best experimental conditions to load OxDC in murine RBCs. We carried out the experiment using the same protocol of human RBCs. However, we obtained an entrapment yield of 18% and a recovery of 55%. These values are significantly lower than those obtained with human RBCs. The difference is due to the fact that murine RBCs are much more fragile than human erythrocytes (Rossi *et al.*, 2014). Nevertheless, our result was very satisfying if compared with other encapsulation procedures (Rossi *et al.*, 2014).

CONCLUSIONS

In this chapter we have setup one of the first steps necessary for the preclinical investigation to use RBCs-loaded with OxDC as bioreactors to detoxify oxalate in PH. We demonstrated that OxDC can be efficiently encapsulated inside RBCs and it does not lose activity during the encapsulation process. Moreover, enzyme loading does not compromise RBC morphological parameters.

Overall these data provide the proof-of-principle for the feasibility of a therapy for PH based on the administration of RBCs loaded with an oxalate-degrading enzyme. The next step to validate this approach are tests in a murine model of disease. In this regard, the success of the encapsulation in murine RBCs provide the necessary premise to proceed with *in vivo* experiments that are currently under way.

6

**PROTEIN ENGINEERING
STRATEGY TO SELECT AN
IMPROVED FORM OF O_xDC
AT NEUTRAL pH**

Background information

The biochemical characterization of OxDC at neutral pH has revealed that the enzyme maintains its global structural properties but, as expected, displays a strongly reduced catalytic activity. Moreover, under conditions mimicking a physiological environment, the enzyme shows a reduced thermal stability, probably due to an influence of the different state of protonation of key amino acid residues. Therefore, although the administration of OxDC is considered as a promising strategy against the various forms of hyperoxaluria, the reduced activity and stability at neutral pH represents a major problem. In this regard, the acidic optimum pH of OxDC has been historically attributed to the protonation state of oxalate (Anand *et al.*, 2002; Just *et al.*, 2004), but some recent papers suggest that the pH-dependence of the catalytic activity could be also governed by small changes in the active site of the protein that could stabilize the +3 oxidation state of the Mn ion (Zhu *et al.*, 2016). Based on these considerations, we reasoned that mutations of key protein residues could in principle shift the optimum pH toward the neutral range. Therefore, we decided to apply protein engineering techniques to generate mutant forms of OxDC possibly endowed with higher activity and/or higher stability at neutral pH. As described in early 90s by Gupta *et al.*, protein engineering approaches are presented as “a highly promising techniques within the frame of biocatalyst engineering to improve enzyme stability and efficiency in low water systems” (Gupta *et al.*, 1992). Nowadays, many strategies are available to “evolve” a protein with a desired function or property (Chen 2001). They can be classified in two main classes (Figure 21):

- (i) Rational design, for which the knowledge of the structure and function of the target protein represents an essential prerequisite. The term rational refers to the perfect control of the desired change to be introduced into the protein. A rational gene mutation is planned by using *in silico* analyses and by taking into account the information available on the biochemical properties of the protein. This is followed by designed changes in the gene of the protein cloned in a specific vector for heterologous expression, and into the purification of specific

mutants. The final step is a screening based on an assay reporting on the success of the change (Arnold 1993).

One of the well-known successful application of rational design is the engineering of the enzyme subtilisin to avoid its inactivation by bleach (Bryan 2000). Subtilisin is a protease which is added to detergents to improve their efficiency, but is inactivated by bleach. Thanks to the knowledge of the catalytic mechanism and to the availability of the crystal structure, it has been found that the inactivation was due to the oxidation of the methionine at position 22. Using site-directed mutagenesis this residue has been changed to alanine, thus resulting in a mutant enzyme showing improved activity and stability in the presence of bleach (Stauffer and Etson, 1969).

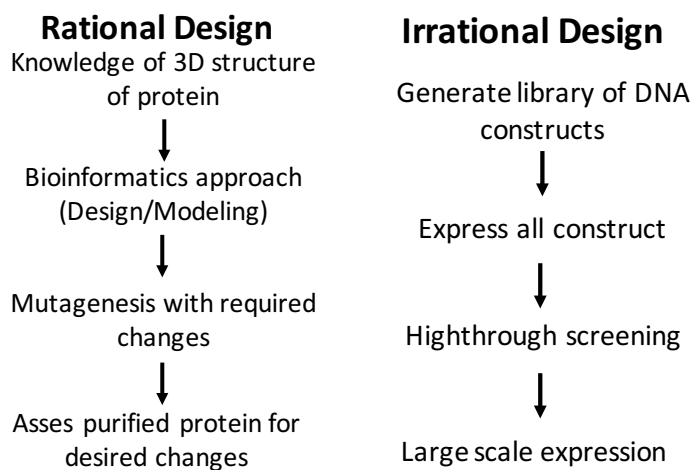


Figure 21. Flow-chart illustrating the basic steps of rational and irrational protein design approaches.

- (ii) Irrational design, also called direct evolution. It is mainly applied when the structure of the target protein is not available. In this method, random changes (mutations) are inserted into the protein, the best mutants are selected based on a phenotypic assay, and the inserted mutations are finally analysed. Direct evolution mimics the process of natural

selection. In fact, the target gene undergoes iterative rounds of mutagenesis that create libraries of variants which are selected for the desired function and expressed on a large scale.

Direct evolution has been largely used to improve protein stability (Beadle and Shoichet, 2002; Tokuriki *et al.*, 2008), substrate binding affinity (Dalby 2003; Park *et al.*, 2005), substrate specificity (Paramesvran *et al.*, 2009; Bougioukou *et al.*, 2009) and optimum pH (Tomschy *et al.*, 2002; van Tilbeurgh *et al.*, 1992).

The born of direct evolution strategies dates back to 1980s when George Smith pioneered phage-display technology for the engineering of proteins with desired binding specificities (Smith, 1985). In the following years, other irrational design techniques have been developed. Among them, error prone PCR is used to generate randomized genomic libraries. It allows the initiation of DNA amplification, starting with tiny amounts of the parent molecule, and produces a considerable number of mutated genes. The principle of this technique is based on the ability of Taq polymerase to anneal incompatible base-pairs to each other under conditions favouring an erroneous interaction. In this way, the polymerase makes mistakes in the newly synthesized complementary DNA resulting in a new gene with unknown mutations.

Another direct evolution technique is DNA shuffling, which is used to rapidly increase the size of a library because it permits the recombination of homologous gene fragments. The target genes are randomly fragmented by DNaseI, and fragments of the desired size are purified from an agarose gel. These fragments are then reassembled using cycles of denaturation, annealing, and extension by a polymerase. Recombination occurs when fragments from different parents anneal in a region of high sequence identity. Following this reassembly reaction, PCR amplification with primers is used to generate full-length chimeras suitable for cloning into an expression vector.

In light of these considerations, it is difficult to understand which one of these strategies is the more suitable to generate improved forms of a target protein because either the rational and the irrational design present some disadvantages. In the rational design technique, besides a lot of successful results, numerous attempts have failed, probably due to an incomplete understanding of mechanism required to enhance the enzymatic properties. Moreover, a unique substitution in a specific site could give an inactive enzyme without the desired properties due to an undesired conformational change. Finally, this approach could be tedious and expensive and might be impractical for multiple cycles of mutagenesis. In fact, at each mutation cycle, the inserted mutation must be confirmed by sequencing and the properties of the corresponding variant in the purified form must be defined before proceeding to other mutagenesis cycles. On the other hand, the irrational design does not need the previous knowledge of the protein structure, but the introduction of mutations in unknown sites can often result in deleterious effects such as deletions, insertions or duplications. Moreover, a detailed screening of the obtained libraries is required, to avoid the exclusion of clones with improved features.

In our project, we decide to use both rational and irrational design techniques in order to develop mutant forms endowed with higher activity and stability at neutral pH.

RESULTS AND DISCUSSION

6.1 Rational approach

Based on the knowledge of sequence, crystal structure, biochemical features and catalytic mechanism of OxDC we decided to use three different strategies for the rational engineering of the protein: (i) change of metal specificity, (ii) site-saturation mutagenesis of Glu162, (iii) substitution of residues in the proximity of the active site.

- (i) **Change of metal specificity.** It has been reported for many metalloenzymes that the change of the metal acting as cofactor could improve catalytic efficiency (van Tilbeurgh *et al.*, 1992). This is possible only if the new metal is able to maintain the same distance between residues, usually histidines, implicated in the coordination of the natural cofactor. In the specific case of OxDC, we wonder if a metal change could change the pH-dependence and improve the activity at neutral pH. Since in OxDC the presence of Mn in a redox state II is fundamental for the correct start of reaction, we thought to substitute this metal with another one with a similar oxidation state (van Tilbeurgh *et al.*, 1992). To incorporate different metals, we included them at millimolar concentration as supplement in the medium of the bacterial culture. As for other Mn-dependent enzymes (van Tilbeurgh *et al.*, 1992) we decided to substitute Mn^{2+} with magnesium (Mg^{2+}), zinc (Zn^{2+}), cobalt (Co^{2+}) or cadmium (Cd^{2+}). Moreover, we used an expression protocol similar to that used for Mn incorporation (see Materials and Methods), to try to maintain the same yield of protein recovery and the same molar ratio of cofactor per monomer. Unfortunately, in the presence of Co^{2+} and Zn^{2+} the expression of OxDC was almost completely depleted, as shown in Figure 22. This is probably due to the toxic effect of these metal ions, which possibly influence the fitness of bacterial cells and/or decrease the efficiency of protein folding.

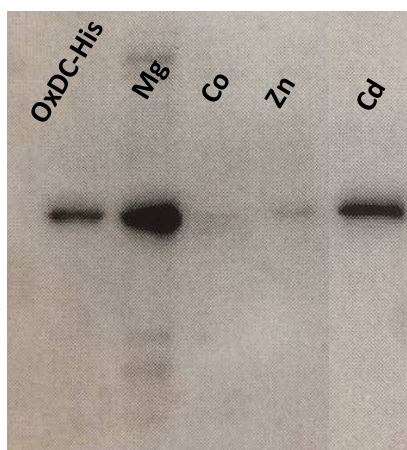


Figure 22. Western blot analyses of purified OxDC-His expressed in the presence of different metal ions. 0.1 ug of OxDC-His (lane 1), 8 ug of OxDC magnesium induced (lane 2), cobalt induced (lane 3), zinc induced (lane 4) and cadmium induced (lane 5). Upon SDS-PAGE, proteins transferred on nitrocellulose membrane were revealed using an anti-His-HRP antibody (1:5000).

On the other hand, in the presence of Mg^{2+} and Cd^{2+} ions the expression of the protein was even higher than that obtained in the presence of Mn (Figure 22). In line with previous reports, Mg-complexed OxDC maintained a catalytic activity at pH 4.2 equal to 90% with respect to that of Mn-complexed OxDC (Anand *et al.*, 2002). However, the activity at pH 7.2 was undetectable, probably due to the incapacity of the metal cofactor to reach the oxidation state suitable to carry on catalysis. In the case of the Cd^{2+} -complexed enzyme, no activity was detected at both acidic and neutral pH, although the protein was correctly expressed and folded, thus suggesting that cadmium at the active site could negatively impact the OxDC catalytic mechanism.

- (ii) **Site-saturation mutagenesis of Glu162.** Site-saturation mutagenesis is usually included among irrational techniques. It consists in the change of a specific protein residue with all other possible amino acid residues. However, we exploited the principle of this technique to substitute Glu162, an OxDC active-site residue, with some other

residues chosen in a rational way. Glu162 is an acid-base catalyst involved in the protonation of the the formyl radical intermediate during the OxDC reaction. For this reason, we wonder if the substitution of Glu162 with amino acids positively charged at neutral pH such as histidine and lysine could promote oxalate decarboxylation. Moreover, we also tested the substitution with glutamine which shows a steric hindrance similar to that of glutamate, but could act as proton donor. We constructed, expressed and purified the mutants E162H, E162K and E162Q, which did not display any gross conformational alteration with respect to the wild-type enzyme. Unfortunately, when we tested their oxalate degrading ability at pH 4.2 and 7.2, we did not detect any catalytic activity, indicating that histidine, lysine and glutamine are not able to substitute glutamate as proton donors. These results are not completely unexpected, since it has been already reported that the mutation of E162Q caused a complete loss of activity at acidic pH (Svedružić *et al.*, 2007).

- (iii) **Substitution of residues in the proximity of the active site.** Various protein engineering studies have shown that the kinetic power of an enzyme can be influenced by residues not directly involved in the catalytic pathway, but located in the proximity of the active site and possibly interacting with the substrate during its channelling. This idea is supported by a previous study where xylose isomerase, a metalloenzyme, has been engineered to increase its optimum pH by changing Glu186, an active site residue not directly involved in catalysis, to Gln. (Tomschy *et al.*, 2002).

Based on these premises, we elaborated the hypothesis that the presence of a proton donor at the entrance of the OxDC active site could improve the activity at neutral pH by inducing oxalate protonation. Therefore, we performed an initial bioinformatic analysis that allowed the identification of three glutamate residues (Glu60, Glu99 and Glu198) which are not directly involved in metal binding or in the catalytic

mechanism of OxDC. We replaced them by amino acids able to act as proton donors at neutral pH (Figure 23).

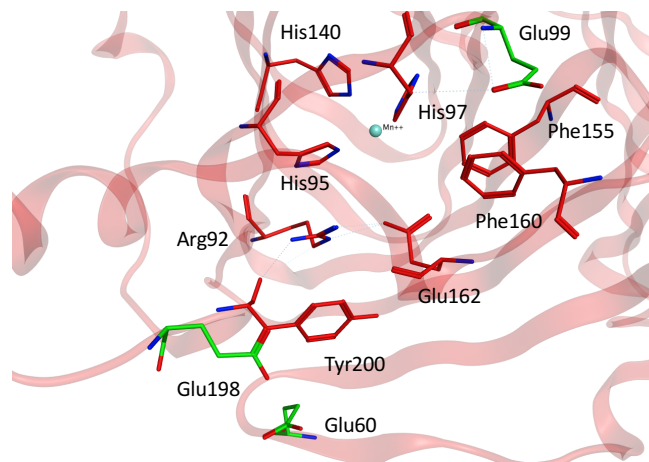


Figure 23. OxDC active site architecture. Residues involved in the formation of the active site pocket are shown as red sticks, while glutamate residues located at the entrance of the active site are represented as green sticks. The Mn^{2+} ion is depicted as a blue sphere.

Their substitution with charged amino acids such as lysine, arginine and histidine could create at neutral pH a positive channel where oxalate could be protonated before reaching the active site, thus becoming in a state suitable for catalysis.

Although we started from a rational approach to choose glutamate residues to be subjected to site-directed mutagenesis, we performed a casual insertion of the selected mutations by using a mixture of primers in a single mutagenesis reaction to obtain all possible mutants: E60H, E60K, E60R, E99H, E99K, E99R, E198H, E198K, E198R. We used the vectors encoding each mutant to transform *E. coli* cells, and we measured the decarboxylase activity on the obtained lysates at pH 5.5 and 6.5. The latter choice was dictated by the necessity to detect even minimal increases of the optimum pH. The screening revealed the presence of two mutants, E60K and E198H, which showed a slight increase in catalytic activity. In particular, E60K presented an increased catalytic efficiency of 1.4-fold at both pHs, whereas E198H showed a 1.3-fold increase in activity only at pH 6.5. We decided to test the effect of the combination

of the two mutations, but the double mutant did not show any improvement of catalytic activity, as reported in Figure 24.

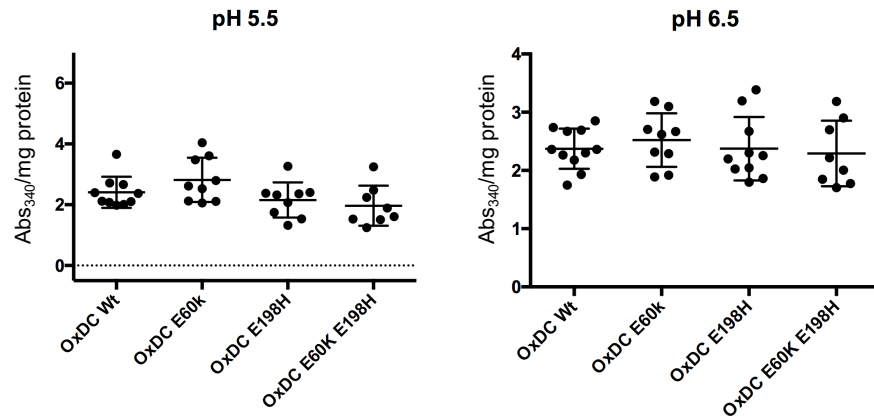


Figure 24. Oxalate oxidase activity of mutants of the pool of colonies selected after transformation and induction of *E. coli* BL21 cells. Here is reported the decarboxylase activity in the lysate of cells expressing OxDC. The measurement of single clones has been repeated 12-fold at two different pHs. For assay condition see Materials and Methods.

The E60K mutant, which showed the highest specific activity in the bacterial lysate, was also expressed and purified, and a complete analysis of activity as a function of pH was carried out (data not shown). Unfortunately, the purified protein did not show any difference with respect to wild-type OxDC, thus indicating that the small increase observed in the bacterial lysate could be related to an improved folding efficiency that increases the amount of protein present inside the cell.

From the analysis of the OxDC active site entrance, shown in Figure 25, we also noticed the presence of aromatic residues which are not in direct contact with residues of the active site, but could be involved in substrate channelling and possibly influence the pH-dependence of catalytic activity: Phe155, Phe160 and Tyr200.

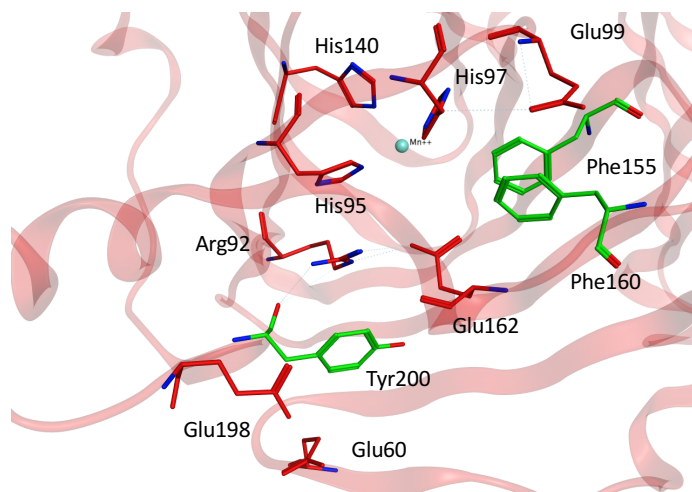


Figure 25. OxDC active site architecture. Residues involved in the formation of the active site pocket are shown as red sticks while aromatic residues located at the entrance of the active site are represented as green sticks. Mn ion is depicted as a blue sphere.

In order to change as less as possible the active site architecture, we mutated the three amino acids to histidine and we produced both the single mutants (F155H, F160H and Y200H) and the combined double and triple mutants. The clones obtained and their decarboxylase specific activity at pH 5.5 and 6.5 are shown in Figure 26. Unfortunately, no significant improvements of catalytic activity were noticed. We also tried to combine the mutation of glutamate and aromatic residues, to investigate if the combination of mutations could generate a mutant with improved features, as shown in Figure 26, but the strategy was not successful.

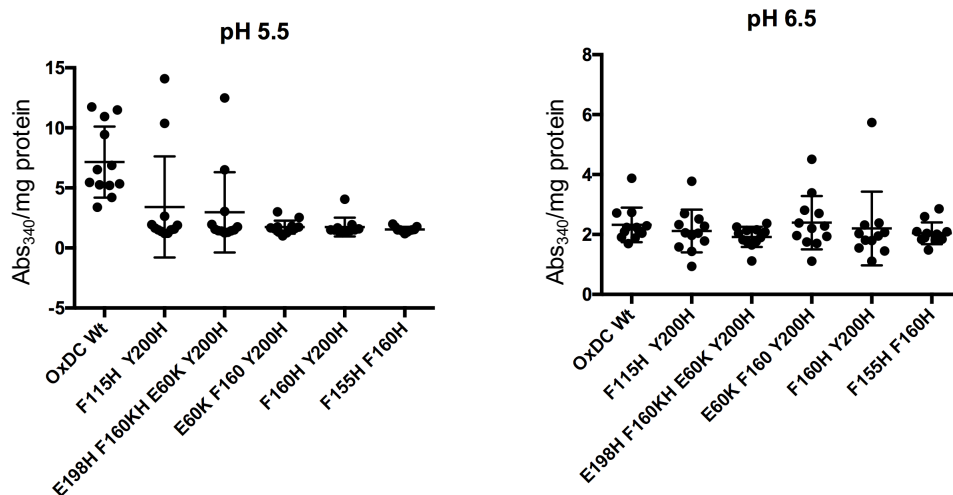


Figure 26. Oxalate oxidase activity of mutants of the pool of colonies selected after transformation and induction of *E. coli* BL21 cells. Here is reported the decarboxylase activity in the lysate of cells expressing OxDC. The measurement of single clones has been repeated 12-fold at two different pHs. For assay condition see Materials and Methods.

In conclusions, we used three different strategies to engineer OxDC to change its optimum pH toward the neutral range. None of our attempts produced significant results. This is probably due to the complex catalytic mechanism of the enzyme. In fact, a monoprotonated substrate and/or a correct ionization state of the metal cofactor is necessary to produce the formyl radical. In this process Glu162 plays a key role and other residues are probably involved in maintaining the overall active site geometry suitable to promote catalysis. Therefore, it is possible to conclude that any alteration could negatively influence the catalytic mechanism. In a previous study, a pH-shift of a metalloenzyme, xylose isomerase, was obtained thanks to protein engineering approaches (van Tilbeurgh *et al.*, 1992). This enzyme catalyses an aldoses/ketose isomerization and requires bivalent cations such as Mg^{2+} , Mn^{2+} or Co^{2+} . The active site of the enzyme contains two metal ions that are involved in substrate binding and participate to the hydride shift between the C1 and C2 atoms of the substrate. Similarly to OxDC, a glutamate residue is present at the active site but not in contact with the substrate nor with the metal cofactor. The authors of the study found a mutation, the E186Q, which preserved most of the activity, but drastically shifted the optimum pH from 7.5 to 6.5 (Tomschy *et al.*, 2002).

In the case of OxDC, however, we did not find any active site residue that do not directly participates to catalysis. This could be the main reason underlying the lack of success of our rational design strategies and prompted us to attempt irrational approaches on residues distant from the active site.

6.2 Irrational approach

Based on the unsatisfactory results obtained by the different strategies employed in the rational approach to obtain an OxDC showing improved activity at neutral pH, we decided to focus our efforts on protein engineering methods based on irrational approaches. The latter strategy could in principle allow to find mutations of residues spread over the entire sequence that improve the functional parameters and/ or the thermodynamic stability of a protein.

It is well-known that one of the main problems of protein directed evolution methods is the high rate of gene combinations and the consequent high number of produced variants, which imply a high number of screening procedures and a low global efficiency of the process (Rockah-Shmuel *et al.*, 2014). In fact, the frequency of beneficial mutations in randomly mutated variants is very low (Lang and Murray, 2008) and combinations of multiple beneficial mutations are often needed to obtain a significant improvement of a desired property (Chen, 2001). Considering all these shortcomings, we reasoned that a totally irrational approach could not be applied to efficiently select a good OxDC variant in our laboratory setting. One of the methods recently employed to reduce the dimension of screening libraries is to produce the so called “smart libraries”, (Lane and Seelig, 2014), i.e. libraries that are less complex but of high-quality and are endowed with a high potential of containing functional variants. To build those libraries, a targeted mutagenesis guided by structural or phylogenetic information, along with methods allowing an improved speed of selection, should be applied.

Among the available methods, we utilized the consensus-mutants based approach (Porebski and Buckle, 2016). Consensus design, like ancestral sequence reconstruction, utilises evolutionary history. However, rather than inferring phylogenetic hierarchy, all sequences are aligned and the most frequently observed

amino acid identified at each position in the alignment are considered potentially beneficial. Moreover, in order to speed-up the selection, we took advantage of the epistatic effect of mutations. Usually, each mutation alone could have neutral or deleterious effects. However, when two or more mutations are combined in a sequence space, they can give rise to a structural improvement (higher thermostability or stress resistance, higher surface adaptability, etc) or to a functional change (altered K_m or k_{cat} , shift of optimum pH, substrate promiscuity). The technique that we employed to combine the selected mutations is named Incorporation of Synthetic Oligonucleotides During Gene Shuffling (ISOR) (Rockah-Shmuel *et al.*, 2014). This technique, which is described in detail in the Materials and Methods section, permits to explore a large number of potentially beneficial mutations in a combinatorial manner such that individual library variants carry a limited number of mutations. The efficacy of this technique is demonstrated by the fact that its rate of success is comparable to that achieved by several rounds of evolution using random mutagenesis approaches (Rockah-Shmuel *et al.*, 2014). In summary, the strategy that we used for the OxDC direct evolution involves (i) a consensus-based approach to select residues spread over the entire sequence and identify possibly beneficial mutations, followed by (ii) the combinatorial insertion of the selected mutations by the ISOR technique (Figure 27). As a read-out of our study, we tested both the stability and the activity of the enzyme at neutral pH.

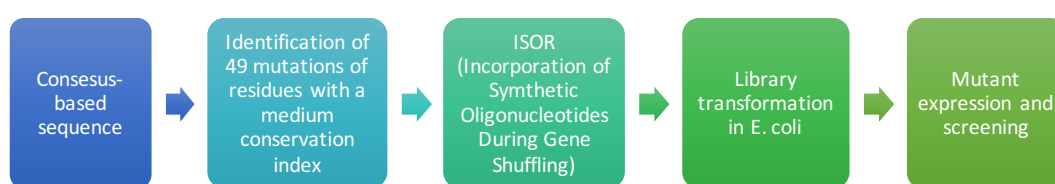


Figure 27. Overall strategies for the irrational design of OxDC

6.2.1 Identification of target mutations by the consensus based-approach

The consensus based-approach involves the following four steps: (i) identification of a domain of the protein to be targeted, (ii) acquisition and pre-processing of homologous sequences, (iii) iterative assessment of several multiple sequence alignments (MSA) and (iv) calculation of sequence conservation. To apply the

consensus-based approach to OxDC we selected 200 proteins displaying an homology sequence from 35 to 95% with OxDC from the UniProt database and we carried out a first multiple sequence alignment using the software MUSCLE on the Consurf server, and then analysed the consensus sequence generated by Jalview program. The output of this analysis allowed us to define the conservation score of each residue with respect to the other analysed sequences. In Figure 28 is reported a slice of the results where the intensity of the blue colour is related to the conservation grade of each residue. In order to confirm the results obtained, we also performed a conservation analysis based on a structural alignment using the MSA obtained previously. We obtained the consensus structural-based alignment, where the conservation score takes into account structural information. At this point, we decided to cross the two outputs (sequence and structure based alignment) and select only the consensus residues common to both predictions. As final step, we mapped the consensus residues identified in the OxDC crystal structure, and we chose the target mutations based on the position and the degree of conservation of each residue.

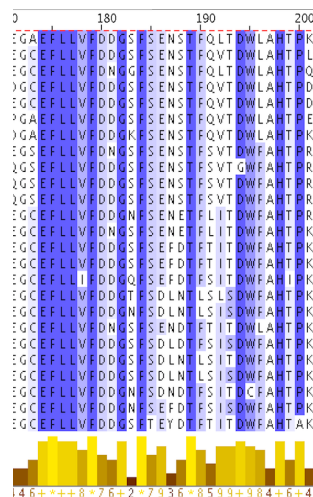


Figure 28. Portion of the sequence alignment of OxDC. Results of sequence alignment of OxDC with 200 proteins with a homology sequence from 35 to 95% obtained using the software CONSURF. A darker colour indicates an higher conservation index of the residue. Yellow bars represent the degree of conservation of each residue.

It should be mentioned that the most conserved residues of a protein are not good candidates for a directed evolution approach, because they usually play an essential role for the structure and/or the biologic activity (Mesa-Torres *et al.*, 2014). Rather,

in order to uncover or evolve properties of a protein that are possibly hidden, one should look for residues with a low conservation score. This usually avoids gross structural/functional alterations. In the case of OxDC, we observed that most of the strongly conserved residues are located at the active site, such as the His involved in manganese binding. On the other hand, we noticed that other regions contain many residues characterized by a low degree of conservation. Among them, we looked for amino acids that are strongly conserved in all or most of the two-hundred proteins used as query for the alignment, but are not highly conserved in OxDC. We then choose to convert each of these residues to that present in the other sequences but absent in OxDC. The analysis gave us 38 mutations, which are listed in Table 5 and represent the starting point for *in vitro* analyses.

Table 5: List of mutations obtained from bioinformatics analyses. Blue, green and red colour indicates mutations involving residues located on the protein surface, at the monomer-monomer interface, or at the entrance of active site, respectively. The black colour indicates mutations involving residues distributed on the other parts of the structure.

M48L	D124A	A246V	H339R
N57M	L138I	K252P	Y340F
E60Q	A144G	A268G	L349M
A65S	A149C	I285L	M351L
S76A	L168I	N304D	F356L
A90G	T169S	Q306R	
I91V	L172F	V321I	
E99Q	L194I	E322Q	
V112I	E198Q	I324T	
I114A	E203Q	I334M	
E117Q	Y228H	D337S	

We mapped each residue on the OxDC crystal structure (Figure 29), and we observed that they are spread over the entire structure of the monomer. We thus grouped the selected mutations based on the position of the mutated amino acids. It can be observed that some are located on protein surface areas, other on stretches involved in monomer-monomer interactions, or in regions located at the entrance of active site.

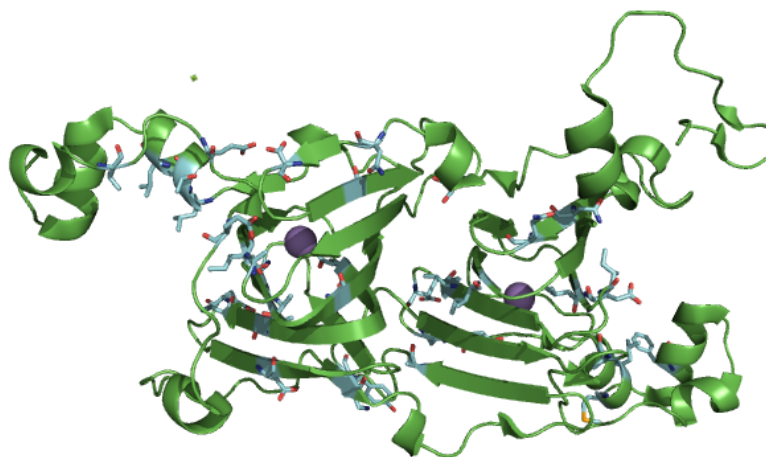


Figure 29. Cartoon representation of the OxDC monomer (PDB: 1J58) showing the map of the residues target of the mutations identified by bioinformatic analyses and listed in Table 4. Mutated residues are shown as light blue sticks, while the Mn²⁺ ion is shown in violet.

6.2.2 Library construction with the ISOR method and screening of the OxDC variants upon expression in *E. coli*

The ISOR method is a molecular biology technique used to create libraries of mutants of a target protein by combining in a stochastic manner a selected number of mutations (Rockah-Shmuel *et al.*, 2014). The overall protocol involves three steps, as summarized in figure 30:

- (i) DNA SHUFFLING: it consists in the random breaking of the cDNA of the target protein using DNaseI;
- (ii) ASSEMBLY PCR: it is a particular type of PCR in which all the oligonucleotides containing the selected mutations and annealing in overlapping regions are used concomitantly. It gives rise to products of different lengths containing random combinations of the selected mutations;
- (iii) NESTED PCR: it consists in the amplification of each of the different constructs obtained in the previous step to obtain enough amount of cDNA of each variant of the target protein for the subsequent cloning step.

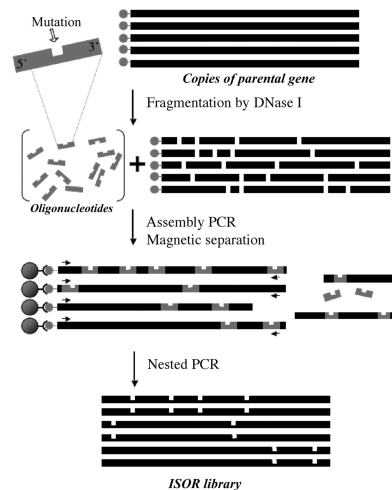


Figure 30. Brief summary of ISOR technique.

We first setup the Assembly PCR to obtain 2- to 4 mutations by preparing a suitable mixture of primers (equal molar concentration of each mutagenic primer, sense or antisense strand). We then performed the NESTED PCR to increase the yield of the assembled DNA, we purified the product, and we cloned them in a pET21(a) vector by using restriction enzymes. The cloning procedure was setup according to Rockah-Shmuel *et al.* 2014 (see Materials and Methods).

As a final step, we verified the success of the cloning procedure by gel electrophoresis of the vector using the empty vector and the vector containing the wild-type OxDC gene as negative and positive control, respectively.

We transformed the OxDC library into competent BL21 *E. coli* cells. We obtained several plates where each colony represents a putative variant. We then setup the screening procedure by performing a small-scale growth and induction of each bacterial colony in 96-well plates, followed by lysis of the culture of each well, and analysis of the soluble lysate.

As read-out, we determined the oxalate decarboxylase specific activity of the bacterial lysate at pH 5.5 and 6.5, and we compared the obtained values with those of wild-type OxDC and of the untransformed bacteria as positive and negative control, respectively. Technical details are given in Materials and Methods.

In the first set of experiments, we screened enough colonies to cover most of the possible combinations of mutants (Rockah-Shmuel *et al.*, 2014). Unfortunately, we

did not obtain any variant showing an improved activity at physiological pH. Thus, we decided to test the possible epistatic effect of the selected mutations and to combine all the selected changes in a single run, i.e. to use conditions in which a large number of mutations at a time is inserted in each DNA sequence. It should be mentioned that a similar approach would require the screening of a very high number of clones to cover the whole mutational space. Since our experimental setting did not allow to test thousands of colonies, in order to have a preliminary idea of the possible success of this procedure, we decided to limit our testing to approximately 1000 clones.

The screening of the second set of mutants allowed to identify 31 clones showing an improved decarboxylase activity at pH 5.5 and 6.5 with respect to wild-type OxDC. We then performed a second run in which each positive clone was screened in triplicate at both pHs to exclude false positives possibly resulting from the intrinsic variability of the assay and/or of the screening procedure. The results are shown in Figure 31 and allowed us to select four clones showing improved activity at pH 5.5 and 6.5. Since the sequence of each clone was unknown, we named them based on their position in the screening plate as D7, G2, G10 and G11.

Among the positive clones, we decided to proceed our study only with G2, because it was the only mutant showing a significant change of specific activity with respect to wild-type OxDC.

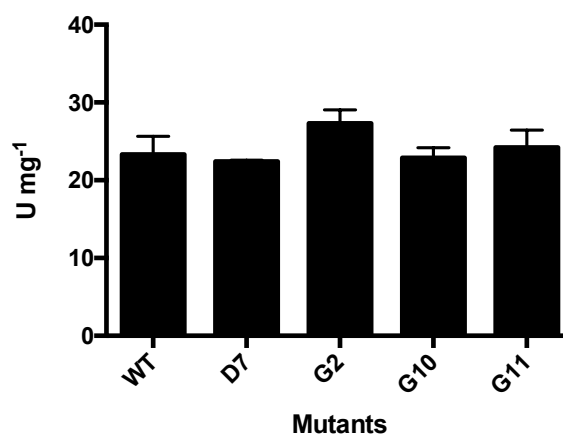


Figure 31. Results of the second-run screening of OxDC mutants. The bars show the oxalate decarboxylase specific activity at pH 6.5 measured in the cellular lysate of bacteria expressing each variant. The screening procedure is described in the Materials and Methods section.

6.2.3 Analysis of the G2 clone

Upon sequencing of the vector expressing the G2 clone we noticed that the variant is characterized by the combination of mutations reported in Table 6.

Table 6. Mutations identified in the G2 clone of OxDC.

N57M	E99Q	I180L
E60Q	L138I	E198Q
A65S	A144G	E203Q
S76A	A149C	Y228H
I91V	T169S	K252P

The visual inspection of the mapped mutations (Figure 32) reveals that the mutated residues are only part of the cupin domain I. Some of them, such as Glu198 and Ala65, are located at the entrance of active site, while others, such as Tyr228 and Lys252, are involved in the interaction with cupin domain II, and others, such as Ala144, Iso180 and Glu203, are located on the protein surface. It has been demonstrated that cupin domain I is the catalytic site for OxDC, while cupin domain II plays a structural role (Just *et al.*, 2007). Thus, we could speculate that mutations of residues belonging to the cupin domain II could have deleterious effects on OxDC folding, and thus strongly compromise protein fitness, while mutations of residues belonging to the cupin domain I could be better tolerated. This could explain why the mutations present on the G2 variant are only located in domain I.



Figure 32. Cartoon representation of the OxDC monomer (PDB: 1J58) showing the map of the residues mutated the G2 mutant. Mutated residues are shown as light blue sticks, while the Mn²⁺ ion is shown in violet.

It should be mentioned that a screening based on the specific activity measured in the bacterial lysate does not allow to distinguish between variations caused by an altered intrinsic catalytic activity of a protein, variations due to an altered expression level, and variations resulting from a combination of both factors. Thus, in order to substantiate the improved features of the G2 variant, we performed a large scale expression and we purified the protein to homogeneity.

We first investigated the pH-profile of the variant by determining the oxalate decarboxylase activity in the range of pH from 4.2 to 7.2. We did not notice any significant shift of the optimum pH with respect to wild-type OxDC (data not shown). However, when we analysed the thermostability at neutral pH by monitoring the loss of the CD signal at 222 nm with time, as reported in Figure 33, we found an improved stability. In fact, under the same experimental conditions, the mutant shows a T_m of 79°C, while wild-type OxDC shows a T_m of 39°C.

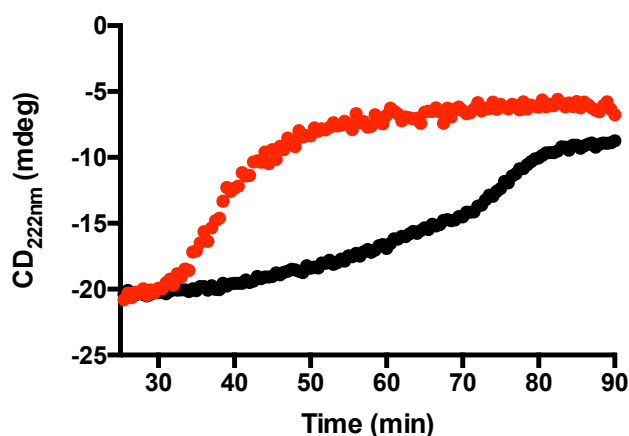


Figure 33. Thermal stability of OxDC WT and G2 mutant. Change in the CD signal at 222 nm at increasing temperature from 25° to 90°C (heating rate 1.5°C/min). All measurements were performed at 0.5 mg/ml enzyme concentration, in 16 mM Tris-HCl pH 7.2, 140 mM NaCl (red line) or 52 mM sodium acetate pH 4.2, 140 mM NaCl (black line), at 25°C. The colour code is the following: red, wild-type OxDC; black, G2 mutant.

Thus, we can conclude that the improved specific activity of the G2 variant is not due to an increase of intrinsic catalytic activity of the enzyme, but is probably the consequence of an improved expression yield of the protein caused by its increased thermodynamic stability.

At the moment it is difficult to define which of the mutations present on the G2 mutant contributes to the gain of stability, or if the improvement results from the combination of more than one mutation. The second option is the more probable based on the location of mutations which are spread over the structure of domain I. It can be speculated that one or more than one mutation leads to a different orientation of some amino acids which play a key role in the maintenance of the OxDC three-dimensional structure, or in influencing the aggregation propensity of the protein, thus resulting in an improved intracellular stability that in turn leads to an higher expression level. Similar results have been obtained in 2016 by Mesa-Torres *et al.*, who used a consensus-based approach to produce a mutant form of alanine:glyoxylate aminotransferase showing an increased kinetic stability. Moreover, in 2018 Cirri *et al.*, using consensus mutagenesis obtained a thermostable human excitatory amino acid transporter variant that shared up to 95% amino acid identity with the wild type transporters, but remained natively folded and functional for a long time under thermal stress conditions.

Studies are under way to better define the biochemical features of the G2 variants, the role of each mutation, and the possible occurrence of epistatic effects.

CONCLUSIONS

An optimum pH of OxDC in the neutral range is one of the more desirable features for the therapeutic use of the protein. In fact, notwithstanding its high activity at strongly acidic pH values, OxDC is considered as a new frontier in treatment of hyperoxaluria, where the enzyme should be active and stable at neutral pH (Grujic *et al.*, 2009; Langman *et al.*, 2016). Our study is the first aiming at improving the optimum pH of the enzyme through the use of protein engineering techniques. The strategy that we used is two-fold: 1) a rational approach, which did not give us any significant improvements of activity, and 2) an irrational approach based on the combination of a consensus-based approach and of the ISOR technique. Overall, the irrational approach was not able to give us an OxDC with improved activity at neutral pH. Nevertheless, we obtained a new enzyme showing an improved stability at neutral pH. The significance of this discovery is not only related to a better definition of the biochemical features of OxDC, but also to the selection of an enzyme with a remarkable resistance under conditions mimicking a physiological environment. This could represent a key property in the light of the application of the mutant as biological drug. In particular, we will exploit this property by encapsulating the mutant in RBCs and by comparing the half-life of the loaded protein with that of wild-type OxDC.

7

**OPPOSITE EFFECT OF
POLYMORPHIC MUTATIONS ON
THE ELECTROSTATIC
AGGREGATION OF HUMAN
ALANINE:GLYOXYLATE
AMINOTRANSFERASE:
IMPLICATIONS FOR THE
PATHOGENESIS OF PRIMARY
HYPEROXALURIA TYPE I.**

Background Information

The propensity to aggregation is an inevitable issue for most proteins and protein aggregates formation is the basis of several misfolding diseases, including those displaying loss-of-function pathogenesis. Different types of aggregates can be formed and they can lead to different effects in cells and organisms. For example, in age-related neurodegenerative disorders like Alzheimer's disease, a protein undergoes a conformational change favouring the formation of ordered oligomers and fibrillar aggregates that exert a toxic effect on a specific cell type (Oliva *et al.*, 2015; Roberts *et al.*, 2014). In other cases, like in diseases caused by protein deficits, pathogenic mutations can promote the aggregation of the protein involved causing the formation of amorphous aggregates that undergo degradation. The consequent reduction in the folding yield leads to a deficit of activity specific of the protein, as the CFTR chloride transporter in the case of cystic fibrosis (Walsh *et al.*, 2010; Pallas *et al.*, 2006), or the sphingolipid catabolism in the case of Gaucher disease (Torok *et al.*, 2002; Cuthbert *et al.*, 1992).

Although aggregation is often attributed to the population of intermediates exposing hydrophobic surfaces, the contribution of electrostatic forces has recently gained attention. The process of electrostatic aggregation is based on the attraction between complementary charged domains of a protein surface and it usually decreases at high ionic strength, due to screening effects (Sarkadi *et al.*, 1992). Studies aimed at improving protein aggregation resistance have indicated that surface charge strongly influences protein stability and that the controlling factor is the spatial location of charges (Mistry *et al.*, 2017; Wajnera *et al.*, 2004; Wang *et al.*, 2010). In fact, the main factor governing the aggregation extent is protein charge anisotropy, i.e. the asymmetric distribution of charged residues on the exterior of a particular protein.

Human alanine:glyoxylate aminotransferase (AGT) as described in the Introduction section, is associated with Primary Hyperoxaluria Type I. The majority of disease-causing mutations on the *AGXT* gene encoding AGT are missense mutations (Morris *et al.*, 2009; Fink *et al.*, 1998). Data obtained in prokaryotic and eukaryotic models as well as analyses on variants in the purified form, indicate that many mutations reduce the folding efficiency of AGT by promoting its aggregation

(Neves-Petersen *et al.*, 2003; Majhi *et al.*, 2006; Ugolini *et al.*, 2001). In some case the aggregation is due to a low dimer stability, which allows the formation of monomers exposing hydrophobic surfaces and prone to self-association (Austerberry *et al.*, 2017). In other case however, an aggregation driven by electrostatic interactions between folded dimers showing an increased surface charge anisotropy has been reported (Neves-Petersen *et al.*, 2003).

AGT exists as two polymorphic variants named major (AGT-Ma, the most frequent) and minor (AGT-Mi, present in 20% of Caucasian population) (Lee *et al.*, 2001; Der *et al.*, 2013). AGT-Mi shows an increased aggregation propensity and a reduced stability with respect to AGT-Ma, both *in vitro* and in the cell (Majhi *et al.*, 2006, Lee *et al.*, 2016). This effect has been attributed to a reduced stability of the dimeric structure (Austerberry *et al.*, 2017; Lee *et al.*, 2016; Perchiacca *et al.*, 2011). However, it cannot be excluded that either the P11L and/or the I340M substitutions typical of the minor allele could also influence the electrostatic surface of the protein. Moreover, it has been reported that several pathogenic mutations that lead to PH1 associated with the minor allele, play their effects by increasing the AGT aggregation propensity (Majhi *et al.*, 2006; Ugolini *et al.*, 2001; Lee *et al.*, 2016) and can functionally synergize with the minor allele polymorphism.

So, we decided to combine computational and *in vitro* studies to investigate the aggregation process of AGT in the recombinant purified form. These findings, by increasing the knowledge of the biochemical properties of AGT and of the pathogenesis of PH1, constitute the base to design new strategies able to improve the stability of the protein as a possible premise for the development of innovative therapeutic approaches.

RESULTS AND DISCUSSION

7.1 *In silico* analysis of the AGT surface

Based on the known 3D structure of AGT-Ma in the holo-form (PDB: 3R9A), we evaluated the distribution of hydrophobic surfaces as well as the electrostatic map. As reported in Figure 34A and B, AGT-Ma shows only few hydrophobic patches on its surface, mainly located along the dimerization interface in line with the finding that mutations inducing AGT monomerization favour aggregative processes driven by hydrophobic attractions (Dindo *et al.*, 2016).

Moreover, the electrostatic map of AGT-Ma reveals an asymmetric distribution of negative and positive charges on the dimeric surface (Figure 34C). In particular, four main negative patches are present in one face of the dimer.

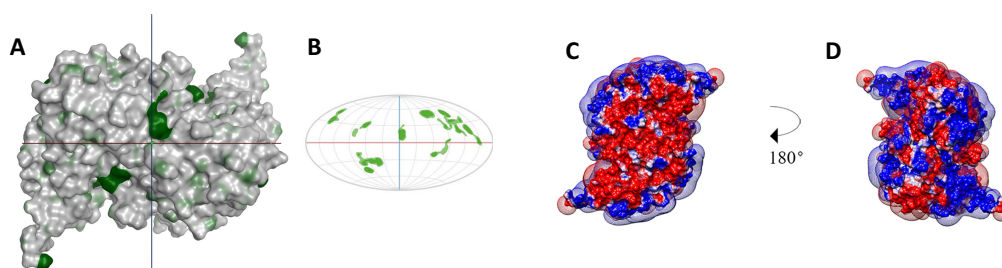


Figure 34. Distribution of hydrophobic patches and electrostatic potential around AGT-Ma. (A) Hydrophobic patches of dimeric AGT shown as green areas on a gray background. (B) Representation of the hydrophobic patches around AGT on a 2D map. The red and blue lines indicate the equatorial and central meridian projection axes, respectively. (C,D) Electrostatic potential contours shown as mesh (-0.5 (red) and $+0.5$ (blue) kT/e) around AGT obtained by using the *pdb2pqr* tool for structure preparation, *propka 3.0* for the protonation state of the residues of AGT and the adaptive poisson-boltzmann solver (APBS) tool to generate the electrostatic potential map. Each tool was run on the Opal web service. The visualization of the potential electrostatic map was performed using the UCSF chimera 1.11 program setting 0.06 M KP, pH 7.4 as buffer at 37 °C

On the other hand, as shown in Figure 34D, four main positive patches are present on the other side. So, we decided to compare the electrostatic map of AGT with those of other PLP-dependent aminotransferases belonging to the Fold type I family such as human cytosolic aspartate aminotransferase (PDB: 3WZF), human ornithine aminotransferase (PDB: 1OAT) and human tyrosine aminotransferase

(PDB: 3DYG) as well as with proteins showing a sequence similarity $\geq 30\%$ with AGT. All the latter proteins (except alanine:glyoxylate aminotransferase from *Aedes aegypti* that displays some positive patches), show an unvarying negative potential on their surface (data not shown) suggesting us that the peculiar distribution of surface charges in human AGT could promote its electrostatic self-association. Following this view, pH and ionic strength could critically influence aggregation rate and/or extent. Moreover, mutations of surface residues could change the charge distribution and negatively or positively influence the self-association process.

7.2 Effect of pH and ionic strength on the aggregation propensity of AGT-Ma

We evaluated the self-association propensity of AGT-Ma by dynamic light scattering (DLS) experiments performed at various pHs and ionic strengths. Preliminary analyses were carried out to guarantee that almost all the protein was present in the dimeric form. We monitored the increase in the mean count rate, a parameter that represents the average scattering intensity during the measurement and directly reports on aggregated species present in solution. To determine the aggregation rate, we have fitted the data on the time-dependent increase in count using the analytic equation proposed by Morris *et al.*, 2008. This equation is related to the minimalistic/”Ockham’s razor” Finke-Watzky (F-W) two-step model, which has been used to analyse the aggregation data of a wide set of proteins (Watzky *et al.*, 2008; Morris *et al.*, 2008). In this model, a continuous nucleation step ($A \rightarrow B$, rate constant k_1) is followed by a fast, autocatalytic growth step ($A + B \rightarrow 2B$, rate constant k_2). $A \rightarrow B$ and $A + B \rightarrow 2B$ processes are composites of multiple elementary steps and therefore the resultant rate constants, k_1 and k_2 , are experimental average values. In our experiments, we assumed that A is the dimeric form of AGT, B is the polymeric aggregation nucleus, k_1 and k_2 correspond to the average rate constants for nucleation and growth, respectively.

It is well-known that a lot of proteins tend to have decreased solubility near the pI , often referred to as isoelectric precipitation, where the low net charge of the protein corresponds to the loss of repulsive forces. AGT has a predicted pI of 8.59. So, we

decided to perform the analyses at 37°C in 0.1 M potassium phosphate buffer (KP) in the pH range 5.5-8.0, to avoid protein unfolding due to strong acid or alkaline conditions. HoloAGT-Ma does not show any significant increase in count rate from pH 8 down to 6.5, while a slight aggregation propensity can be seen at pH 5.5 and 6 (Figure 35A). At pH 5.5, the values of k_1 and k_2 were equal to $1.70 \pm 0.02 \cdot 10^{-2} \text{ min}^{-1}$ and $7.3 \pm 0.5 \cdot 10^{-4} \text{ min}^{-1} \mu\text{M}^{-1}$, respectively. In contrast, apoAGT-Ma showed an increase in count rate along the whole pH range, with extent and rate of aggregation higher than the corresponding of holoAGT-Ma (Figure 35B). The values of k_1 and k_2 increase as the pH is lowered from 8 to 5.5, giving values of pK_{spec} of 6.0 ± 0.1 , and 6.18 ± 0.09 , respectively (Figure 35C).

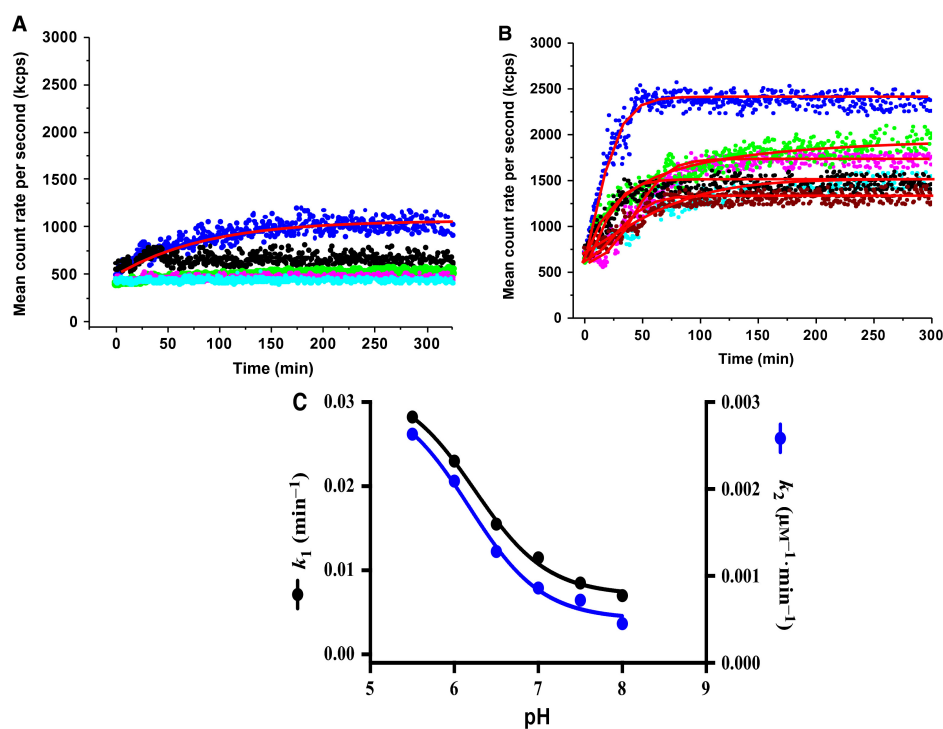


Figure 35. Aggregation profiles of holoAGT-Ma (A) and apoAGT-Ma (B) and trend of the rate constants values of apoAGT-Ma (C) as a function of pH. (A) Time-dependent changes of the total count rate (measured as kilocounts per second) of holoAGT-Ma. (B) Time-dependent changes of the total count rate (measured as kilocounts per second) of apoAGT-Ma. (C) Plot of k_1 (black circles) and k_2 (blue circles) rate constants of apoAGT-Ma. Measurements were performed at 10 μM enzyme concentration, 0.1 M KP, 37 °C. The color code for (A, B) is the following: blue, pH 5.5; black, pH 6.0; green, pH 6.5; purple, pH 7.0; red, pH 7.5; and cyan, pH 8.0.

Thus, the aggregation extent is higher at pHs where the protein net charge shows the highest values. It also be mentioned that the aggregation process leads to the

formation of aggregates of size spanning from 400 to 800 nm (data not shown), which confirms that aggregates are the main responsible for the scattering signal and that the count rate increase is a suitable parameter to follow the aggregation process, as already reported (Bemporad *et al.*, 2009). However, the signal of the dimer is always visible in the whole pH range, thus indicating that the dimer still remains the more represented species in solution.

By monitoring the aggregation process of apoAGT-Ma at pH 5.5 and 8 at various protein concentrations (Figure 36A and B) we found an increase in k_1 and k_2 values at increasing AGT concentrations under both conditions. When we studied the aggregation process of apoAGT-Ma at pH 5.5 varying KP concentration from 0.05 to 1 M, we found that the aggregation rate decreases at increasing ionic strength of the buffer. In particular, aggregation is completely prevented at values equal or higher than 0.2 M, and occurs with k_1 values of $3.1 \pm 0.3 \cdot 10^{-2} \text{ min}^{-1}$ and $2.2 \pm 0.2 \cdot 10^{-2} \text{ min}^{-1}$, and k_2 values of $2.9 \pm 0.3 \cdot 10^{-3} \text{ min}^{-1} \mu\text{M}^{-1}$ and $2.0 \pm 0.2 \cdot 10^{-3} \text{ min}^{-1} \mu\text{M}^{-1}$, at 0.05 M and 0.1 M, respectively (Figure 36C). These data indicate that the process is not mediated by hydrophobic attractions, which would have been enhanced by increased salt concentrations. Rather, it depends on electrostatic interactions, which are reduced or suppressed at high ionic strength due to screening effects.

In order to investigate if aggregation was accompanied by an unfolding process, we registered the dichroic signal at 222 nm, indicative of the secondary structure content, of 10 μM apoAGT-Ma in KP 0.05 M pH 5.5, 37°C, i.e. under conditions in which a strong aggregation phenomenon is observed. Since we did not observe any loss of secondary structure with time during aggregation up to 300 minutes (Figure 36D), we concluded that the process is not dependent on a partial unfolding, but occurs starting from a native or native-like form of the protein. Furthermore, by exploiting the different behaviour of the protein in the apo- and holo-form, we found that aggregation is not reversible. In fact, the addition of 100 μM PLP to an aggregating mixture of 10 μM apoAGT-Ma at pH 5.5 in 0.05 M KP was able to stop but not to revert the self-association process.

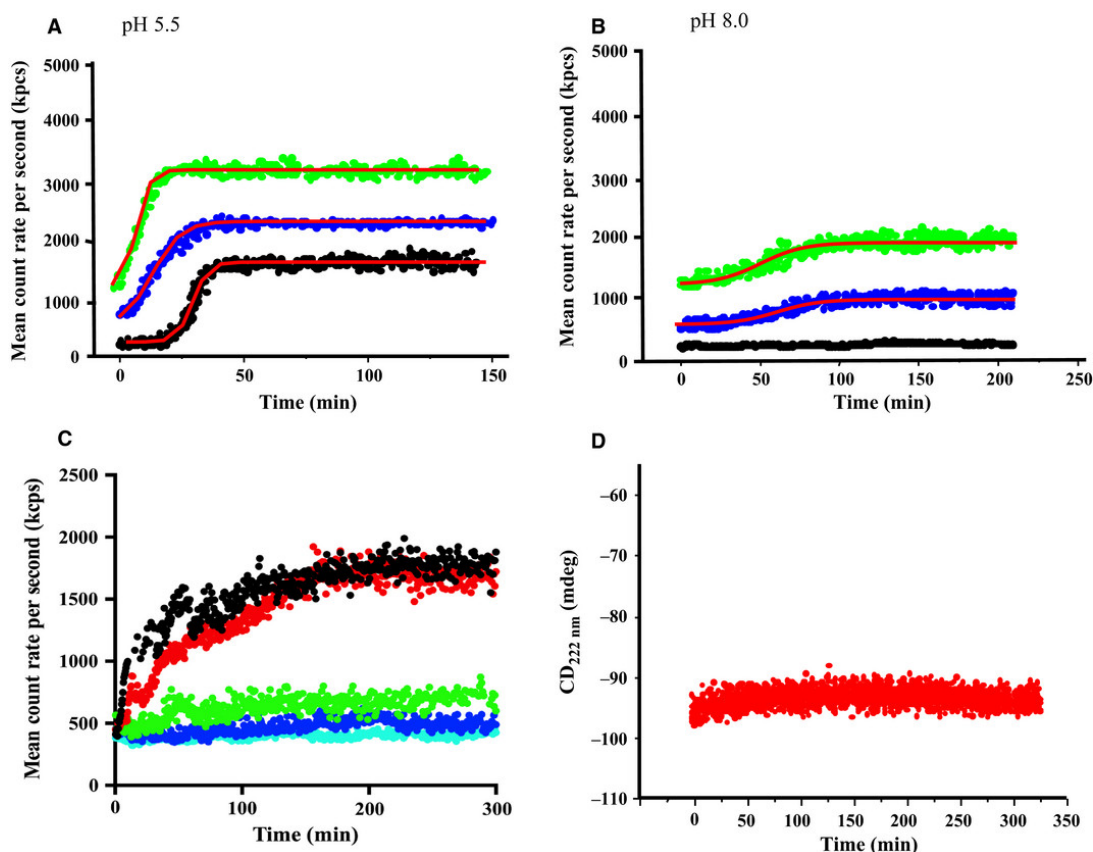


Figure 36. Aggregation of apoAGT-Ma at different protein concentrations and ionic strengths. (A,B) Time dependence of total count rate (measured as kilocounts per second) of apoAGT-Ma at 2 μM (black), 10 μM (blue) and 20 μM (green) concentration, in 0.1 M KP buffer, 37 $^{\circ}\text{C}$ at the indicated pH value. (C) Time-dependent changes of the total count rate (measured as kilocounts per second) of 10 μM apoAGT-Ma at 37 $^{\circ}\text{C}$ in KP buffer pH 5.5 at 0.05 M (black), 0.1 M (red), 0.2 M (green), 0.5 M (blue), and 1 M (cyan). (D) Time-dependent changes in the CD signal at 222 of apoAGT-Ma in 0.1 M KP, pH 5.5, 37 $^{\circ}\text{C}$, 10 μM enzyme concentration.

Altogether, these data allow us to conclude that the aggregation of AGT-Ma is not an isoelectric precipitation phenomenon, because it is not influenced by the global net charge of the protein, and is not due to the formation of disulphide bonds. Rather, it depends on the electrostatic interaction between patches of opposite charge present on the native dimeric species as a consequence of the charge anisotropy of the protein surface. A similar aggregation mechanism has been already reported for β -Lactoglobulin, which shows a strong aggregation phenomenon at pH values below the pI (Majhi *et al.*, 2006).

7.3 Effects of the P11L and I340M polymorphic mutations on the aggregation process

We analysed the aggregation process of apo- and holoAGT-Mi as a function of pH by DLS under the same experimental conditions used for AGT-Ma and we have found that the aggregation rate increases at decreasing ionic strength, thus indicating that the process is mediated by electrostatic forces (data not shown). The trends of the k_1 and k_2 as a function of pH of holo- and apoAGT-Mi, reported in Figure 37, reveal that both species show an increased aggregation propensity at acidic pH with estimated values of pK_{spec} of 5.8 ± 0.3 and 5.7 ± 0.1 for k_1 and 6.4 ± 0.1 and 6.2 ± 0.3 for k_2 of apo and holoAGT-Mi, respectively. Moreover, the species populating during AGT-Mi aggregation were similar to those formed by AGT-Ma but characterized by a higher molecular weight (~ 1000 nm diameter).

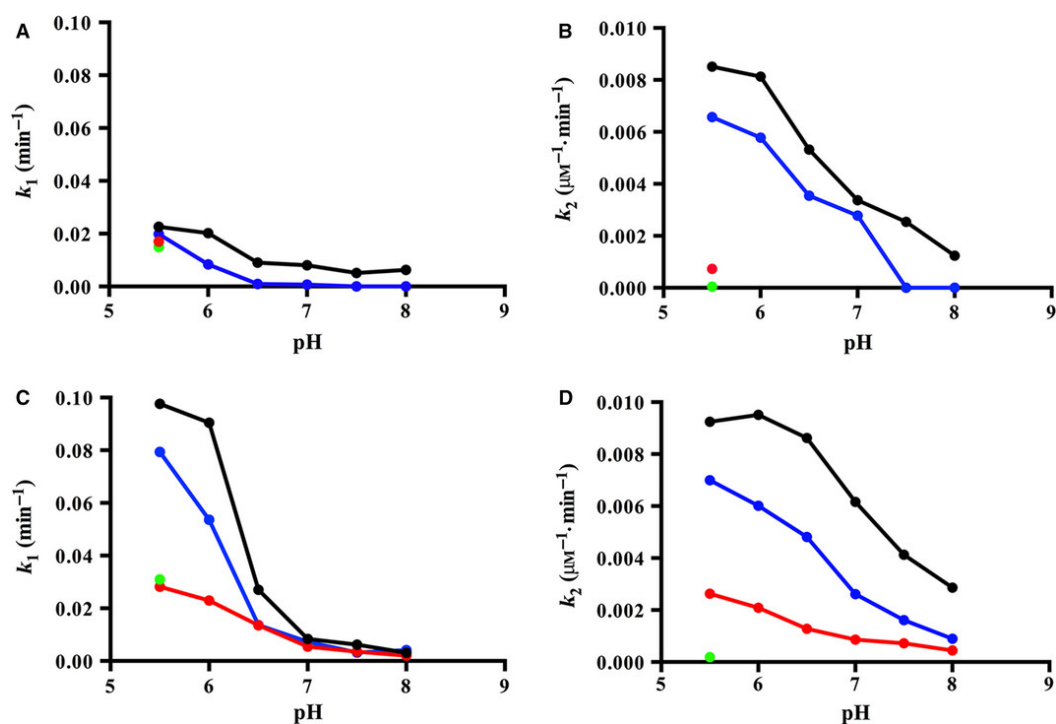


Figure 37. Trends of k_1 and k_2 of AGT-Mi, P11L, and I340M as a function of pH. The proteins either in the holo (A,B) or apo (C,D) form were incubated in 0.1 M KP at different pH values at 37 °C and the mean count rate in DLS was monitored. The values of k_1 and k_2 were obtained by fitting the data to Eq. 8 (see Materials and Methods). The color code is the following: AGT-Mi, blue; P11L, black; I340M, green. The values of AGT-Ma (red) are also shown for comparison.

At both 5.5 and pH 8, the aggregation rate is proportional to protein concentration (data not shown) and no unfolding is detected during aggregation, as indicated by CD spectroscopy experiments (data not shown). By comparing the aggregation rate constants of holo- and apoAGT-Mi with those of the corresponding forms of AGT-Ma we noticed that the minor allelic form shows an increased aggregation propensity. In fact, a visible aggregation event was present at pHs lower or equal to 7 in holoAGT-Mi, while holoAGT-Ma only aggregates at pH 5.5. At the latter pH value, holoAGT-Mi showed k_1 and k_2 values about 2- and 10-fold higher, respectively, as compared with those of holoAGT-Ma. As for the apo-form, the values of k_1 and k_2 were from 1- to 2.5-fold and from 2- to 4-fold higher than those of apoAGT-Ma, respectively (Figure 37).

Overall, these data allow to conclude that AGT-Mi is prone to an electrostatically-driven process of self-association analogous to that already observed for AGT-Ma, but characterized by a higher aggregation rate. The latter effect seems to depend more on an increased autocatalytic growth rate than on an increased nucleation rate. This suggests that one or both of the two polymorphic mutations typical of the minor allele, P11L and I340M, could directly or indirectly change the surface of the protein and somehow influence the interaction between oppositely-charged patches during aggregates growth.

In order to understand the structural determinants responsible for the increased aggregation propensity of AGT-Mi, we expressed, purified and characterized the two single mutants P11L and I340M. Their absorbance and CD spectra in the visible region were similar to the corresponding of AGT-Ma and AGT-Mi (data not shown). Moreover, the P11L and I340M mutations did not affect the $K_{D(PLP)}$ value of AGT as well as the kinetic parameters of the overall transamination reaction, except for a 30% reduction in k_{cat} of the P11L variant (data not shown).

Finally, the two mutations did not alter the quaternary structure of the protein up to 0.3 μM (the detection limit of SEC experiments).

We thus investigated the aggregation behaviour of I340M and P11L single variants. HoloI340M displayed a visible increase in count rate only at pH 5.5 and 6. At pH 5.5 the values of k_1 and k_2 were equal to $1.5 \pm 0.4 \cdot 10^{-2} \text{ min}^{-1}$ and $6.0 \pm 0.1 \cdot 10^{-5} \text{ min}^{-1} \mu\text{M}^{-1}$, respectively. The value of k_1 was similar while that of k_2 was 12-fold

lower than the corresponding of holoAGT-Ma. Accordingly, apoI340M only aggregated at pH 5.5, with a k_1 value similar to that of apoAGT-Ma but a k_2 value 14-fold lower than the corresponding of apoAGT-Ma ($k_1 = 3.20 \pm 0.15 \cdot 10^{-2} \text{ min}^{-1}$, $k_2 = 1.9 \pm 0.1 \cdot 10^{-4} \text{ min}^{-1} \mu\text{M}^{-1}$) (Figure 37). Hence, the I340M mutation has a stabilizing effect on the AGT native structure.

A completely different effect is exerted by the P11L mutation, as shown by the pH-dependence of the k_1 and k_2 values of aggregation of the apo and holo variant, respectively (Figure 38).

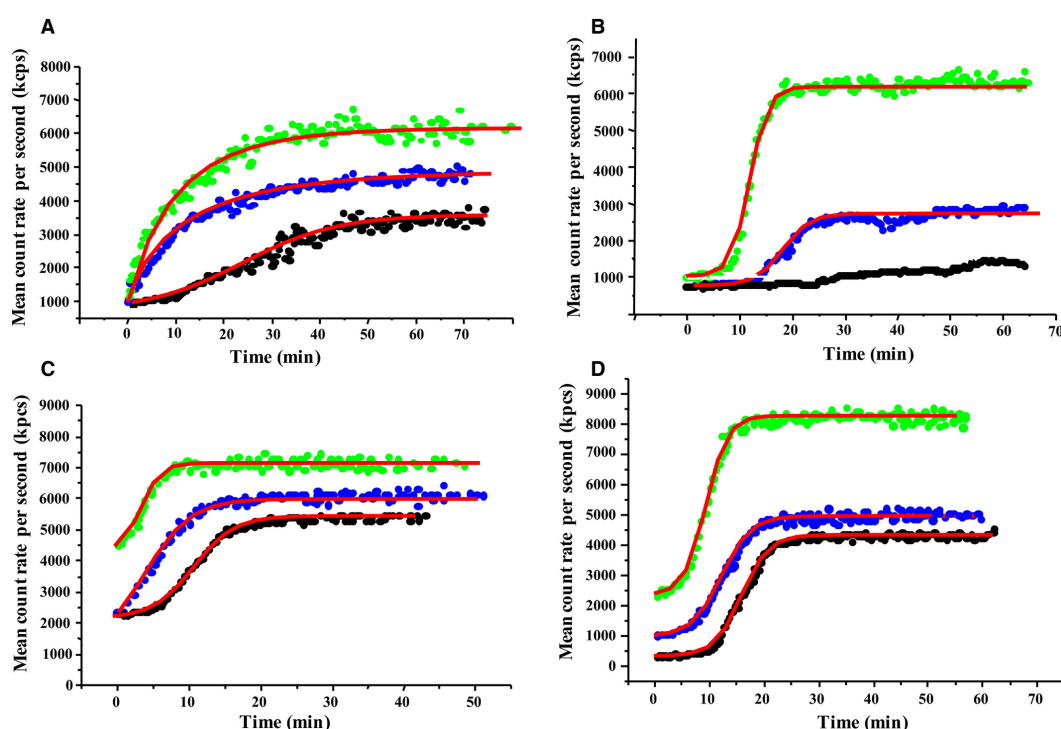


Figure 38. Aggregation profiles of apoAGT-Mi and apoP11L at different protein concentrations. Time dependence of total count rate (measured as kilocounts per second) of apoAGT-Mi (A,B) and apoP11L (C,D) at 2 μM (black), 10 μM (blue) and 20 μM (green dots) protein concentration, in 0.1 M KP buffer, 37 $^{\circ}\text{C}$ at pH 5.5 (panels A and C) or 8 (panels B and D).

An increase in count rate was detectable for both forms in the whole pH range. The aggregation increased at acidic pH with pK_{spec} for k_1 and k_2 of 6.1 ± 0.2 and 6.4 ± 0.2 respectively, for holoP11L, and 6.1 ± 0.4 and 6.9 ± 0.2 , respectively, for apoP11L. These values agree quite well with those previously found for AGT-Ma and AGT-Mi. The aggregation rate increased at increasing protein concentration

(Figure 38C and D) and is not accompanied by loss of secondary structure, thus suggesting a molecular mechanism similar to that already proposed for AGT-Ma and AGT-Mi. The comparison between the aggregation kinetics of the P11L variant with those of AGT-Ma revealed that the mutation increases by approximately 1.5-2 fold and by 2-4 fold the k_1 , and by approximately 9 and 4-fold the k_2 of the holo- and apo-form, respectively. Nevertheless, the signal of the dimer disappeared after ~20 minutes during the aggregation process of P11L. This indicates that a significant portion of the variant is present as aggregated species in agreement with the fact that the mixture displays a visible turbidity at the end of the analysis.

Overall, by comparing the data obtained on AGT-Mi, P11L, and I340M, with those of AGT-Ma, we can conclude that while the I340M mutation exerts a stabilizing effect, the P11L mutation significantly increases the aggregation propensity of AGT. The hypothesis that the two polymorphic mutations could have opposite effects on AGT has been previously advanced. Mesa-Torres *et al.*, 2014 have reported the mutation of Ile340 as one of the consensus amino acids substitutions that contribute to create a form of AGT endowed with a higher stability in solution and in cellular systems. On the other hand, the P11L mutation has been claimed as responsible for the increased sensitivity of AGT-Mi to chemical and thermal stress (Cellini *et al.*, 2010). However, all these data have been interpreted by looking to the possible effects of the two substitutions on dimer stability. Our data indicate that they also play a role on the electrostatic aggregation of the protein. In particular, both mutations seem to mainly influence the autocatalytic growth of the aggregates. However, since k_1 and k_2 in the F-W model do not describe completely independent events, it cannot be excluded that the increase in k_2 is influenced by the increase in k_1 , which would determine a more rapid accumulation of aggregating nuclei that in turn would promote aggregate growth for mass action (Cohen *et al.*, 2012).

Pro11 is located at the monomer-monomer interface. *In silico* analyses predict that its substitution by a leucine residue could increase the flexibility of the N-terminal arm of AGT, possibly promoting its dissociation from the neighbouring subunit. This is also confirmed by biochemical studies showing an increased susceptibility of AGT variants bearing the P11L mutation to proteolytic cleavage at the N-terminus (Cellini *et al.*, 2010; Montioli *et al.*, 2015; Coultier-Mackie *et al.*, 2008).

Based on these data and considerations, we compared the electrostatic map of AGT-Ma with that of a truncated form of the protein deleted by the first 21 residues mimicking the possible detachment of the N-terminal arm (Figure 39).

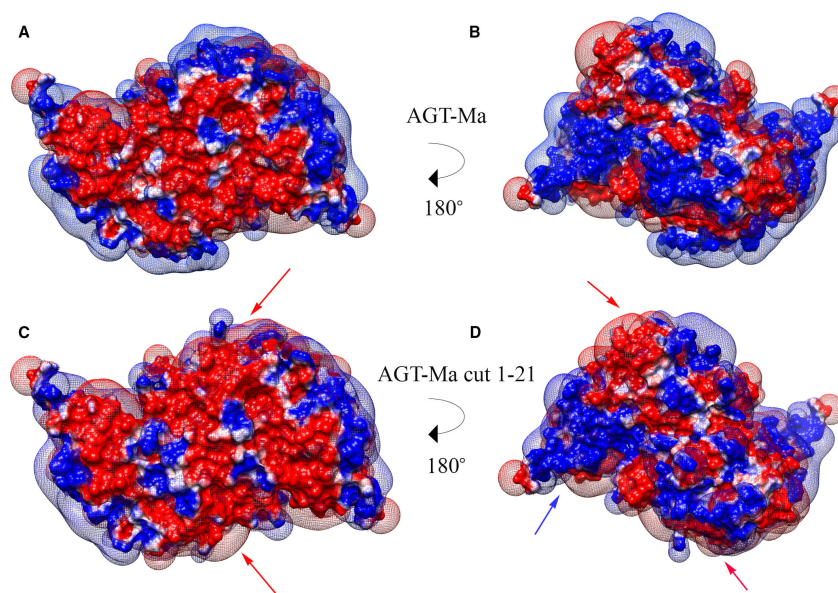


Figure 39. Electrostatic potential contours (-0.5 (red) and $+0.5$ (blue) kT/e) of full length AGT-Ma (A,B) and of a truncated form with residues 1–21 deleted (C,D). We have setted 0.06 M KP, pH 7.4 as buffer at 37 °C. Blue and red arrows indicate the differences between the electrostatic potential map of AGT-Ma and its truncated form.

We found that negatively charged residues would be exposed upon detachment of the N-terminal arm of AGT, including Asp52, Glu59, Asp196, Glu274 and Glu281. It can be hypothesised that the increased flexibility of the N-terminal arm due to the P11L mutation could promote its transient dissociation from the neighbouring subunit, thus causing the exposure of negative areas. This in turn would increase the anisotropy of charge distribution on the AGT surface, thus creating more favourable conditions for the electrostatic interactions between dimers. An analogous mechanism has been already proposed to explain the behaviour of variants bearing mutations at Gly41 (Cellini *et al.*, 2010).

The comparison of the aggregation kinetics of each analysed species in the apo- and holo-form gives other important information. In the case of AGT-Ma and I340M,

we noticed that the holo-form displays a reduction of both k_1 and k_2 with respect to the apo-form, thus indicating that the binding of PLP influences both the nucleation and the autocatalytic growth step. However, it is difficult to draw definitive conclusions since the holo-forms do not aggregate in a wide range of pHs. On the other hand, in both AGT-Mi and P11L, bound PLP mainly influences the nucleation step. In fact, the k_1 values of apoAGT-Mi are 7- to 15-fold higher than the corresponding of holoAGT-Mi in the range of pH 5.5-7.0, while the k_2 values are of the same order of magnitude. Similarly, in the P11L variant the k_1 values of the apo-form are from 4 to 7-fold higher than those of the holo-form, while the k_2 values are of the same order of magnitude. It can be speculated that the stabilizing effect of PLP could be mediated by an overall conformational change induced by the cofactor that would probably disfavour the electrostatic interaction with neighbouring dimers, thus reducing the aggregation rate. Although the crystal structure of apoAGT has not been solved, its dichroic features in the near-UV region indicate that it has a tertiary structure slightly different from that of holoAGT (Oppici *et al.*, 2012), as well as an higher flexibility of the polypeptide chain making it more susceptible to unfolding and proteolytic degradation (Cellini *et al.*, 2012). It has been well documented that the PLP coenzyme is able to play a chaperone role for AGT, an effect mainly interpreted as being due to a quaternary structure stabilization (Dindo *et al.*, 2012). Based on our data, we can suggest that PLP binding could also reduce the exposure of charged residues possibly involved in the aggregation process. In this regard, the finding that in the presence of the P11L substitution PLP binding mainly affects the nucleation step could be explained through an indirect effect of coenzyme binding on the loop 24-32 that is connected to the N-terminal arm on one side, and to the active site on the other side. A role of the coenzyme in inducing conformational changes of the bound apoenzyme has been already proved in other B6-enzymes (Giardina *et al.*, 2011, Giardina *et al.*, 2015), but only the resolution of the crystal structure of apoAGT will shed light on the structural bases of the stabilizing role. To investigate the consequences of the aggregation process for AGT functionality, as well as the effect of the two polymorphic mutations, we measured the residual catalytic activity of AGT-Ma, AGT-Mi, P11L and I340M upon 3 h incubation at

37°C in KP 0.1 M pH 5.5 (to favour aggregation), at a protein concentration of 10 μ M. We then performed the assays in KP 0.1 M pH 7.4 at 25°C in the presence of PLP at saturating substrates concentrations, to stop the aggregation process. Holo and apoAGT-Ma, holo and apoI340M and holoAGT-Mi showed residual catalytic activity >90%. On the other hand, apoAGT-Mi, holo P11L and apoP11L displayed a residual activity of 64%, 48%, and 26%, respectively. In analogy with DLS analyses, the residual activity increased at increasing pH and increasing ionic strength. Moreover, the residual activity of the holo-form is higher than that of the corresponding apo-form under similar experimental conditions (Figure 40).

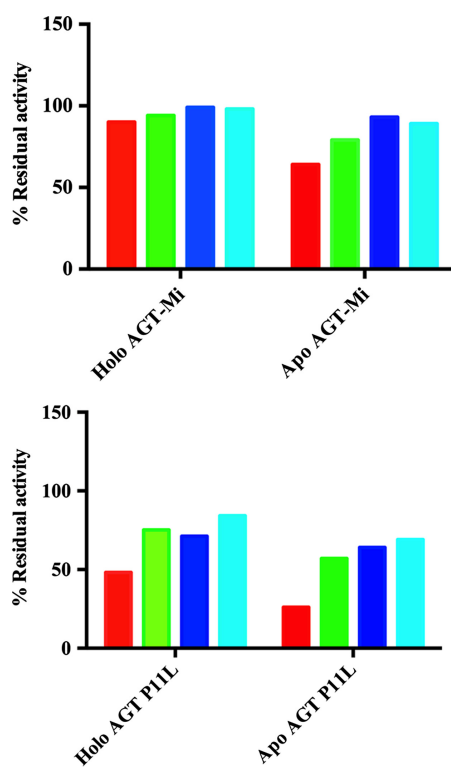


Figure 40. Residual catalytic activity of AGT-Mi and P11L upon incubation under different conditions of pH and ionic strength. Each species was incubated for 3 h at 10 μ M concentration, 37 °C under different conditions. The residual transaminase activity was measured by a standard enzymatic assay at 0.1 μ M concentration as described in Materials and methods. Bars are colored as follows: red, 0.1 M KP, pH 5.5; green, 0.1 M KP, pH 8.0; blue, 0.1 M KP pH 7.0, and cyan, 1 M KP, pH 7.0.

These data are in line with the aggregation mechanism, and confirm the destabilizing effect of the P11L mutation as well as the protective role of the PLP

coenzyme. Notably, the finding that the native-like aggregation process is associated with loss of protein functionality is not in contrast with CD spectroscopy analyses indicating no loss of secondary structure, because it is known that even small conformational changes far from the active site can reduce or abolish AGT catalytic activity (Oppici *et al.*, 2012, Giardina *et al.*, 2011). Thus, it can be hypothesized that the association of native-like dimers could negatively influence enzyme functionality leading to a loss of activity even in the absence of an unfolding process. A loss of activity has been already documented during the native-like aggregation of the acylphosphatase form *Sulfolobus solfataricus* (Bemporad and Chiti 2009).

7.4 Modulation of AGT-Mi aggregation by common PH1-causing mutations

Some of the most common mutations associated with PH1, including the F152I, G170R and I244T (Williams *et al.*, 2009), induce conformational changes on AGT that synergize with those generated by the minor allele polymorphism reducing the overall efficiency of the folding pathway and causing the population of monomeric intermediates kept by mitochondria (Danpure 2006). PLP is able to shift the equilibrium toward the holo-form, by probably promoting the formation of the native dimer, in line with the responsiveness to B6 reported at cellular and/or clinical level (Fargue *et al.*, 2013; Hoyer-Kuhn *et al.*, 2014). Based on the significant influence of the polymorphic mutations on the aggregation propensity of AGT in the native form, we investigated if the F152I, G170R and I244T mutations could also play a role in this process when present on the background of the minor allele.

We determined the aggregation rate of the F152I-Mi, G170R-Mi and I244T-Mi variants in the holo- and apo-form at three different pHs by DLS. As described above for the polymorphic AGT species, the aggregation propensity decreases at increasing pH (Figure 41A). The rate of the process increases at increasing protein concentration and low ionic strengths (data not shown).

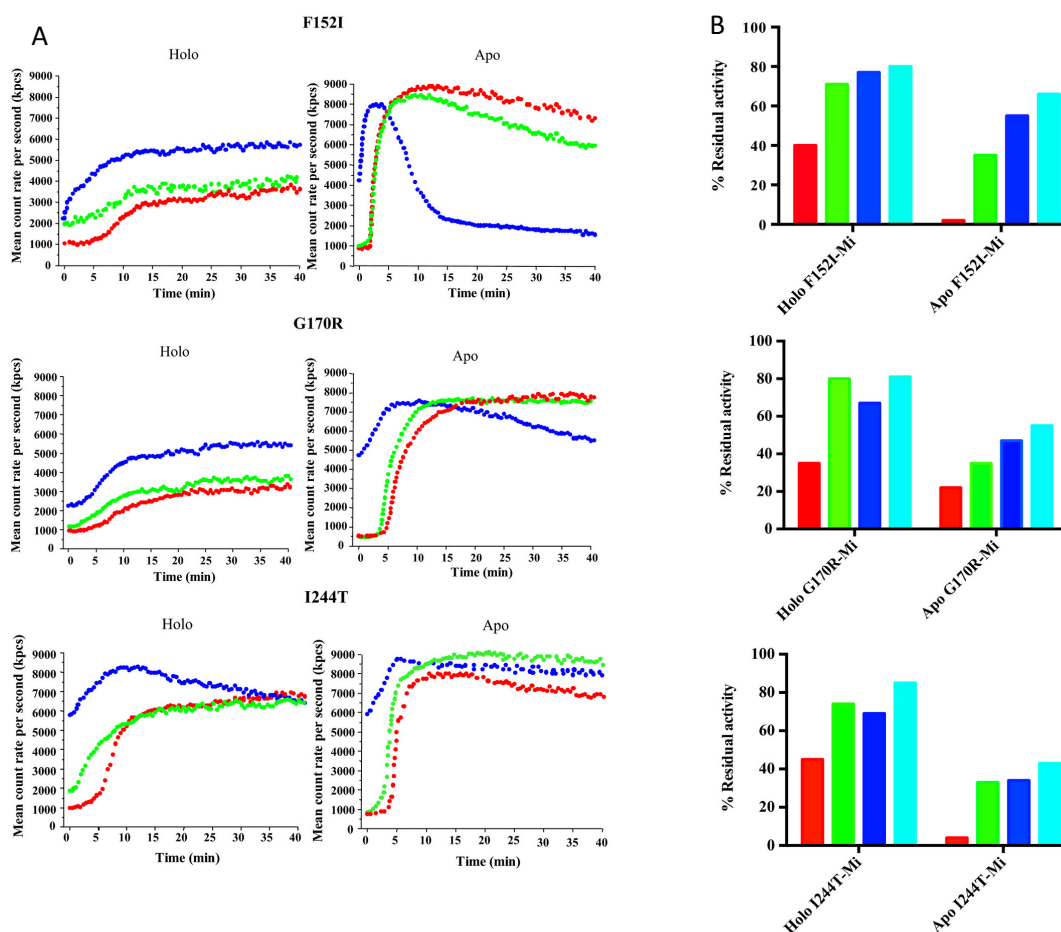


Figure 41. Electrostatic map and time-dependent aggregation of the pathogenic variants F152I-Mi, G170R-Mi, and I244T-Mi in the holo and apo form. (A) Time-dependent changes of the total count rate (measured as kilocounts per second) of the indicated species at 10 μ M concentration in 0.1 M KP at pH 5.5 (blue), 7.0 (green), and 8.0 (red). (B) Residual catalytic activity upon 3 h incubation under different conditions of pH and ionic strength. Each species was incubated for 3 h at 10 μ M concentration, 37 $^{\circ}$ C under different conditions. The residual transaminase activity was measured by a standard enzymatic assay at 0.1 μ M concentration as described in Materials and Methods. Bars are colored as follows: red, 0.1 M KP, pH 5.5; green, 0.1 M KP, pH 8.0; blue, 0.1 M KP pH 7.0, and cyan, 1 M KP, pH 7.0.

At each pH, the values of both k_1 and k_2 of the three variants are higher than the corresponding of AGT-Mi. In line with these results, we found that a significant reduction of catalytic activity occurs upon aggregation, with higher residual activity at increasing pH and ionic strength (Figure 41B). Thus, we can conclude that (i) at neutral and alkaline pH the variants undergo a native-like aggregation process driven by electrostatic forces, which accounts for a significant loss of functionality of the protein, in particular in the apo-form; (ii) at acidic pH, the holovariants show electrostatic aggregation in the native-like form, while the apovariants also undergo

a time-dependent unfolding process, in line with their reduced stability already suggested by chemical or thermal unfolding studies (Mesa-Torres *et al.*, 2014).

A global analysis of the behaviour of the variants allows to hypothesize that the F152I, G170R and I244T mutations synergize with the minor allele polymorphisms not only by interfering with the folding pathway of AGT populating monomeric intermediates prone to hydrophobic aggregation, degradation, and mistargeting to mitochondria, but also by increasing the electrostatic aggregation propensity of the protein once folded. Both phenomena would concur to the strong functional deficit of AGT of cells expressing the three variants, and would explain why they are partly present in the insoluble fraction of the lysate (Oppici *et al.*, 2015).

It should be also pointed out that the F152I-Mi, G170R-Mi and I244T-Mi variants are found to be responsive to Vitamin B6 in a cellular model of PH1 and the responsiveness is confirmed by clinical data in the case of F152I-Mi and G170R-Mi [49]. Previous reports ascribed the responsiveness to the ability of the coenzyme to promote AGT folding and dimerization (Dindo *et al.*, 2016). Our analyses support an additional role of PLP in protecting the native protein from aggregation. In fact, the aggregation extent of each species in the apo-form is higher than that of the corresponding holo-form, an effect mainly driven by the increase in k_2 . It remains to be explained why the coenzyme in the pathogenic variants seems to mainly affect the aggregates growth rather than nucleus formation. In the absence of structural information, we can only speculate that this could be partly due to the different conformational changes induced by polymorphic and pathogenic mutations, and to their synergic action.

We have gained important insights into how point alterations of a protein surface could impact its behavior and stability in solution. Most studies on the pathogenesis of protein deficits interpret the aggregation propensity of disease-causing variants as being due to the population of folding intermediates showing sticky hydrophobic patches (misfolding-based aggregation). Our results, along with those on other proteins of pharmacological interest (Roberts 2014, Austerberry *et al.*, 2017), highlight that a deep analysis of the electrostatic surface should be also carried out to provide insights into possible alterations of the surface charge anisotropy that

could promote electrostatic aggregation of a protein once folded (native-like aggregation). In particular, by combining the data reported here with those of previous reports (Cellini *et al.*, 2009; Cellini *et al.*, 2011; Mesa-Torres *et al.*, 2013), we delineated a more comprehensive picture describing AGT aggregation. Figure 42 illustrates the minimal proposed model of AGT-Ma folding and highlights the differential influence of mutations from a quantitative and qualitative point of view. The protein is prone to aggregate both during the folding pathway, as a consequence of the population of monomeric intermediates exposing hydrophobic surfaces, and once folded, as a consequence of the exposure of oppositely charged surfaces. Polymorphic and pathogenic mutations can increase the propensity of the protein to misfolding-based hydrophobic aggregation and/or to native-like electrostatic aggregation. In addition, the coenzyme PLP plays a wide chaperone role for the protein because it not only favors the folding of intermediates in the apo form and the attainment of the dimeric structure but also stabilizes the protein once folded.

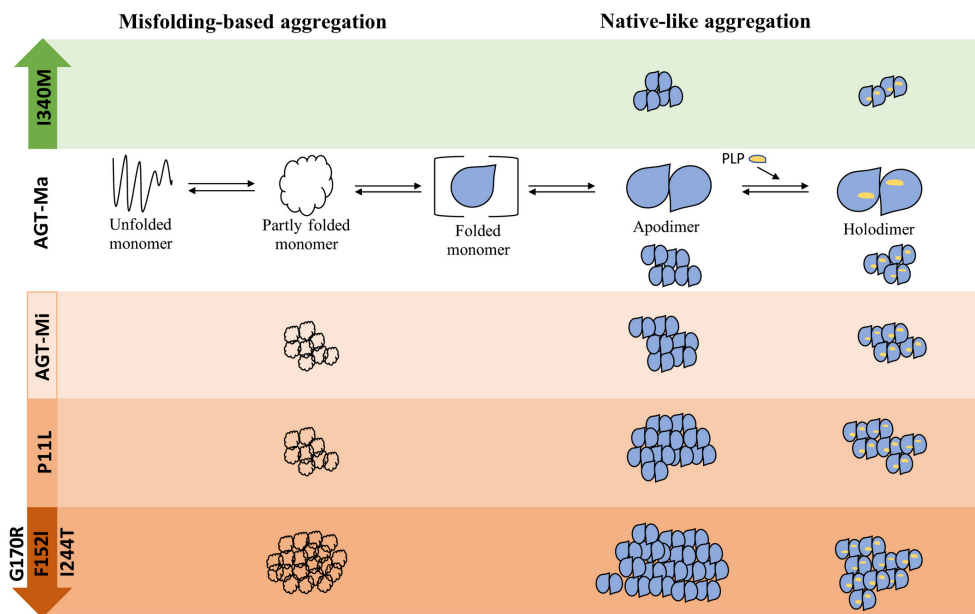


Figure 42. Global scheme describing the influence of polymorphic and pathogenic mutations on the AGT aggregation propensity.

CONCLUSIONS

Here we combined *in silico* and *in vitro* studies to analyse the aggregative behaviour of AGT and to shed light on the possible influence of polymorphic and pathogenic mutations. The results obtained indicate that: (i) the major allelic form of AGT shows a high surface charge anisotropy that makes it susceptible to an aggregation mediated by electrostatic forces; (ii) PLP binding strongly reduces the aggregation of the protein, thus suggesting that the coenzyme could have a more wide chaperone role than previously known (Cellini *et al.*, 2010); (iii) the P11L mutation enhances the aggregation propensity of AGT, while the I340M mutation has a stabilizing effect; (iv) missense mutations associated with PH1 could play their effects by promoting electrostatic aggregation.

We have gained important insights into how point alterations of a protein surface could impact its behaviour and stability in solution. Most studies on the pathogenesis of protein deficits interpret the aggregation propensity of disease-causing variants as being due to the population of folding intermediates showing sticky hydrophobic patches (misfolding-based aggregation) (Camilloni *et al.*, 2016). Our results, along with those on other proteins of pharmacological interest (Roberts 2002), highlight that a deep analysis of the electrostatic surface should be also carried out to provide insights into possible alterations of the surface charge anisotropy that could promote electrostatic aggregation of a protein once folded (native-like aggregation). In particular, by combining the data reported here with those of previous reports (Cellini *et al.*, 2009), we delineated a more comprehensive picture describing AGT aggregation. Fig. 14 illustrates the minimal proposed model of AGT-Ma folding and highlights the differential influence of mutations from a quantitative and qualitative point of view. The protein is prone to aggregate both during the folding pathway, as a consequence of the population of monomeric intermediates exposing hydrophobic surfaces, and once folded, as a consequence of the exposure of oppositely charged surfaces. Polymorphic and pathogenic mutations can increase the propensity of the protein to misfolding-based hydrophobic aggregation and/or to native-like electrostatic aggregation. In addition, the coenzyme PLP plays a wide chaperone role for the protein because it not only

favours the folding of intermediates in the apo-form and the attainment of the dimeric structure, but also stabilizes the protein once folded.

These findings, by increasing the knowledge of the biochemical properties of AGT and of the pathogenesis of PH1, constitute the base to design new strategies able to improve the stability of the protein as a possible premise for the development of innovative therapeutic approaches. Recently, a strategy for the successful administration of recombinant purified AGT based on the conjugation with polymeric carriers has been setup. The knowledge of the influence of surface charge on protein stability will be pivotal for the future development of the conjugates as a biological drug.

8

CONCLUSIONS

During the last years, many efforts have been focused on the development of an effective treatment for Hyperoxaluria (Cowley *et al.*, 2017; Grujic *et al.*, 2009, Langman *et al.*, 2014; Hoppe *et al.*, 2006; Hoppe *et al.*, 2011; Cellini *et al.*, 2011; Monico *et al.*, 2005; Hoyer-Kuhn *et al.*, 2014; Oppici *et al.*, 2015; Moya-Garzon *et al.* 2018; Lai *et al.*, 2018). Some of them are currently in clinical testing and especially address PH1, which is the most severe form of disease. One of the main problem deriving from hyperoxaluria is systemic oxalosis, in which oxalate accumulates in plasma and deposit in many organs including skin, heart and eye. It is well known that oxalate-degrading enzymes are presented in bacteria, fungi and plants, but their direct administration in humans is not feasible. During my PhD, I focused my attention on the possibility of using oxalate decarboxylase (OxDC) from *B. subtilis* as a biological drug, once encapsulated inside red blood cells (RBCs) to prevent its immunogenicity.

Altogether, the data obtained indicate that:

- 1) OxDC and its mutated form OxDC-DSSN (i) display optimal activity at pH 4.2 but retain a detectable residual activity at pH 7.2, the intracellular pH of RBCs, (ii) do not undergo major structural changes at neutral pH, (iii) are able to detoxify oxalate endogenously produced in eukaryotic cells.
- 2) OxDC can be efficiently encapsulated in human and murine RBCs and does not loose catalytic activity during the encapsulation process.
- 3) By using directed evolution approaches, we engineered a mutated form of OxDC more resistant to thermal stress and aggregation under physiological conditions as compared with wild-type OxDC.

Overall these data provide the proof-of-principle for the feasibility of a therapy for Hyperoxaluria based on the administration of RBCs-loaded with an oxalate-degrading enzyme. Future studies will be focused on the testing of the ability of wild-type and engineered OxDC to detoxify oxalate in a mouse model of PH1.

In addition, I participated to a study focused on the effect of pathogenic and polymorphic mutations on the propensity to aggregation of AGT, the enzyme

mutated in PH1. The results obtained indicate that AGT is highly susceptible to an aggregation mediated by electrostatic forces and that the coenzyme PLP strongly reduces the self-association of the protein. The P11L and I340M polymorphic mutations play an opposite role on the aggregation propensity of AGT, while the most common missense mutations associated with PH1 promote the process. These findings improve the knowledge of the pathogenic mechanisms of PH1 and constitute the base to design innovative therapeutic approaches able to improve AGT stability.

ANNEX I

Summary of the results obtained and activities performed during the PhD course

Publications

During my PhD I have focused my research on the study of hyperoxaluria, a pathologic condition due to genetic and non-genetic causes that leads to the deposition of calcium oxalate stones in the urinary tract. Hyperoxaluria can be caused either by the increased amount of endogenous oxalate production (primary hyperoxaluria or PH) or by an increased intestinal oxalate absorption (secondary hyperoxaluria or SH). The most severe form of PH is primary hyperoxaluria type I, which is due to a mutations on the gene encoding alanine:glyoxylate aminotransferase (AGT). Current therapeutic approaches are poorly effective and the development of a new therapeutic strategy is highly desirable. To afford this question, the main project during my PhD was the development of a new strategy based on the encapsulation of an oxalate-degrading enzyme, oxalate decarboxylase from *B. subtilis* (OxDC) inside red blood cells (RBCs) to metabolize plasmatic oxalate. This would in turn contributes to reducing urinary oxalate thus avoiding the precipitation of calcium oxalate in the kidneys.

The first results of my study have been accepted to publication. They describe the characterization of wild-type OxDC and of a mutant form at neutral pH:

- 1) **C. Conter**, E. Oppici, M. Dindo, L. Rossi, M. Magnani and B. Cellini, “Biochemical properties and oxalate-degrading activity of oxalate decarboxylase from *Bacillus subtilis* at neutral pH”, *IUBMB Life*, (2019) doi: 10.1002/iub.2027.

In parallel with my main PhD project, I have been also involved in a second project related to PH1, focused on the study of the effect of polymorphic and pathogenic mutations on the electrostatic aggregation of AGT. The results obtained are reported in the following paper:

- 2) M. Dindo, **C. Conter** and B. Cellini “Opposite effect of polymorphic mutations on the electrostatic aggregation of human alanine:glyoxylate aminotransferase: implications for the pathogenesis of primary hyperoxaluria type I”, *FEBS J.*, (2017) doi: 10.1111/febs.14269.

Finally, I have participated to the writing of a review and a book chapter on the molecular bases of PH:

- 3) M. Dindo*, **C. Conter***, E. Oppici, V. Ceccarelli, L. Marinucci and B. Cellini, “Molecular basis of primary hyperoxaluria: clues to innovative

treatments”, *Urolithiasis*, (2018), doi: 10.1007/s00240-018-1089-z. *Co-first authors.

- 4) E. Oppici, M. Dindo, **C. Conter**, C.B. Voltattorni and B. Cellini “Folding defects leading to Primary Hyperoxaluria” *Handbook of Experimental Pharmacology*, (2017) doi: 10.1007/164_2017_59

Meeting attendance

- 1) 4 June - 6 June 2018 “Sensory Systems in Health Disease”, Verona (Italy).
- 2) 28 May - 30 May 2018 “PROTEINE 2018”, Verona (Italy).
- 3) 14 July -16 July 2017 “12th International Primary Hyperoxaluria Workshop” Tenerife (Spain)
- 4) 30 March – 1 April 2016 “PROTEINE 2016”, Bologna (Italy)

Short oral communications to national and international meetings

- 1) **C. Conter**, “Electrostatic interactions drive native-like aggregation of human alanine:glyoxylate aminotransferase”, “Sensory Systems in Health Disease”, Verona (Italy) - June 4-6, 2018 (Selected from abstract).
- 2) **C. Conter**, “Erythrocytes as carriers of oxalate decarboxylase: an innovative approach for the treatment of Hyperoxaluria”, 12th International Primary Hyperoxaluria Workshop”, Tenerife (Spain) – July 14-16, 2017 (Selected from abstracts).

Visiting experience

- 1) September 4th 2017-December 17th. Visit to the University of Granada, dept. of Chemical Chemistry, under the supervision of Dr. Angel Luis Pey. During these three months I learned the Isothermal Titration Calorimetry and Differential Scanning Calorimetry techniques, that I applied to study the denaturation and aggregation processes of oxalate decarboxylase (OxDC).
- 2) March 20th – 24th 2017. Visit to the University of Urbino “Carlo Bo”, dept. of Biomolecular Science, under the supervision of Prof. Mauro Magnani and Prof. Luigia Rossi. During this week I have setup the encapsulation of OxDC in murine erythrocytes, an important prerequisite for the aim of my PhD project.

- 3) May 2nd – 6th 2016. Visit to the University of Urbino “Carlo Bo”, dept. of Biomolecular Science, under the supervision of Prof. Mauro Magnani and Prof. Luigia Rossi. During this week I learned the techniques of erythrocytes loading and, I have setup the encapsulation of OxDC in human erythrocytes, as the basis to proceed in my PhD project.

BIBLIOGRAPHY

Alagia A, Eritja R (2016) siRNA and RNAi optimization. *Wiley interdisciplinary reviews RNA* 7 (3):316-329.

Albert A (2017) Expression of heterologous oxalate decarboxylase in HEK293 cells confers protection against oxalate induced oxidative stress as a therapeutic approach for calcium oxalate stone disease. *J Enzyme Inhib Med Chem* 32(1): 426-433.

Allen LC, Kadujevic L and Romaschin AD (1989) An enzymatic method for oxalate automated with the Cobas Fara centrifugal analyzer. *Clin Chem.* 35(10): 2098-100.335-45.

Amadasi A, Bertoldi M, Contestabile R, Bettati S, Cellini B, di Salvo ML, Borri-Voltattorni C, Bossa F, Mozzarelli A (2007) Pyridoxal 5'-phosphate enzymes as targets for therapeutic agents. *Curr Med Chem* 14:1291–1324.

Anand R, Dorrestein PC, Kinsland C, Begley TP and Ealick SE (2002) Structure of oxalate decarboxylase from *Bacillus subtilis* at 1.75 Å resolution. *Biochemistry* 41:7659-7669.

Andy V, Horvath P, Wanders RJ (1995) Aminooxy acetic acid: a selective inhibitor of alanine:glyoxylate aminotransferase and its use in the diagnosis of primary hyperoxaluria type I. *Clin chim acta* 243 (2):105-114.

Archer HE, Dormer AE, Scowen EF, Watts RW (1957) Studies on the urinary excretion of Oxalate by normal subjects. *Clinical Science* 16 (3): 405-11.

Arnold, FH. (1993), Engineering proteins for non-natural environments. *The FASEB Journal*, 7 (9): 744-749.

Austerberry JA, Dajania R, Panovab S, Robertsc D, Golovanovd AP, Pluene A, van der Wallef CF, Uddinf S, Warwickerd J, Derricka JP et al. (2017) The effect of charge mutations on the stability and aggregation of a human single chain Fv fragment. *Eur J Pharm Biopharm* 115, 18–30.

Baker NA, Sept D, Joseph S, Holst MJ and McCammon JA (2001) Electrostatics of nanosystems: application to microtubules and the ribosome. *Proc Natl Acad Sci USA* 98: 10037–10041.

Barker S.A., Khossravi D. (2001) Drug delivery strategies for the new millennium. *Drug Discovery Today* 6: 75–77.

Beadle BM, Shoichet BK (2002) Structural bases of stability-function tradeoffs in enzymes. *J. Mol. Biol.* 321, 285–296.

Beck BB, Hoyer-Kuhn H, Gobel H, Habbig S, Hoppe B (2013) Hyperoxaluria and systemic oxalosis: an update on current therapy and future directions. *Expert Opin Investig Drugs* 22:117–129.

- Begley TP and Ealick SE (2004) Enzymatic reactions involving novel mechanisms of carbanion stabilization. *Curr Opin Chem Biol* 8(5): 508-15.
- Behnam, JT (2006) Reconstruction of human hepatocyte glyoxylate metabolic pathways in stably transformed Chinese-hamster ovary cells. *Biochem J* 394: 409-16.
- Bemporad F & Chiti F (2009) “Native-like aggregation” of the acylphosphatase from *Sulfolobus solfataricus* and its biological implications. *FEBS Lett* 583: 2630–2638.
- Ben-Shalom E and Frishberg Y (2015) Primary hyperoxalurias: diagnosis and treatment. *Pediatric nephrology* 30 (10):1781-1791
- Bertoldi M (2005) Folding pathway of the pyridoxal 5'-phosphate C-S lyase MalY from *Escherichia coli*. *Biochem J*, 389: 885-98.
- Bhasin B, Urekli HM and Atta MG (2015) Primary and secondary hyperoxaluria: understanding the enigma. *World J Nephrol* 4:235–244.
- Biagiotti S, Paoletti MS, Fraternali A, Rossi L and Magnani M (2011) Drug Delivery by Red Blood Cells *IUBMB Life*, 63(8): 621–631.
- Booth MP, Connors R, Rumsby G, Brady RL (2006) Structural basis of substrate specificity in human glyoxylate reductase/hydroxypyruvate reductase. *Journal of molecular biology* 360 (1):178-189.
- Bougioukou DJ, Kille S, Taglieber A, Reetz MT (2009) Directed evolution of an enantioselective enoate-reductase: testing the utility of iterative saturation mutagenesis. *Adv. Synth. Catal.* 351, 3287–3305.
- Bryan PN (2000) Protein engineering of subtilisin. *BBA* 1543: 203-222
- Burrell MR, Just VJ, Bowater L, Fairhurst SA, Requena L, Lawson DM, Bornemann S. (2007) Oxalate decarboxylase and oxalate oxidase activities can be interchanged with specific switch of up to 282 000 mutating an active side lid. *Biochemistry* 46:12327-12336.
- Camilloni C, Sala BM, Sormanni P, Porcari R, Corazza A, De Rosa M, Zanini S, Barbiroli A, Esposito G, Bolognesi M et al. (2016) Rational design of mutations that change the aggregation rate of a protein while maintaining its native structure and stability. *Sci Rep* 6: 255-59.
- Canales BK and Gonzalez RD (2014) Kidney stone risk following Roux-en-Y gastric bypass surgery. *Translation Andrology and Urology* 3: 242–249.

Carrasco A, Jr., Granberg CF, Gettman MT, Milliner DS, Krambeck AE (2015) Surgical management of stone disease in patients with primary hyperoxaluria. *Urology* 85 (3):522-526.

Cassland (2010) Evaluation of oxalate decarboxylase and oxalate oxidase for industrial applications. *Appl Biochem Biotechnol*, 2010. 161(1-8): 255-63.

Castello R, Borzone R, D'Aria S (2016) Helper-dependent adenoviral vectors for liver-directed gene therapy of primary hyperoxaluria type I. *Gene Therapy* 23(2):129–134.

Cellini B (2017) Treatment options in primary hyperoxaluria Type I. *Expert Opinion on Orphan Drugs* 5 (4):11.

Cellini B, Bertoldi M, Montioli R, Paiardini A, and Borri Voltattorni C (2007) Human wild-type alanine:glyoxylate aminotransferase and its naturally occurring G82E variant: functional properties and physiological implications. *Biochem J* 408(1):39-50.

Cellini B, Lorenzetto A, Montioli R, Oppici E, Voltattorni CB (2010a) Human liver peroxisomal alanine:glyoxylate aminotransferase: different stability under chemical stress of the major allele, the minor allele, and its pathogenic G170R variant. *Biochimie* 92:1801–1811.

Cellini B, Montioli R, Bianconi S, Lopez-Alonso JP & Voltattorni CB (2008) Construction, purification and characterization of untagged human liver alanine-glyoxylate aminotransferase expressed in *Escherichia coli*. *Protein Pept Lett* 15, 153–159.

Cellini B, Montioli R, Oppici E, Astegno A & Voltattorni CB (2013) The chaperone role of the pyridoxal 50-phosphate and its implications for rare diseases involving B6-dependent enzymes. *Clin Biochem* 47, 158–165.

Cellini B, Montioli R, Paiardini A, Lorenzetto A, Maset F, Bellini T, Oppici E, Voltattorni CB (2010b) Molecular defects of the glycine 41 variants of alanine glyoxylate aminotransferase associated with primary hyperoxaluria type I. *Proc Natl Acad Sci U S A* 107:2896–2901.

Cellini B, Montioli R, Paiardini A, Lorenzetto A, Voltattorni CB (2009) Molecular insight into the synergism between the minor allele of human liver peroxisomal alanine:glyoxylate aminotransferase and the F152I mutation. *J Biol Chem* 284:8349–8358.

Cellini B, Montioli R, Voltattorni CB (2011) Human liver peroxisomal alanine:glyoxylate aminotransferase: characterization of the two allelic forms and their pathogenic variants. *BBA* 1814 (11):1577-1584.

Cellini B, Oppici E, Paiardini A and Montioli R (2012) Molecular insights into primary hyperoxaluria type 1 pathogenesis. *Front Biosci (Landmark Ed)* 17:621-634.

Cellini B *et al.*, (2006) Dimerization and folding processes of *Treponema denticola* cystalysin: the role of pyridoxal 5'-phosphate. *Biochemistry*, 45(47): 14140-54.

Chadwick VS, Modha K, Dowling RH (1973) Mechanism for hyperoxaluria in patients with Ileal dysfunction. *N Engl J Med* 289: 172-176.

Cirri E., Brier S, Reda Assal, Canul-Tec, Chamot-Rooke, Reyes N., *eLife* 2018;7:e40110.

Cochat P and Groothoff J (2013) Primary hyperoxaluria type 1: practical and ethical issues. *Pediatric nephrology* 28 (12):2273-2281.

Cochat P and Rumsby G (2013) Primary hyperoxaluria. *N Engl J Med* 369:649–658.

Cochat P, Fargue S and Harambat J (2010) Primary hyperoxaluria type 1: strategy for organ transplantation. *Curr opin organ transp* 15 (5):590-593.

Cochat P, Hulton SA, Acquaviva C, Danpure CJ, Daudon M, De Marchi M, Fargue S, Groothoff J, Harambat J, Hoppe B, Jamieson NV, Kemper MJ, Mandrile G, Marangella M, Picca S, Rumsby G, Salido E, Straub M, van Woerden CS, OxalEurope (2012) Primary hyperoxaluria Type 1: indications for screening and guidance for diagnosis and treatment. *Nephrology, dialysis, transplantation: official publication of the European Dialysis and Transplant Association - European Renal Association* 27 (5):1729-1736.

Cohen SI, Vendruscolo M, Dobson CM & Knowles TP (2012) From macroscopic measurements to microscopic mechanisms of protein aggregation. *J Mol Biol* 421, 160–171.

Coulter-Mackie MB and Lian Q (2008) Partial trypsin digestion as an indicator of mis-folding of mutant alanine:glyoxylate aminotransferase and chaperone effects of specific ligands. Study of a spectrum of missense mutants. *Mol Gen Metab* 94, 368–374.

Coulter-Mackie MB and Lian Q (2006) Consequences of missense mutations for dimerization and turnover of alanine:glyoxylate aminotransferase: study of a spectrum of mutations. *Mol Genet Metab* 89(4):349-359

Coulter-Mackie MB, Tung A, Henderson HE, Toone and Applegarth DA (2003) The AGT gene in Africa: a distinctive minor allele haplotype, a polymorphism (V326I), and a novel PH1 mutation (A112D) in Black Africans. *Mol Genet Metab* 78(1):44-50.

Cowley (2017) In vitro and in vivo safety evaluation of Nephure. *Regul Toxicol Pharmacol*, 86: 241-252.

Cowley AB (2010) 14-day repeat-dose oral toxicity evaluation of oxazyme in rats and dogs. *Int J Toxicol*, 2010 29(1): 20-31.

Cregeen DP, Williams EL, Hulton S and Rumsby G (2003) Molecular analysis of the glyoxylate reductase (GRHPR) gene and description of mutations underlying primary hyperoxaluria type 2. *Hum Mutat* 22:497

Cuthbert AW (1992) The biochemical defect in cystic fibrosis. *J R Soc Med* 85, 1–5.

Danpure CJ (2006) Primary hyperoxaluria type 1: AGT mistargeting highlights the fundamental differences between the peroxisomal and mitochondrial protein import pathways. *Biochim Biophys Acta* 1763, 1776–1784.

Danpure CJ and Jennings PR (1986) Peroxisomal alanine:glyoxylate aminotransferase deficiency in primary hyperoxaluria type I. *FEBS Lett* 201 (1): 20-24.

Danpure CJ and Rumsby G (2005) Molecular etiology of primary hyperoxaluria and its implications for clinical management. *Expert Rev Molec Med* 6 (1): 1-16.

De Baets G, Van Doorn L, Rousseau F and Schymkowitz J (2015) Increased aggregation is more frequently associated to human disease-associated mutations than to neutral polymorphisms. *PLoS Comput Biol* 11, e1004374.

Der BS, Kluwe C, Miklos AE, Jacak R, Lyskov S, Gray JJ, Georgiou G, Ellington AD & Kuhlman B (2013) Alternative computational protocols for supercharging protein surfaces for reversible unfolding and retention of stability. *PLoS ONE* 8, e64363.

Dindo M, Conter C and Cellini B. (2017) Opposite effect of polymorphic mutations on the electrostatic aggregation of human alanine:glyoxylate aminotransferase: implications for the pathogenesis of primary hyperoxaluria type I', *FEBS J.*, doi: 10.1111/febs.14269.

Dindo M, Montioli R, Busato M, Giorgetti A, Cellini B, Borri Voltattorni C (2016) Effects of interface mutations on the dimerization of alanine glyoxylate aminotransferase and implications in the mistargeting of the pathogenic variants F152I and I244T. *Biochimie* 131:137–148.

Dindo M, Oppici E, Dell'Orco D, Montone R, Cellini B (2018) Correlation between the molecular effects of mutations at the dimer interface of alanine-glyoxylate aminotransferase leading to primary hyperoxaluria type I and the cellular response to vitamin B6. *J inherit met dis* 41 (2):263-275

Dolinsky TJ, Niesen JE, McCammon JA & Baker NA (2004) PDB2PQR: an automated pipeline for the setup, execution, and analysis of Poisson-Boltzmann electrostatics calculations. *Nucleic Acids Res* 1, 665–667.

Dumas B, Freyssinet G, Pallett KE (1995) Tissue-Specific Expression of Germin-Like Oxalate Oxidase during Development and Fungal Infection of Barley Seedlings. *Plant Physiology* 107: 1091–1096.

Duncan SH, Richardson AJ, Kaul P, Holmes RP, Allison MJ and Stewart CS (2002) *Oxalobacter formigenes* and its potential role in human health. *Appl. Environ. Microbiol.* 68: 3841–3847.

Dutta C, Avitahl-Curtis N, Pursell N, Larsson Cohen M, Holmes B, Diwanji R, Zhou W, Apponi L, Koser M, Ying B, Chen D, Shui X, Saxena U, Cyr WA, Shah A, Nazef N, Wang W, Abrams M, Dudek H, Salido E, Brown BD, Lai C (2016) Inhibition of Glycolate Oxidase With Dicer-substrate siRNA Reduces Calcium Oxalate Deposition in a Mouse Model of Primary Hyperoxaluria Type 1. *Molecular therapy: the journal of the American Society of Gene Therapy* 24 (4):770-778.

Emiliani E. and Bekes P (1964) Enzymatic Oxalate Decarboxylation in *Aspergillus Niger*. *Arch Biochem Biophys*, 105: 488-93.

Fargue S, Lewin J, Rumsby G, Danpure CJ (2013a) Four of the most common mutations in primary hyperoxaluria type 1 unmask the cryptic mitochondrial targeting sequence of alanine: glyoxylate aminotransferase encoded by the polymorphic minor allele. *J Biol Chem* 288:2475–2484.

Fargue S, Milliner DS, Knight J, Olson JB, Lowther WT and Holmes RP (2018) Hydroxyproline Metabolism and Oxalate Synthesis in Primary Hyperoxaluria. *J Am Soc Nephrol.* 29(6):1615-1623.

Fargue S, Rumsby G and Danpure CJ (2013b) Multiple mechanisms of action of pyridoxine in primary hyperoxaluria type 1. *Biochim Biophys Acta* 1832: 1776–1783.

Fink AL (1998) Protein aggregation: folding aggregates, inclusion bodies and amyloid. *Fold Des* 3, R9–R23.

Fodor K, Wolf J, Erdmann R, Schliebs W and Wilmanns M (2012) Molecular requirements for peroxisomal targeting of alanine-glyoxylate aminotransferase as an essential determinant in primary hyperoxaluria type 1. *PLoS Biol* 10, e1001309.

Fontana A, de Laureto PP, Spolaore B, Frare E, Picotti P, Zambonin M (2004) Probing protein structure by limited proteolysis. *Acta Biochim Pol* 51:299–321.

Giafi CF and Rumsby G (1998) Kinetic analysis and tissue distribution of human D-glycerate dehydrogenase/glyoxylate reductase and its relevance to the diagnosis of primary hyperoxaluria type 2. *Annals of Clinical Biochemistry* 35: 104–109.

Giardina G, Brunotti P, Fiascarelli A, Cicalini A, Costa MG, Buckle AM, di Salvo ML, Giorgi A, Marani M, Paone A et al. (2015) How pyridoxal 50-phosphate differentially regulates human cytosolic and mitochondrial serine hydroxymethyltransferase oligomeric state. *FEBS J* 282, 1225–1241.

Giardina G, Montioli R, Gianni S, Cellini B, Paiardini A, Voltattorni CB & Cutruzzola F (2011) Open conformation of human DOPA decarboxylase reveals the mechanism of PLP addition to Group II decarboxylases. *Proc Natl Acad Sci USA* 108, 20514– 20519.

Grujic D, Salido EC, Shenoy BC, Langman CB, McGrath ME, Patel RJ, Rashid A, Mandapati S, Jung CW and Margolin AL (2009) Hyperoxaluria is reduced and nephrocalcinosis prevented with an oxalate-degrading enzyme in mice with hyperoxaluria. *American Journal of Nephrology* 29: 86-93.

Guerard N, Oder D, Nordbeck P, Zwingelstein C, Morand O, Welford RWD, Dingemans J, Wanner C (2018) Lucerastat, an Iminosugar for Substrate Reduction Therapy: Tolerability, Pharmacodynamics, and Pharmacokinetics in Patients With Fabry Disease on Enzyme Replacement. *Clinical pharmacology and therapeutics* 103 (4):703-711.

Gupta, MN. (1992). Enzyme function in organic-solvents. *European Journal of Biochemistry* 203: 1-2.

Gutierrez-Millan C, Sayalero ML, Castaneda AZ and Lanao JM (2004) Drug, enzyme and peptide delivery using erythrocytes as carriers. *J Control Rel* 95:27-49

Guyton AC (1996) Red blood cells, anemia and polycitemia. *Textbook of Medical Physiology*, Philadelphia.

Harambat J, Fargue S, Bacchetta J, Acquaviva C and Cochat P (2011) Primary hyperoxaluria. *International journal of nephrology* 2011:864580.

Hatch M, Freel RW (2008) The roles and mechanisms of intestinal oxalate transport in oxalate homeostasis. *Seminars in nephrology* 28 (2):143-151.

Hatch M, Freel RW (2013) A human strain of *Oxalobacter* (HC-1) promotes enteric oxalate secretion in the small intestine of mice and reduces urinary oxalate excretion. *Urolithiasis* 41 (5):379-384.

Hatch M, Gjymishka A, Salido EC, Allison MJ, Freel RW (2011) Enteric oxalate elimination is induced and oxalate is normalized in a mouse model of primary hyperoxaluria following intestinal colonization with *Oxalobacter*. *American journal of physiology Gastrointestinal and liver physiology* 300 (3): 461-469.

Hatch M, Cornelius J, Allison M, Sidhu H, Peck A and Freel RW (2006) *Oxalobacter* sp. reduces urinary oxalate excretion by promoting enteric oxalate

secretion. *Kidney International*, 69:691–698.

Hiatt WR (1987) Oxalic acid removal in beer production.

Holmes RP, Goodman HO and Assimos DG (2001) Contribution of dietary oxalate to urinary oxalate excretion. *Kidney International* 59: 270–276.

Hopp K, Cogal AG, Bergstralh EJ, Seide BM, Olson JB, Meek AM, Lieske JC, Milliner DS, Harris PC, Rare Kidney Stone C (2015) Phenotype-genotype correlations and estimated carrier frequencies of primary hyperoxaluria. *J Am Soc Nephrol* 26:2559–2570.

Hoppe B (2012) An update on primary hyperoxaluria. *Nat Rev Nephrol* 8:467–475

Hoppe B, Beck B, Gatter N, von Unruh G, Tischer A, Hesse A, Laube N, Kaul P, Sidhu H (2006) *Oxalobacter formigenes*: a potential tool for the treatment of primary hyperoxaluria type 1. *Kidney international* 70 (7):1305-1311.

Hoppe B, Dittlich K, Fehrenbach H, Plum G, Beck BB (2011) Reduction of plasma oxalate levels by oral application of *Oxalobacter formigenes* in 2 patients with infantile oxalosis. *American journal of kidney diseases: the official journal of the National Kidney Foundation* 58 (3):453-455. doi:10.1053/j.ajkd.2011.05.012

Hoppe B, Leumann E and von Unruh G (2003) Diagnostic and therapeutic approaches in patients with secondary hyperoxaluria. *Frontiers in Bioscience*, 8: e437–e443.

Hoppe B and vonUnruh G. (2005) Oxalate degrading bacteria: new treatment option for patients with primary and secondary hyperoxaluria. *Urological Research*, 33:372-5.

Hopper ED, Pittman AM, Fitzgerald MC and Tucker CL (2008) In vivo and in vitro examination of stability of primary hyperoxaluria-associated human alanine:glyoxylate aminotransferase. *J Biol Chem* 283(45):30493-30502.

Hoskins J. and Gray A (1982) Phenylalanine ammonia lyase in the management of phenylketonuria: the relationship between ingested cinnamate and urinary hippurate in humans. *Res. Commun. Chem. Pathol. Pharmacol* 35: 275-282

Hoyer-Kuhn H, Kohbrok S, Volland R, Franklin J, Hero B, Beck BB and Hoppe B (2014) Vitamin B6 in primary hyperoxaluria I: first prospective trial after 40 years of practice. *Clin J Am Soc Nephrol* 9: 468–477.

Jain S and Jain NK (1997) Engineered erythrocytes as a drug delivery system. *Indian Journal of Pharmaceutical Sciences* 59: 275–281.

Just VJ, Burrell MR, Bowater L, McRobbie I, Stevenson CEM, Lawson DM and

Bornemann S. (2007) The identity of the active site of oxalate decarboxylase and the importance of the stability of active site lid conformations. *Biochemical Journal* 407(3): 97–406.

Just VJ, Stevenson CEM, Bowater L, Tanner A, Lawson DM and Bornemann S (2004) A closed conformation of *Bacillus subtilis* oxalate decarboxylase OxdC provides evidence for true identity of the active site. *The Journal of Biological Chemistry* 279:19867-19874.

Karaolani G, Lionaki S, Moris D, Palla VV and Vernadakis S (2014) Secondary hyperoxaluria: a risk factor for kidney stone formation and renal failure in native kidneys and renal grafts. *Transplantation reviews* 28 (4):182-187.

Konno T (2001) Amyloid-induced aggregation and precipitation of soluble proteins: an electrostatic contribution of the Alzheimer's b (25–35) amyloid fibril. *Biochemistry* 40: 2148–2154.

Kopp N and Leumann E. (1995) Changing pattern of primary hyperoxaluria in Switzerland. *Nephrology Dialysis Transplantation*, 10 (12): 2224–2227.

Lai C et al., (2018) Specific Inhibition of Hepatic Lactate Dehydrogenase Reduces Oxalate Production in Mouse Models of Primary Hyperoxaluria. *Mol Ther.* 26(8):1983-1995.

Lane MD and Seelig B (2014) Advances in the directed evolution of proteins. *Curr Opin Chem Biol.* 0: 129–136.

Lang GJ and Murray AG (2008) Estimating the per-base-pair mutation rate in the yeast *Saccharomyces cerevisiae*. *Genetics*, 178 (1): 67-82.

Langman, CB, et al., (2016) A Double-Blind, Placebo Controlled, Randomized Phase 1 Cross- Over Study with ALLN-177, an Orally Administered Oxalate Degrading Enzyme. *Am J Nephrol* 44(2): 150-8.

Langman LJ and Allen LC (1998) An enzymatic method for oxalate automated using the Hitachi 911 analyzer. *Clin Biochem* 31(5): 429-32.

Lee CC, Julian MC, Tiller KE, Meng F, DuConge SE, Akter R, Raleigh DP & Tessier PM (2016) Design and optimization of anti-amyloid domain antibodies specific for b-amyloid and islet amyloid polypeptide. *J Biol Chem* 291, 2858–2873.

Lee LP & Tidor B (2001) Barstar is electrostatically optimized for tight binding to barnase. *Nat Struct Biol* 8, 73–76.

Lee E., et al., (2014) Expression of the gene encoding oxalate decarboxylase from *Bacillus subtilis* and characterization of the recombinant enzyme. *BMC Res Notes* 7: 598.

Liebow A, Li X, Racie T, Hettinger J, Bettencourt BR, Najafian N, Haslett P, Fitzgerald K, Holmes RP, Erbe D, Querbes W, Knight J (2016) An Investigational RNAi Therapeutic Targeting Glycolate Oxidase Reduces Oxalate Production in Models of Primary Hyperoxaluria. *Journal of the American Society of Nephrology JASN*. doi:10.1681/ASN.2016030338

Lumb MJ and Danpure CJ (2000) Functional synergism between the most common polymorphism in human alanine:glyoxylate aminotransferase and four of the most common disease-causing mutations. *J Biol Chem* 275(46):36415-36422.

Lumb MJ, Drake AF and Danpure CJ (1999) Effect of N-terminal alpha- helix formation on the dimerization and intracellular targeting of alanine:glyoxylate aminotransferase. *J Biol Chem* 274(29):20587-20596.

Lvarez FEA and Lichtiger B (1995) Bacterial contamination of cellular blood components. *Current Issues in Transfusion Medicine* 3 (3).

Magnani M, Rossi L, Bianchi M, Fornaini G, Benatti U, Guida L, Zocchi E and De Flora A (1988) Improved metabolic properties of hexokinase-overloaded human erythrocytes. *Biochimica et Biophysica Acta* 972(1):1-8.

Magnani M, Rossi L, Fraternali A, Bianchi M, Antonelli A, Crinelli R and Chiarantini L. (2002) Erythrocyte-mediated delivery of drugs, peptides and modified oligonucleotides. *Gene Therapy* 9 (11): 749– 751.

Magro PM and Di Lena P (1988) Enzymatic oxalate decarboxylation in isolates of *Sclerotinia sclerotiorum*. *FEMS Microbiology Letters*, 49(1): 49-52

Majhi PR, Ganta RR, Vanam RP, Seyrek E, Giger K & Dubin PL (2006) Electrostatically driven protein aggregation: beta-lactoglobulin at low ionic strength. *Langmuir* 24, 9150–9159.

Mandrile G, Woerden CS, Berchiolla P, Beck BB, Bourdain CA, Hulton SA and Rumsby G., on behalf of OxalEurope Consortium (2014) Data from a large European study indicate that the outcome of primary hyperoxaluria type 1 correlates with the AGXT mutation type. *Kidney International* **86**, 1197–1204.

Marangella M, Petrarulo M and Cosseddu D (1994) End-stage renal failure in primary hyperoxaluria type 2. *N Engl J Med* 330:1690.

Marengo SR and Romani AM (2008) Oxalate in renal stone disease:the terminal metabolite that just won't go away. *Nature Clinical Practice Nephrology* 14: 368-377.

Marshall RW, Cochran M and Hodgkinson A. (1972) Relationships between calcium and oxalic acid intake in the diet and their excretion in the urine of normal

and renal-stone-forming subjects. *Clinical Science* 43 (1): 91-9.

Martin-Higueras C, Luis-Lima S, Salido E (2016) Glycolate Oxidase Is a Safe and Efficient Target for Substrate Reduction Therapy in a Mouse Model of Primary Hyperoxaluria Type I. *Molecular therapy : the journal of the American Society of Gene Therapy* 24 (4):719-725.

Martinez-Zaguilan, R., et al., (1991) Simultaneous measurement of intracellular pH and Ca²⁺ using the fluorescence of SNARF-1 and fura-2. *Am J Physiol.* **260**:297-307.

Mdluli K, Booth MP, Brady RL, Rumsby G (2005) A preliminary account of the properties of recombinant human Glyoxylate reductase (GRHPR), LDHA and LDHB with glyoxylate, and their potential roles in its metabolism. *Biochimica et biophysica acta* 1753 (2):209-216.

Mesa-Torres N, Cristina Yunta, Israel Fabelo-Rosa, Juana María Gonzalez-Rubio, José M. Sánchez-Ruiz, Eduardo Salido, Armando Albert, Angel L. Pey (2014) The consensus-based approach for gene/enzyme replacement therapies and crystallization strategies: the case of human alanine-glyoxylate aminotransferase *Biochem. J.* 462: 453–463 (Printed in Great Britain).

Mesa-Torres N, Fabelo-Rosa I, Riverol D, Yunta C, Albert A, Salido E, Pey AL (2013) The role of protein denaturation energetics and molecular chaperones in the aggregation and mistargeting of mutants causing primary hyperoxaluria type I. *PLoS One* 8:e71963.

Mesa-Torres N, Salido E and Pey AL (2014) The lower limits for protein stability and foldability in primary hyperoxaluria type I. *Biochim Biophys Acta* 1844: 2355–2365.

Mesa-Torres N, Yunta C, Fabelo-Rosa I, Gonzalez- Rubio JM, Sanchez-Ruiz JM, Salido E, Albert A & Pey AL (2014) The consensus-based approach for gene/enzyme replacement therapies and crystallization strategies: the case of human alanine-glyoxylate aminotransferase. *Biochem J* 462, 453–463.

Mistry PK, Lopez G, Schiffmann R, Barton NW, Weinreb NJ & Sidransky E (2017) Gaucher disease: progress and ongoing challenges. *Mol Genet Metab* 120, 8–21.

Mittal RD and Kumar R (2004) Gut inhabiting bacterium Oxalate Formigenes: role in calcium oxalate urolithiasis. *Journal of Endourology* 18:418-24.

Monico CG, Olson JB, Milliner DS (2005) Implications of genotype and enzyme phenotype in pyridoxine response of patients with type I primary hyperoxaluria. *American Journal of Nephrology* 25 (2), 183-8.

Monico CG, Rossetti S, Olson JB, Milliner DS (2005) Pyridoxine effect in type I

primary hyperoxaluria is associated with the most common mutant allele. *Kidney international* 67 (5):1704-1709.

Montioli R, Oppici E, Dindo M, Roncador A, Gotte G, Cellini B & Borri Voltattorni C (2015) Misfolding caused by the pathogenic mutation G47R on the minor allele of alanine:glyoxylate aminotransferase and chaperoning activity of pyridoxine *Biochim Biophys Acta* 1854, 1280–1289.

Montioli R, Dindo M, Giorgetti A, Piccoli S, Cellini B, and Voltattorni CB, (2014) A comprehensive picture of the mutations associated with aromatic amino acid decarboxylase deficiency: from molecular mechanisms to therapy implications. *Human Molecular Genetics* 23 (20): 5429–5440.

Moomaw, E.W., et al., (2013) Kinetic and spectroscopic studies of bicupin oxalate oxidase and putative active site mutants. *PLoS One*. 8(3): p. e57933.

Morris AM, Watzky MA & Finke RG (2009) Protein aggregation kinetics, mechanism, and curve-fitting: a review of the literature. *Biochim Biophys Acta* 1794, 275–397.

Morris AM, Watzky MA, Agar JN & Finke RG (2008) Fitting neurological protein aggregation kinetic data via a 2-step, minimal/“Ockham’s razor” model: the Finke-Watzky mechanism of nucleation followed by autocatalytic surface growth. *Biochemistry* 47, 2413–2427.

Moss HA, Tebbs SE, Faroqui MH, Herbst T, Isaac JL, Brown J and Elliott TS (2000) A central venous catheter coated with benzalkonium chloride for the prevention of catheter-related microbial colonization. *European Journal of Anaesthesiology* 17 (11): 680– 687.

Moya-Garzoń D et al., (2018) Salicylic Acid Derivatives Inhibit Oxalate Production in Mouse Hepatocytes with Primary Hyperoxaluria Type 1. *J. Med. Chem.* 61: 7144–7167

Mufarrij, P.W., et al., (2013) The effects of Oxazyme on oxalate degradation: results and implications of in vitro experiments. *J Endourol*, 2013. 27(3): 284-7.

Neves-Petersen MT & Petersen SB (2003) Protein electrostatics: a review of the equations and methods used to model electrostatic equations in biomolecules—applications in biotechnology. *Biotechnol Annu Rev* 9: 315–395.

Noel-Hocquet S, Jabbouri S, Lazar S, Maunier JC, Guillaumet G, Ropars C, in: Magnani M., DeLoach J. R. (Eds.) *The Use of Resealed Erythrocytes as Carriers and Bioreactors*, *Advances in Experimental Medicine and Biology*, vol. 326, 1992, pp. 215–221.

Oliva A, Llabrés M & Farina JB (2015) Fitting bevacizumab aggregation kinetic data with the Finke-Watzky two-step model: effect of thermal and mechanical stress. *Eur J Pharm Sci* 18: 170–179.

Olsson MH, Sondergaard CR, Rostkowski M & Jensen JH (2011) PROPKA3: consistent treatment of internal and surface residues in empirical pKa predictions. *J Chem Theory Comput* 7: 525–537.

Oppici E, Fargue S, Reid ES, Mills PB, Clayton PT, Danpure CJ & Cellini B (2015a) Pyridoxamine and pyridoxal are more effective than pyridoxine in rescuing folding-defective variants of human alanine:glyoxylate aminotransferase causing primary hyperoxaluria type I. *Hum Mol Genet* 24: 5500–5511

Oppici E, Montioli R and Cellini B (2015b) Liver peroxisomal alanine:glyoxylate aminotransferase and the effects of mutations associated with primary hyperoxaluria type I: an overview. *Biochim Biophys Acta* 1854:1212–1219.

Oppici E, Montioli R, Dindo M, Maccari L, Porcari V, Lorenzetto A, Chellini S, Voltattorni CB, Cellini B (2015) The Chaperoning Activity of Amino-oxyacetic Acid on Folding-Defective Variants of Human Alanine:Glyoxylate Aminotransferase Causing Primary Hyperoxaluria Type I. *ACS chemical biology* 10 (10):2227-2236.

Oppici E, Roncador A, Montioli R, Bianconi S, Cellini B (2013) Gly161 mutations associated with primary hyperoxaluria type I induce the cytosolic aggregation and the intracellular degradation of the apo-form of alanine:glyoxylate aminotransferase. *Biochim Biophys Acta* 1832:2277–2288. <https://doi.org/10.1016/j.bbadis.2013.09.002>

Osswald H, Hautmann R. (1979) Renal elimination kinetics and plasma half-life of oxalate in man. *Urologia Internationalis* 34 (6): 440–450.

Pace CN, Vajdos F, Fee L, Grimsley G and Gray T (1995) How to measure and predict the molar absorption coefficient of a protein. *Protein Sci* 4: 2411–2423.

Pace CN and Thompson BAS (1989) Measuring the Conformational Stability of a Protein. *Protein Structure, a Practical Approach*, oxford: IRL Press.

Pallas M and Camins A (2006) Molecular and biochemical features in Alzheimer's disease. *Curr Pharm Des* 12, 4389–4408.

Paramesvaran J, Hibbert EG, Russell AJ, Dalby PA, (2009) Distributions of enzyme residues yielding mutants with improved substrate specificities from two different directed evolution strategies. *Protein Eng. Des. Sel.* 22: 401–411.

Park S, Morley, KL, Horsman GP, Holmquist M, Hult K and Kazlauskas R.J (2005) Focusing mutations into the P. fluorescens esterase binding site increases enantioselectivity more effectively than distant mutations. *Chem. Biol.* 12: 45–54.

Parkinson IS, Kealey T, and Laker MF (1985) The determination of plasma oxalate concentrations using an enzyme/bioluminescent assay. *Clin Chim Acta*, 1985. **152**(3):2-10.

Pettersen EF, Goddard TD, Huang CC, Couch GS, Greenblatt DM, Meng EC and Ferrin TE (2004) UCSF Chimera—a visualization system for exploratory research and analysis. *J Comput Chem* 25, 1605–1612.

Pey AL, Albert A and Salido E (2013) Protein homeostasis defects of alanine-glyoxylate aminotransferase: new therapeutic strategies in primary hyperoxaluria type I. *Biomed Res Int* 2013:687658.

Pey AL, Salido E & Sanchez-Ruiz JM (2011) Role of low native state kinetic stability and interaction of partially unfolded states with molecular chaperones in the mitochondrial protein mistargeting associated with primary hyperoxaluria. *Amino Acids* 41, 1233–1245.

Phang JM, Hu CA and Valle D (2001) Disorders in proline and hydroxyproline metabolism. *The Metabolic and Molecular Bases of Inherited Disease*, 1821-1838.

Philo JS and Arakawa T (2009) Mechanism of protein aggregation. *Curr Pharm Biotechnol* 10: 348–351.

Plakoutsi, G., et al., (2004) Aggregation of the Acylphosphatase from *Sulfolobus solfataricus*: the folded and partially unfolded states can both be precursors for amyloid formation. *J Biol Chem*, **279**(14):14111-9.

Porebski BT and Buckle A (2016) Consensus protein design *Protein Engineering, Design & Selection* 29 (7):245–251

Powers ET, Morimoto RI, Dillin A, Kelly JW, Balch WE (2009) Biological and chemical approaches to diseases of proteostasis deficiency. *Annual review of biochemistry* 78:959-991.

Purdue PE, Allsop J, Isaya G, Rosenberg LE and Danpure CJ (1991) Mistargeting of peroxisomal L-alanine:glyoxylate aminotransferase to mitochondria in primary hyperoxaluria patients depends upon activation of a cryptic mitochondrial targeting sequence by a point mutation. *Proc Natl Acad Sci U S A* 88(23):10900-10904

Purdue PE, Takada Y, & Danpure CJ (1990) Identification of mutations associated with peroxisome-to-mitochondrion mistargeting of alanine/glyoxylate aminotransferase in primary hyperoxaluria type 1) *J Cell Biol* 111(6 Pt 1):2341-2351

Reinhardt LA, Svedruzic D, Cleland WW and Richards NGJ (2003) Heavy atom isotope effects on the reaction catalyzed by the oxalate decarboxylase from *Bacillus subtilis*. *Journal of American Chemical Society* 125: 1244–1252.

Ren J, Williams N, Clementi L, Krishnan S and Li WW (2010) Opal web service for biomedical applications. *Nucleic Acids Res* 38: 724–731.

Requena L. and Bornemann S, Barley (*Hordeum vulgare*) oxalate oxidase is a manganese- containing enzyme (1999) *Biochem J*, 343(1): 185-90.

Ringe D, Petsko GA (2009) What are pharmacological chaperones and why are they interesting? *Journal of biology* 8 (9):80.

Roberts CJ (2014) Therapeutic protein aggregation: mechanisms, design, and control. *Trends Biotechnol* 32, 372–380.

Robijn S and Hoppe B (2011) Hyperoxaluria: a gut-kidney axis? *Kidney International* 80:1146– 58.

Rockah-Shmuel, Dan S. Tawfik, and Moshe Goldsmith Generating Targeted Libraries by the Combinatorial Incorporation of Synthetic Oligonucleotides During Gene Shuffling (ISOR) Elizabeth M.J. Gillam et al. (eds.), *Directed Evolution Library Creation: Methods and Protocols*, Methods in Molecular Biology, vol. 1179, DOI 10.1007/978-1-4939-1053-3_8, © Springer Science+Business Media New York 2014

Roncador A, Oppici E, Talelli M, Pariente AN, Donini M, Dusi S, Voltattorni CB, Vicent MJ & Cellini B (2016) Use of polymer conjugates for the intraperoxisomal delivery of engineered human alanine: glyoxylate aminotransferase as a protein therapy for primary hyperoxaluria type I. *Nanomedicine* 13, 897– 907.

Rossi L, Pierigè F, Carducci C, Gabucci C, Pascucci T, Canonico B, Bell SM, Fitzpatrick PA, Leuzzi V and Magnani M (2014) Erythrocyte-mediated delivery of phenylalanine ammonia lyase for the treatment of phenylketonuria in BTBR-Pahenu2 mice. *Journal of Controlled Release* 194: 37-44.

Sala AJ, Bott LC, Morimoto RI (2017) Shaping proteostasis at the cellular, tissue, and organismal level. *J Cell Biol* 216:1231–1241.

Salido E, Pey AL, Rodriguez R, and Lorenzo V (2012) Primary hyperoxalurias: disorders of glyoxylate detoxification. *Biochim Biophys Acta* 1822(9):1453-1464.

Salido EC, Li XM, Lu Y, Wang X, Santana A, Roy-Chowdhury N, Torres A, Shapiro LJ and Roy-Chowdhury J (2006) Alanine-glyoxylate aminotransferase-deficient mice, a model for Primary hyperoxaluria that responds to adenoviral gene transfer. *PNAS USA* 103 (48): 18249- 54.

Salido E, Pey AL, Rodriguez R and Lorenzo V (2012) Primary hyperoxalurias: Disorders of glyoxilate detoxification. *Biochimica et Biophysica Acta* 1822: 1453-

1464.

Salido E, Rodriguez-Pena M and Santana A (2011) Phenotypic correction of a mouse model for primary hyperoxaluria with adeno-associated virus gene transfer. *Molecular Therapy* 19(5):870–875.

Santana A, Salido E, Torres A, Shapiro LJ (2003) Primary hyperoxaluria type 1 in the Canary Islands: a conformational disease due to I244T mutation in the P11L-containing alanine: glyoxylate aminotransferase. *Proc Natl Acad Sci U S A* 100:7277–7282.

Sarkadi B, Bauzon D, Huckle WR, Earp HS, Berry A, Suchindran H, Price EM, Olson JC, Boucher RC and Scarborough GA (1992) Biochemical characterization of the cystic fibrosis transmembrane conductance regulator in normal and cystic fibrosis epithelial cells. *J Biol Chem* 267: 2087–2095.

Sarkissian CN et al., (2008) Preclinical evaluation of multiple species of PEGylated recombinant phenylalanine ammonia lyase for the treatment of phenylketonuria. *Proc Natl Acad Sci U S A*, 105(52): 20894-9.

Scriver CR and Kaufman S *Hyperphenylalaninemia: phenylalanine hydroxylase deficiency*. R. Scriver, A.L. Beaudet, W.S. Sly, D. Valle, B. Childs, B. Vogelstein (Eds.), *The Metabolic and Molecular Bases of Inherited Disease*, McGraw Hill, New York (2001), pp. 1667-1724

Shemesh E, Deroma L, Bembi B, Deegan P, Hollak C, Weinreb NJ, Cox TM (2015) Enzyme replacement and substrate reduction therapy for Gaucher disease. *The Cochrane database of systematic reviews* (3):CD010324.

Sjöde AW, Nilvebrant S, Jönsson, LJ (2008) Enzyme-based control of oxalic acid in the pulp and paper industry. *Enzyme and microbial technology* 43(2): 78-83.

Smid BE, Ferraz MJ, Verhoek M, Mirzaian M, Wisse P, Overkleeft HS, Hollak CE, Aerts JM (2016) Biochemical response to substrate reduction therapy versus enzyme replacement therapy in Gaucher disease type 1 patients. *Orphanet journal of rare diseases* 11:28.

Smith GP (1985) Filamentous fusion phage: novel expression vectors that display cloned antigens on the virion surface. *Science* 228 (4705): 1315–7.

Smith LH, Van den Berg CJ, Wilson DM. Current concepts in nutrition – nutrition and urolithiasis. *N Eng J Med* 1978; **298**: 87–89.

Stauffer DE (1969) The effect on subtilisin activity of oxidizing a methionine residue, *J. Biol. Chem.* 244 (1969) 5333-5338.

Sugai Y, Sugai K and Fuse A. (2001) Current status of bacterial contamination of

autologous blood for transfusion. *Transfusion and Apheresis. Science* 24: 255– 259.

Svedružić D, Liu T, Reinhardt LA, Wroclawska E, Wallace CW and Richards NGJ (2007) Investigating the roles of putative active site residues in the oxalate decarboxylase from *Bacillus subtilis*. *Archives of Biochemistry and Biophysics* 464:36-47.

Svedruzic D., et al., (2005) The enzymes of oxalate metabolism: unexpected structures and mechanisms. *Arch Biochem Biophys*, **433**(1): 176-92.

Tanner A and Bornemann S (2000) *Bacillus subtilis* yVrK is an acid-induced oxalate decarboxylase. *Journal of Bacteriology* 182: 5271-3.

Tanner A, Bowater L, Fairhurst SA and Bornemann S (2001) Metal Dependence of Oxalate Decarboxylase Activity. *The Journal of Biological Chemistry* 276: 43627–43634.

Tokuriki N, Tawfik DS (2009). Chaperonin overexpression promotes genetic variation and enzyme evolution. *Nature* 459: 668–673.

Tomschy AR, Brugger M, Lehmann A, Svendsen K, Vogel D, Kostrewa SF, Lassen D, Burger A, Kronenberger C, van Loon (2002) . *Appl. Environ. Microbiol*, 68 (2002): 1907-1913

Torok M, Milton S, Kayed R, Wu P, McIntire T, Glabe CG and Langen R (2002) Structural and dynamic features of alzheimer's ab peptide in amyloid fibrils studied by site- directed spin labeling. *J Biol Chem* 277: 40810–40815.

Twahir UT, Ozarowski A, and Angerhofer A (2016) Redox Cycling, pH Dependence, and Ligand Effects of Mn(III) in Oxalate Decarboxylase from *Bacillus subtilis*. *Biochemistry* 55(47): 6505-6516.

Ueland PM, Ulvik A, Rios-Avila L, Midttun O, Gregory JF (2015) Direct and Functional Biomarkers of Vitamin B6 Status. *Annual review of nutrition* 35:33-70. doi:10.1146/annurev-nutr-071714-034330

Ugolini R, Ragona L, Silletti E, Fogolari F, Visschers RW, Alting AC and Molinari H (2001) Dimerization, stability and electrostatic properties of porcine b-lactoglobulin. *Eur J Biochem* 268: 4477–4488.

Uversky VN, et al., (2001) Stabilization of partially folded conformation during alpha-synuclein oligomerization in both purified and cytosolic preparations. *J Biol Chem*, 276(47):43495-8.

Valbonesi M, Bruni R, Florio G, Zanella A and Bunkens H (2001) Cellular contamination of plasma collected with various apheresis systems. *Transfusion and Apheresis. Science* 24: 91– 94.

van Tilbeurgh H, Jenkins J, Chiadmi M, Janin J, Wodak SJ, Mrabet NT and Lambeir AM (1992) Protein engineering of xylose (glucose) isomerase from *Actinoplanes missouriensis*. 3. Changing metal specificity and the pH profile by site- directed mutagenesis. *Biochemistry* 31: 5467–5471.

Wajnera A, Michelina K, Burinb MG, Piresb RF, Pereira ML, Giugliani R & Coelho JC (2004) Biochemical characterization of chitotriosidase enzyme: comparison between normal individuals and patients with Gaucher and with Niemann-Pick diseases. *Clin Biochem* 37, 893–897.

Walsh G (2010) Biopharmaceutical benchmarks 2010. *Nat Biotechnol* 28, 917–924.

Wang W, Nema S and Teagarden D (2010) Protein aggregation–pathways and influencing factors. *Int J Pharm* 390, 89–99.

Watzky MA, Morris AM, Ross ED & Finke RG (2008) Fitting yeast and mammalian prion aggregation kinetic data with the Finke-Watzky two-step model of nucleation and autocatalytic growth. *Biochemistry* 47, 10790–10800.

Williams EL, Acquaviva C, Amoroso A, Chevalier F, Coulter-Mackie M, Monico CG, Giachino D, Owen T, Robbiano A, Salido E, Waterham H, Rumsby G (2009) Primary hyperoxaluria type 1: update and additional mutation analysis of the AGXT gene. *Hum Mutat* 30:910–917.

Wojtaszek P. (1997) Oxidative burst: an early plant response to pathogen infection. *Biochemical Journal*, 322: 681–692.

Worcester EM (2002) Stones from bowel disease.. *Endocrinology Metabolism Clinics of North America*, 31: 979–999.

Zarembski PM and Hodgkinson A. (1969) Some factors influencing the urinary excretion of oxalic acid in man. *Clinica Chimica Acta* 25 (1):1-10.

Zhang X *et al.* (2003) Crystal structure of alanine:glyoxylate aminotransferase and the relationship between genotype and enzymatic phenotype in primary hyperoxaluria type 1 *J Mol Biol* 331(3):643-652

Zhang Z, Collinge D, Thordal-Christensen H. (1995) Germin-like oxalate oxidase, a H₂O₂- producing enzyme, accumulates in barley attacked by the powdery mildew fungus. *The Plant Journal*, 8: 139–145.

Zhu W, Wilcoxon J, Britt RD and Richards NGJ (2016) Formation of Hexacoordinate Mn(III) in *Bacillus subtilis* Oxalate Decarboxylase Requires Catalytic Turnover. *ACS Biochemistry* 55:429–434.

Zocchi E, Tonetti M, Polvani C, Guida L, Benatti U, De Flora A (1989) Encapsulation of doxorubicin in liver-targeted erythrocytes increases the therapeutic index of the drug in a murine metastatic model. PNAS U. S. A. 86: 2040– 2044.